UNIVERSITÀ DEGLI STUDI DI PAVIA
DOTTORATO DI RICERCA IN FISICA – XX CICLO

Boron Neutron Capture Therapy of Disseminated Tumours

Silva Bortolussi

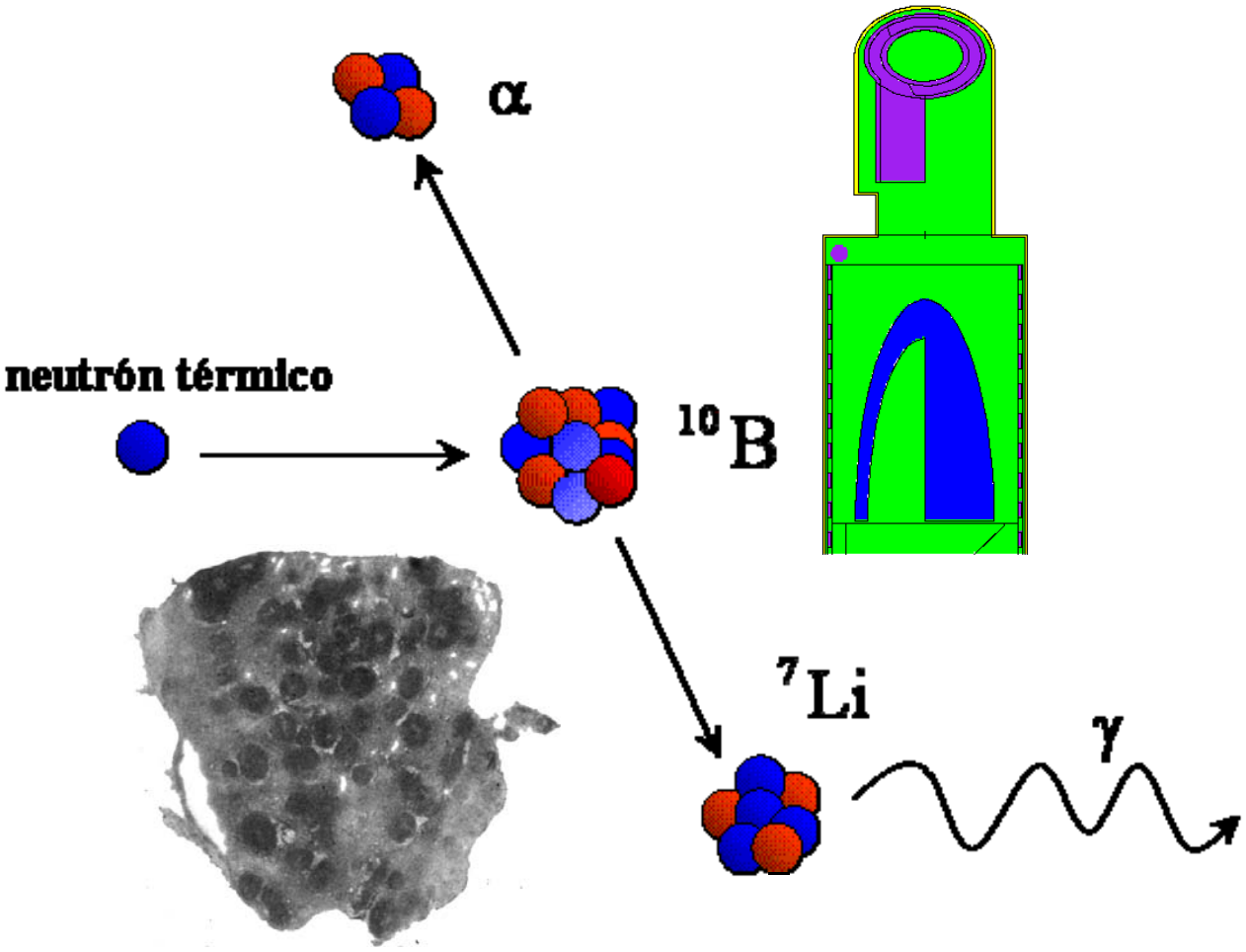

Supervisor: Dr *Saverio Altieri*

Tesi per il conseguimento del titolo

Università
degli Studi
di Pavia

Dipartimento di Fisica
Nucleare e Teorica

Istituto
Nazionale di
Fisica Nucleare

DOTTORATO DI RICERCA IN FISICA – XX CICLO

Boron Neutron Capture Therapy of Disseminated Tumours

dissertation submitted by

Silva Bortolussi

to obtain the degree of

DOTTORE DI RICERCA IN FISICA

Supervisor: Dr Saverio Altieri
Referee: Dr Raymond Moss

Cover

Center	The neutron capture reaction in Boron
Righ, topt:	ADAM anthropomorphic model. More details can be found in this thesis, on Chapter 3.
Left, bottom:	A neutron autoradiography of a lung tissue sample containing Boron. More details on Chapter 2.

Boron Neutron Capture Therapy of Disseminated Tumours
Silva Bortolussi
PhD thesis – University of Pavia
Printed in Pavia, Italy, November 2007
ISBN 978-88-95767-05-5

Dedico este trabajo a Argentina:
a su historia, a sus luchas
y a lo que me enseñó

Contents

Summary

Boron Neutron Capture Therapy of Disseminated Tumours

Boron Neutron Capture Therapy (BNCT) is an experimental form of binary radiotherapy, based on the irradiation with thermal neutrons of a tumour that is previously enriched with ^{10}B. The selective boron uptake of the tumour makes the irradiation deliver a potentially therapeutic dose to the malignancy, with a substantial sparing of the normal surrounding tissues. This selective effect is a promising novelty in the field of cancer therapy. Since it was proposed for the first time, it has been studied and applied to the tumours with a poor response to traditional therapies such as surgery, γ radiotherapy and chemotherapy. The first tumour treated by BNCT was Glioblastoma Multiforme, using borated compounds and neutron beams extracted from nuclear reactors in the USA, Japan and Europe. Nowadays, feasibility studies and clinical trials are being carried out all over the World. BNCT is applied to a number of other tumours, using neutrons in wider energy ranges, and boron carriers of a new generation. Furthermore, research is going on to produce intense neutron beams using accelerators, with the advantage of obtaining a suitable neutron source inside the hospitals.

The possibility to gain a selective effect based on the boron distribution rather than on the irradiation field, makes BNCT a valid option in the treatment of tumours that invade a whole organ, like the metastatic disseminations. The cause of the poor outcome of the traditional treatments often lies in the difficult diagnosis of all the metastases, especially the micrometastases. Moreover, in the case of multiple and multi-focal tumours a total surgery removal is often impossible, and also the traditional radiotherapy cannot destroy all the metastasis without causing unacceptable damage in the healthy tissue. This kind of tumours has been the subject of the BNCT research in Pavia, since the TAOrMINA project began twenty years ago, aiming to apply this therapy to the multiple metastases invading the liver after the resection of a primary colon adenocarcinoma. For the first time in the world, the BNCT was applied to an isolated organ, infused with boron, extracted from the patient, irradiated in the thermal column of the TRIGA reactor in Pavia and re-implanted in the patient. This pathology was chosen because it is quite common that, after the resection of the primary colon carcinoma,

a metastatic spread in the liver is fatal for the patient, even if there are no metastases in the other organs. Curing the organ would thus ensure a longer survival in good life conditions. Other tumours are extremely difficult to control due to their dissemination and the lack of effective strategies to treat them, for example the lung tumours. Four years ago, in Pavia, a new investigation was initiated to apply BNCT to lung tumours, and for this purpose a different strategy was conceived, consisting in irradiating the organ with external epithermal neutron beams.

This thesis is a summary of the research work performed in Pavia, aimed to the development of new methods and to the consolidation of the existing ones for the BNCT application to the diffuse tumours. The main problem dealing with such kind of tumours is that the tumoural cells are mixed with the normal ones, and the boron concentration measured in the different kind of tissues is not straightforward. An accurate knowledge of the tissue samples composition is needed, together with a map of the boron accumulation inside the tumour, healthy tissues and necrosis. The research carried out in Pavia developed a detailed protocol for the samples analysis: all the facilities for each step of the measurement (preparation of the samples, neutron autoradiography, α spectrometry) were constructed and the times and strategies for the measurement procedures were optimized. The results are useful for other research groups that are investing effort and resources to start new BNCT trials dedicated to the treatment of disseminated tumours; for this reason we are involved in a number of international collaborations.

In the following chapters we describe the feasibility study for the treatment of lung metastases, the studies to export the BNCT liver autotransplant method to other facilities in Europe, and a collaboration work with research groups in Argentina, which are realizing a new challenging concept of liver BNCT with autotransplant. The presented work mainly focuses on the experimental measure of boron concentrations in tissues and on the simulations of the neutron flux and dose distributions inside the organs using Monte Carlo methods.

The thesis is divided into four chapters. The first one is a general introduction, in which the basic concepts of BNCT are explained, with a brief historical description of the BNCT trials in the world and a presentation of the autotransplant method developed in Pavia. The second chapter presents the experimental part of the research on lung BNCT, consisting in the measurement of ^{10}B concentration in tumoural and healthy tissue. In fact, the first step of a BNCT feasibility study should demonstrate that the boron concentration obtained in the tumour and in the normal lung is compatible with a safe and effective irradiation. The third chapter describes the simulations performed with MCNP and the anthropomorphic model ADAM, in order to study the dose distribution in the lung and in the surrounding tissues due to epithermal neutron irradiation. The last chapter deals with the liver BNCT. Following the Pavia experience, a number of research groups in the world began new projects to apply BNCT with the autotransplant method. One of the most important requirements for this protocol is to build an irradiation facility to ensure a thermal flux distribution inside the explanted organ as homogeneous as possible. Different geometries of the irradiation facility were tested in the past using MCNP; in this chapter the extension of these studies to

other reactors is described.

Finally, the work made in Argentina during a research period spent at the Atomic Center of Ezeiza (Buenos Aires) is reported. A description of the Argentinean project that consists of explanting and irradiating only 2 segments of the human liver and the current state of this research are presented, from the biological and physical point of view.

Pavia, October 2007
Silva Bortolussi

Chapter 1

Introduction

Boron Neutron Capture Therapy is based on the reaction of low energy neutrons with ^{10}B producing two high LET[1] particles: a ^{7}Li ion and an α particle. The cross section of the ^{10}B(n,α)^{7}Li reaction is very high: 3837 b at thermal energies, and the Q-value is 2.790 MeV. With a probability of 94%, the reaction gives rise to the Li ion in an excited state, which returns to its fundamental level with a γ emission of 478 KeV. In the rest of the cases the reaction takes place at the fundamental level. The particles coming from the neutron capture in ^{10}B have thus two possible energies, that are reported in Tab. 1.1

The principle of the therapy is that tumoural cells can be loaded with ^{10}B and subsequently irradiated with thermal neutrons. When the reaction takes place inside a cell, the two ionizing particles can cross the nucleus and cause non-reparable damages to the DNA, as double strand breaks. When an α particle crosses a human cell nucleus 2 to 6 times the cell is lethally damaged, as it was proven in [1]. Moreover, the kinetic energy of the two particles is almost entirely dissipated inside the cell where they were originated. In other words their ranges are comparable to a cell diameter. This is an advantage for the therapy because the surrounding healthy cells would be spared from radiation damages coming from the capture reactions occurring in the tumoural cells that accumulate higher boron concentrations[2].

Some calculations were made to assess the number of boron atoms needed inside a tumoural cell to be killed by irradiation with a thermal neutron fluence of 10^{12} neutrons/cm^2. It resulted that 10^9 boron atoms per cell would be enough

[1] Linear Energy Transfer

[2] In this work, 'boron' always indicates the isotope ^{10}B.

Table 1.1: Energies of the particle coming from neutron capture in ^{10}B

	94%	6%
α	1.47 MeV	1.78 MeV
^{7}Li	0.84 MeV	1.01 MeV
γ	0.48 MeV	-

to produce 2 to 3 neutron captures and destroy the cell.

The potential efficacy of BNCT lies in its selectivity, in fact using proper borated compounds the tumoural cells can be loaded with higher boron concentration compared to the normal cells. This fact was experimentally observed since two drugs were synthesized and used in BNCT research. These compounds are the Borophenylalanine (BPA) and the Sodium-Dodecaborane (BSH), which are still used in the BNCT research programs for their ability to concentrate the boron atoms preferably in tumoural cells. The aim of the therapy is to deliver a therapeutic radiation dose to the tumour, keeping the dose absorbed by normal parenchyma under the tolerance levels. When irradiating the tissue with neutrons, the total absorbed dose is made up of different components. Some of these dose components are a non-selective background radiation that cannot be avoided, as they originate from the interaction with tissue elements. The selective dose delivery is based on the boron concentration ratio between the tumour and the healthy tissue, that must be as high as possible. In this chapter some of these points will be further explained, after a brief history of the BNCT trials in the world.

1.1 The BNCT history and present status

The first idea to use the boron neutron capture for therapeutic purposes was born in 1936, proposed by Locher [2], few years after the neutron discovery by Chadwick in 1932. The *in vitro* research on cell cultures and *in vivo* on mice began in the 1940s, but the first clinical applications of BNCT took place at the beginning of the 1950s in the USA. The diseases regarded as the best target for BNCT treatment were the cerebral gliomas, for the poor outcome of the patients treated with the best available radiation therapies of that time. Firstly, patients were treated at Brookhaven National Laboratory (BNL), and later at the Massachusetts Institute of Technology (MIT) using thermal neutron beams extracted from the reactors of the two laboratories and a borated compound named Borax [3]. This first phase concluded in 1959, when the trials were stopped due to the disappointing clinical outcomes, explained with the low selectivity of the drug employed, and the poor penetration of thermal neutrons in the tissues. This fact was the cause of severe damages to the scalp when deep seated tumours were treated [4]; also the removal of the scalp during the irradiation did not improve the results.

In 1968 a new clinical trial started in Japan, due to the introduction of new borated compounds that were able to deliver a higher boron concentration inside the tumoural cells [5] [6] [7]. This second phase of BNCT application to brain tumours gave better results, even if the mean survival was no longer than the one obtained with conventional radiotherapy. Nevertheless the high number of patients treated (120 patients in Japan) pushed the research to go on and improve the clinical results.

In 1994 a new clinical trial started at the BNL, USA: it was the first time that epithermal neutrons were used to irradiate patients [8] [9]. This novelty allowed to reach a better penetration, to spare the skin and to deliver a higher BNCT dose in the tumour, thanks to the neutron thermalization in the first layers of tissue

(skin, scalp). Besides, a new generation of borated compounds was realized, in particular BPA-f (Borophenylalanine-fructose complex), that was able to carry the boron atoms inside the cells penetrating the cell membrane. In the same year a trial for the treatment of cutaneous melanoma started at MIT [10], and 2 years later another trial for intra-cerebral melanoma or glioblastoma started in the same laboratory [11]. In 1997 a similar research program started in Europe, at the High Flux Reactor (HFR) in Petten, The Netherlands, for the treatment of cerebral tumours, in collaboration with Amsterdam (NL) and Essen (Germany) university hospitals [12] [13] [14]. In 1999 and 2000 similar trials started in Sweden and Finland [15][16].

In 2001 a liver with multiple metastases of a patient that was affected by a primary colon carcinoma, was treated at the TRIGA reactor in Pavia (Italy), with a new method developed at the University [17]. It consisted in irradiating the explanted liver previously infused with BPA in the Thermal Column of the reactor and in the subsequent re-implantation in the patient. This represented the birth of a new BNCT field dedicated to the treatment of tumours dissemination in whole vital organs, which could not be treated with collimated external beams. This topic will be explained later in this chapter and in the following ones.

In 2003, a trial for the application of BNCT to the skin Melanoma started in Argentina [18] and a trial for the brain metastases from melanoma at the HFR in Petten, in collaboration with MIT [19]. Other research is currently being developed in Czech Republic [20], South-Korea, Taiwan and Russia.

What is the present status of the trials started around the world in the last years? The trials dedicated to the treatment of the brain diseases are going on mainly in Japan, where also a new research on lung began [21]. The tumours in the lung are a new target for BNCT research: in Italy (Chapters 2 and 3 of this thesis and [24][25][22]) and in the USA [26]. Also the liver BNCT with the autotransplant method is being studied and projects have been created to modify the thermal column of TRIGA reactors around Europe (see Chapter 4), and to realize irradiation facilities around epitermal beams such as in Petten [27]. Head and neck cancers [28], oral tumours, hepatocellular carcinomas [29] [30], and other kinds of malignancies are currently under evaluation for a possible BNCT treatment, as also reported in the Proceedings of the 12th International Congress on Neutron Capture Therapy, held at Takamatsu, (Japan) in October 2006 [31]. A detailed description of the most important BNCT trials with a review of BNCT characteristics and developments is reported in [32]. Unfortunately, two large projects for BNCT development and applications were closed: the BNCT research at BNL (USA) and at Studsvik (Sweden).

The hope towards a BNCT outcome in the treatment of many different kinds of tumours lies in the progress that the research made during the last years in all the involved fields of physics, surgery and radiotherapy. Nevertheless, the BNCT whole community agrees on the fact that a future dramatic improvement is bound to the development of new drugs, that would ensure a higher boron concentration ratio between tumour and healthy tissue. This would mean shorter irradiation times and the possibility to irradiate larger targets, with a high dose delivery to

the tumour and an almost total sparing of the healthy tissues.

1.2 The boron carriers used for BNCT

The development of new boron carriers in the 1950s allowed the birth of new BNCT trials, and since their introductions almost no further enhancement was reached in the field of the boron selective transportation into the tumour. The borated compounds that are currently used in clinical BNCT are in fact the BPA (Borophenylalanine) and the BSH (Sodium Dodecaborane).

The latter ($Na_2B_{12}H_{11}SH$) was mainly used for the brain tumours, because its selective uptake is based on its capacity to cross the Blood Brain Barrier only in the zones where it is destroyed by the disease. The concentration ratio obtained between tumour and blood is never larger than 2, because the accumulation in the tumour is passive.

The BPA ($C_9H_{12}{}^{10}BNO_4$) was synthesized in 1950, and it gave positive results to *in vitro* and *in vivo* tests. It was applied for the first time to the cutaneous melanoma. The BPA was proven to have an active mechanism of transportation inside the cell, and to lead to an uniform boron distribution inside the nucleus and the cytoplasm [33]. Even if the active transportation results in an higher boron concentration in blood, in the tumour the concentration is 2-4 times higher. In Pavia the preclinical research and the clinical application to the liver were carried out using BPA. As explained later in this thesis, BPA allowed to reach a boron concentration in the metastases that is about 5 times higher than in the liver of the treated patients. Presently, a pharmacokinetic study is being performed to verify and quantify the selective uptake in lung metastases from colon Adenocarcinoma in a BPA-mediated lung BNCT feasibility study.

Other compounds are currently being studied and tested. The aim is principally to take advantage of some specific agents that only the tumour would recognize, in other words, to make the uptake really selective for each kind of tumour.

A significant exception is represented by the study of a drug named GB-10, which does not deposit boron selectively in tumour cells, but has been demonstrated to cause a selective effect on tumour, sparing the normal tissue. This selective effect would be the result of differential damage to the angiogenic, more radiosensitive tumour blood vessels [34]. This research is being performed in Argentina, using a hamster model to verify the effects of BNCT irradiations mediated by BPA, GB-10 and BPA+GB-10 [35].

Another possibility lies in the development of the nanotechnologies. It would be possible to build empty structures like silicon nanoparticles, with diameters of some nanometers, that could be loaded with boron. Besides, on the surface of the nano-carrier, it would be possible to place some receptors for specific targets. This field could be a valid option not only for BNCT but also for the cancer therapy in general and for diagnostic purposes [36].

Liposomes are an option that have been studied since years. Some experiments demonstrated that the liposomes can transportate boron inside cells both *in vivo*

and *in vitro*. To increase the selectvity a target agent can be added to liposomes, in such a way that the liposome can recognize some specific proteins expressed only by tumoural cells [37]. In Italy a group in Florence is studying the possibility to load liposomes with carboranic cages, that carry 10 atoms of boron per molecule. Uptake studies have been recently planned (see the clonclusions of this work).

1.3 The boron concentration measurement

A BNCT treatment plan must be based on a precise knowledge of the boron concentration obtained in the tissues to be irradiated. A number of techniques were developed to measure the boron content in tissues, and can be classified as microscopic or macroscopic methods according to the spatial resolution. Presently, quantities between 100 pg/g and 100 μg/g can be measured in very small samples. Usually a macroscopic technique allows to obtain a mean value of the boron concentration in tissue samples or in blood, while the microscopical methods can measure the boron distribution at cellular or sub-cellular levels.

The most common methods used in the BNCT field to determine boron concentrations are Atomic Emission Spectroscopy (AES), Mass Spectrometry (IC-MS, DC-MS), Prompt Gamma Neutron Activation Analysis (PGNAA) and Secondary Ion Mass Spectrometry (SIMS) [39].

In Pavia we developed a new radio-analytical method, that allows to determine the boron concentration by spectroscopy of the α particles coming from the reaction ^{10}B(n,α)^{7}Li. The technique is macroscopic, because thin slices of tissue samples are irradiated in front of a Silicon detector that collects the charged particles produced by neutron interaction in the tissue. The spectrum is then analyzed and the boron content calculated. The final value obtained from the sample irradiation does not take into account the sample composition. This is not a problem in case of healthy tissue samples, where the boron is uniformly distributed. In this case, the measurement gives the value of the boron concentration that must be accounted for in the irradiation plan to preserve the normal parenchyma. In case of tumoural samples the mean value is not enough. In fact, especially in the case of disseminated metastases, a tumoural sample is always made up of different kind of tissues: active tumoural cells, necrotic zones, mucus and normal parenchyma. Therefore, the mean value obtained in the measurement of different samples taken from the same tumour can vary a lot, increasing the uncertainties and the risk of a bad evaluation of the dose delivered to the tissues. For this reason an imaging method that helps to reveal the different components of each analyzed sample should be employed. In Pavia we have been using the authoradiography technique coupled to histological analysis. Groups of three slices are cut from the tissue samples: the first one deposited on mylar for quantitative measurements by α spectrometry, the second deposited on glass for histological analysis and the third deposited on films for neutron autoradiography. The films are irradiated in the Thermal Column; the α particles and the Li ions coming from the neutron capture in boron leave tracks that are subsequently made visible by etching. The etched film is a map of the boron distribution in the tissue slice. Comparing this

map with the histological preparation, the selective uptake in the tumour can be visualized and the contribution of each different kind of tissue can be evaluated. With this the factors used to correct the quantitative results can be determined, and the boron concentration values of the tumoural and the normal cells can be separated.

This thesis reports about the BNCT research work to which the author contributed, dealing with two applications of the BNCT to two organs and using very different strategies. The problem of obtaining a correct and reliable boron concentration was and is always a background topic of all the research made in Pavia. The quantitative measure by α spectrometry, coupled with the neutron autoradiography is described in detail in Chapter 2.

1.4 The BNCT application to whole organs

As already mentioned, the application of BNCT to the treatment of diffuse tumours, when no other therapies are effective, is the ambitious objective of our research group. In this section the BNCT applications to the liver and the lung tumours are presented.

1.4.1 The BNCT of the liver with the autotransplant method

The BNCT history shows that the first and most studied BNCT application has been dedicated to brain tumours, due to the lack of effective therapies and the extremely short survival of the patients with those pathologies. Nonetheless, the selective uptake of boron is a powerful BNCT characteristic which is in principle also applicable to other organs, which are invaded by unresectable tumours. The colon adenocarcinoma, for example, is a primary tumour that is surgically easy to remove, but in 2/3 of the cases it gives origin to hepatic metastases. Their multifocal nature makes the surgery and the traditional radiotherapy not effective, and they often cause the patient death for deficiency of hepatic functionalities. Chemotherapy is a feasible option that may produce response in 20% of patients [40]. The idea of the treatment of the liver explanted from the patient and irradiated inside the thermal column of the reactor, was constructed with the TAOrMINA project, which began with the preliminary studies, the realization of the irradiation facility in the reactor, and the *in vitro* and *in vivo* measurements [17] [41]. Using the tumoural cell line DHD/K12/Trb of rat colon adenocarcinoma, liver metastases were obtained in BDIX rats, that were treated with BPA and sacrificed at different intervals of time after the drug administration. Then both tumoural and healthy samples were obtained from the rat livers, and irradiated in the thermal column for the quantitative measurement of the boron concentration. The curve of the concentration ratio between tumour and normal liver tissue as a function of the time, demonstrated that after 2 hours after the BPA infusion the ratio was larger than 4. Then the whole procedure of autotransplantation and irradiation was tested on rats. The irradiation facility was realized as a channel inside the Thermal Column of the reactor by removing

some graphite bars. Two Bismuth walls were installed between the liver position and the reactor core to attenuate the γ background that would be a source of non-selective damaging dose. Many Monte Carlo simulations were performed in order to characterize the facility and to study the thermal neutron flux and dose distribution inside the explanted liver. A Teflon phantom was built to measure the neutron flux by means of neutron activation analysis (see Chapter 4).

The protocol for the eligibility of the patients imposed a young age (less than 55 y), the presence of metastases only in the liver, a good state of the other vital organs, and liver functions not seriously impaired. According to these instructions, two patients were treated, the first in 2001 and the second in 2003. The preclinical studies, the details of the surgical phases and the post-operative follow-ups are described in detail in [45]. During the transplantation operations, two biopsies were taken, one from the center of a metastasis and the other from a zone of normal tissue, for the boron concentration measurement by means of α spectrometry coupled with neutron autoradiography. These data allowed to decide the irradiation plan, that fixed an irradiation time about 10 minutes long for both the treated livers. During the irradiation the liver was inside a Teflon bag filled with physiological solution to keep it in a good condition which was placed inside a Teflon holder covered with dry ice to keep the temperature at 4^oC. The temperature was continually monitored using thermocouples. After the irradiation the liver was transported back to the surgery room, where it was re-implanted in the patient.

The first patient was affected by multiple bi-lobar metastases, coming from a primary colon adenocarcinoma. The whole procedure lasted 21 h, with an anhepatic phase of 5 h 30'. After the early post-operative period, characterized by hepatic and renal insufficiency and other severe disturbs, the general conditions improved, with a progressive return to normal laboratory values and an increasing of the liver functions. The CT scans of the liver showed that the sites occupied by metastases before the BNCT application, had been replaced by large necrotic areas. The intra-operative ultrasound examination and the following CT scans, demonstrated also that the number of metastases invading the liver was greater than the evaluation made before the operation. This is an hint of the efficacy of the method, that allows to destroy the tumoural nodules regardless of their spatial distribution or their sizes. The subsequent course of the first patient was good and without signals of tumour re-apparition until August 2003, when an extrahepatic nodule was removed and an adjutant chemotherapy regime was started. 33 months after BNCT, a regrowth of hepatic and extrahepatic metastases required other operations and pharmacological therapies, but the clinical state worsened 44 months after and in August 2004 the patient died. The regrowth of the tumour could not be attributed to the presence of active tumoural cells remained inside the liver after BNCT, simply because too much time had passed after the irradiation. The extra-hepatic spread that could not be overcome followed the laws of tumour recurrence. Studies are currently being done on the possibility of the existence of tumoural cells that were not active at the irradiation time but could have awaken later to origin another hepatic metastatic spread [46]. The

exceptional survival time of this patient is a great success of the method, considering that he lived for 44 months enjoying a good quality of life, comparing to the median life of 4-10 months expected in similar clinical conditions without BNCT treatment. Besides, no lethal damages were observed in the normal liver. In fact, despite a post-irradiation syndrome observed in both the patients, in this case the liver function kept improving after BNCT maintaining optimum values also several months later. The second patient had a similar early peri-operative period. The same metastases evolution to necrosis was observed, and again the number of necrotic zones detected after the BNCT treatment was greater than the number of metastases that could be diagnosed by a CT scan before the operation. Unfortunately the general situation of the second patient worsened towards a month after the operation, for a thrombosis of the hepatic artery followed by a cardiac failure in the 33th post operative day. The weak general conditions of this patients when BCNT was prescribed, and the presence of a dilatative cardiomyophaty were already bad indications for the outcome of the treatment. However, also this case contributed to clarify the positive aspects of this method, most of all the ability to selectively kill the metastases, definitively demonstrated by the postmortem examination of the patient liver. Along the peryphery of the metastases replaced by necrosis microscopical evaluations showed the presence of some neoplastic cells suffering from a mitotic delay, that would have lead to a progressive death for radiation damages. In fact, one of the effects of cells irradiation is to induce apoptosis: a controlled self extinction of a severely damaged cell.

Undoubtedly all these positive aspects make BNCT with autotransplant an extremely interesting and promising technique, that has to be further studied and improved. Clearly this is a therapy aimed to cure the liver metastases, that otherwise would cause the patient death in few months. The tumour recurrences, due to the presence of tumoural cells in the blood circulation, is an event that in no way could be faced with this BNCT treatment. Other aspects of this method are still to be understood and fixed, as for example the pharmacological therapy to be followed to help the body clean and absorb the massive necrotic tissue created by the neutron irradiation. This kind of problems would obviously be fixed with an appropriate, long-term clinical trial, which will increase the statistics of the results and enable more detailed conclusions.

1.4.2 The BNCT of the lung

The good premises for a successful BNCT application to explanted liver encouraged us to continue in this research, in particular to export the technique to other facilities, to create the starting point for a new clinical program. The lack of financial support and/or willingness to go on with this kind of research is due to the risk that the patient faces in undergoing the procedure. Often this causes some reluctance in the medical world in supporting the therapy, because even if the eligible patients have a prognosis of few months, it is thought not to be worth exposing them to a risk of death during the treatment, or few days after. For this reason, while the method is being improved and further understood, other strategies are being investigated to face the problem of the disseminated tumours

invading the organs.

This is the case of our research aiming to treat lung tumours. Worldwide, the lung carcinoma is the most common cause of death in men and women, and the 14% 5-year survival rate has not being changed for decades [40]. For this reason the proposal and the validation of a new therapeutic option could be essential. In 2005, a lung project was created to start a feasibility study using the experience and the equipments collected during the extensive liver research. Taking advantage from the low density of the lung tissue when it is inside the chest, a BNCT irradiation of the whole organ can be conceived using epithermal, external neutron beams, with diameters comparable to the lung extension. Explanting the lung would not be easy and still dangerous for the patient. A uniform thermal neutrons field could be created inside the organ irradiating from the outside with epithermal neutrons that are thermalized crossing the first layers of tissues, reaching the tumour site with the optimal energy for the capture reaction. Besides, the neutron flux would not be drastically attenuated in the path across the lung due to its density about 3 times lower than the liver one. By irradiating with multiple beams the thermal neutron field inside the lung could be highly homogeneous. The importance of the field uniformity in the treatment of entire organs is explained later in Chapter 4. An intensive study was performed in order to ensure a good uniformity of the neutron flux inside the explanted liver, that could be reached only by turning the organ halfway during the irradiation time. In case of the lung the uniformity is more straightforward: simulating a chest irradiatied with two opposed beams, antero-posterior and postero-anterior, with an energy of 1 KeV, resulted in an optimum uniformity as described in Chapter 3.

The lung research began with an experimental series of measurements to verify the selective boron uptake in the lung tumour. An animal model was developed and both tumoural and healthy samples were analyzed to determine the optimal interval of time between BPA administration and neutron irradiation. The methodologies and the results of this important part of the project are described in detail in Chapter 2.

Chapter 2

BNCT of Lung Tumours: the ^{10}B concentration measurement in tissues

2.1 Introduction

Boron Neutron Capture Therapy could be a valid option to treat patients affected by lung tumours that are not surgically operable and with no positive response to chemotherapy. Lung carcinoma is the leading cause of cancer mortality worldwide. Despite the introduction over the last years of new therapeutic agents, very little progress has been made in terms of survival, and the prognosis for these patients remains poor. For these reasons any effort to find and validate a new effective therapeutic procedure to treat lung cancer is very essential but time consuming.

The great advantage of BNCT consists in its selectivity: the preferential boron accumulation in the tumour, together with a thermal neutron irradiation inside the whole organ, allows to destroy the tumoural nodules and isolated cells with no need to know the precise spatial distribution of the tumour inside the organ volume. If the boron concentration ratio between tumour and normal tissues is high and the boron concentration in normal tissue is low, a potentially therapeutic dose can be delivered to the tumour keeping the dose absorbed by the normal tissue below the tolerance level.

In Pavia we are presently studying the possibility to apply BNCT to diffuse lung tumours irradiating with external epithermal neutron beams. Therefore in 2005, we initiated the BNCT Lung Project in Pavia, funded by the Ministry of Education, University and Research (MIUR) and by the National Institute of Nuclear Physics (INFN).

The first step of a BNCT feasibility study is verifying that a selective uptake of ^{10}B can be obtained in the tumoural tissues compared to the surrounding normal parenchyma. In particular we started to study the boron pharmacokinetics in tumour and normal lung performing an *in vivo* research with an animal model. A rat model with lung metastases was developed for this purpose, and tumoural

and healthy samples were taken for the measurement of the boron concentration and for the imaging of the boron distribution in tissues. The next sections explain in detail all parts of this study: the development of the animal model, the ^{10}B imaging by neutron autoradiography and the quantitative measuring method by α spectrometry. A preliminary result of the boron concentration in tissues as a function of the interval of time after the drug infusion in the animal, is presented as well.

2.2 The animal model

To obtain pulmonary metastases and normal lung tissue samples we employed BDIX rats with induced lung metastases from colon adenocarcinoma. The choice of this type of tumour is justified by the previous experience gathered in Pavia in the study and application of BNCT for liver metastases. Over the last 20 years the BNCT research in Pavia developed a method for the treatment of diffuse and unresectable metastases invading the liver from a primary colon adenocarcinoma [17][41].

The DHD/K12/TRb colon carcinoma cell line was used to induce the metastases in the animals. The cell line was obtained from a 1,2dimethylhydrazine induced colon adenocarcinoma in syngeneic BDIX rats, selected and cloned for its capacity to induce progressive and metastatic tumours in the hosts [42]. The cells can be maintained at confluence for a long time without apparent changes in cell biology, including tumorigenicity. The cell line grows as confluent, polygonal cells in monolayer in tissue culture flasks in Ham's F10 medium supplemented with 10% fetal calf serum.

In a first phase the metastases were induced in BDIX rats (male, average weight 250 g) by intra-splenic injection of $2 \cdot 10^7$ colon-carcinoma cells under general anesthesia. After injection, splenoctomy was performed. In this way the time interval between the cell injection and the appearance of the lung metastases was too long: 20-27 days. Besides, in some animals the metastatic spread affected only the liver, while the lungs remained healthy. In order to obtain a more efficient model a surgical technique for tumour induction was tested. The tumoural cells were injected via Inferior Vena Cava, with the same dose of $2 \cdot 10^7$ cells. All the injected rats gave positive results: after 10-12 days the lungs presented a macroscopically visible metastatic spread (see Fig. 2.1).

This new method allowed us to administer BPA after 10 days from tumoural cells injection. The BPA solution 0.14 M was prepared combining BPA (^{10}B-enriched, L-isomer) with a 10% molar excess of fructose in water. The pH was adjusted to 9.5-10 with NaOH, the mixture was stirred and after some minutes the pH was readjusted to 7.4 with HCl [8]. Two methods of infusion were tested: intra-venous and intra-peritoneal. Some rats were used to test the efficacy of the administration method, and the intra-peritoneal one was chosen because it was easier to perform and it gave good results regarding the boron concentration values.

The animals were sacrificed at fixed intervals of time after BPA administration,

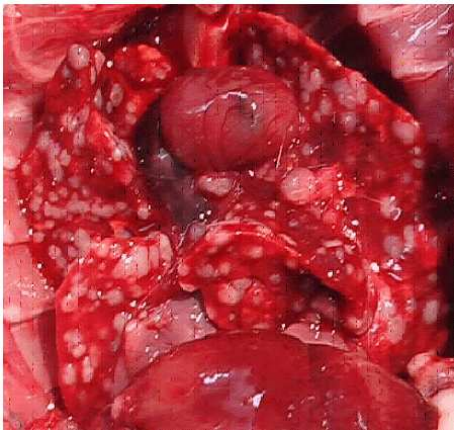

Figure 2.1: Picture of the chest of a rat, 10 days after the DHD/K12/Trb cells injection. The metastatic spread is visible all over the lungs

after which the lungs were taken out and frozen in liquid Nitrogen. To date, a total of 20 rats have been treated of which the results are used for the curve of the BPA pharmacokineticss and the spatial boron distribution in lung tissues.

The frozen organs were cut into thin slices using a Leyca cryostat. The slices of tissues were organized in couples or triplets regarding the kind of analysis. For boron imaging couples of slices were cut, each consisting in a first sample 60 μm thick directly deposited on a sensitive film for neutron autoradiography, and a second one being 10 μm thick, deposited on glass for morphological analysis by standard hematoxilin-eosin staining. For quantitative analysis, a slice of 60 μm thick was deposited on a mylar disk to be irradiated in the Thermal Column of the reactor, a second slice was prepared for morphological analysis and a third slice, again 60 μm thick, was deposited on a film for neutronigraphy.

2.3 The imaging of boron spatial distribution in lung tissues

The spatial imaging of boron in lung tissue samples was performed by neutron autoradiography. The used films were cellulose nitrate films called CN85, produced by Kodak Pathè, on which the lung slices were directly deposited. These films are relatively easy to handle and etch, because they are insensitive to the light and to the γ radiation that is possibly present at the irradiation position. The samples on films were irradiated at a position of the Thermal Column were the thermal neutron flux was $2 \cdot 10^9$ cm^{-2} s^{-1}. The high-LET radiation components coming from the (n,α) reaction induce latent tracks on the film that can be visualized with a proper etching. During the research performed in the past for the liver samples, the optimal parameters to obtain clear images have been fixed by varying the irradiation time, the solution temperature and the etching time. The fixed protocol for the lung samples consisted in irradiating the films for 30 minutes, and

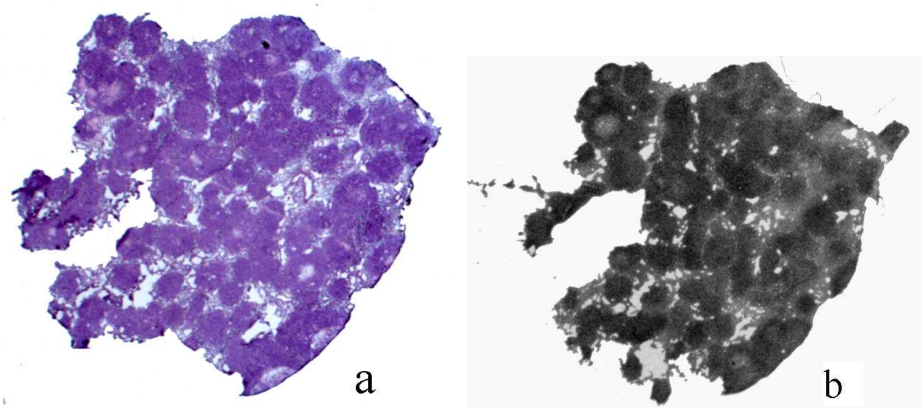

Figure 2.2: Comparison between the image of an histological section (a) and the autoradiography of the subsequent section of lung tissue (b). The sample is invaded by metastases for almost 100% of the volume.

etching them in a NaOH solution 10% in weight, at a costant temperature of 60^o C for 20 minutes.

The autoradiography method could be used for a quantitative measurement of boron concentration. To this end, the irradiation time and the etching parameters must be calculated in order to obtain separate tracks, that can be counted by a dedicated algorithm. The main aim of the autoradiography performed in Pavia for BNCT purposes is the boron imaging. The etched films visualize in a gray scale the difference between the boron concentration accumulated in the tumoural nodules with respect to the surrounding normal tissues. Each image obtained by etching the films was compared with the image of the histological section that was cut just after the one deposited on the film. To acquire the images we used a Leyca imaging system made up of a stereomicroscope connected to a digital camera and a Personal Computer. The system is equipped with software for image analysis (QWin 500). The darker zones in the neutronigraphy images correspond to the areas that absorbed a higher boron concentration, resulting in a higher track density in the film. Comparing these areas with the tumoural nodules visible in the histological glass, the selective uptake can be visualized.

In Fig. 2.2, 2.3, 2.4 some examples of autoradiographies compared to correspondent histological preparations are reported. In the couple of images in Fig. 2.3, a difference of track density can be recognized inside the metastatic nodules. As shown by histology the structure of a nodule is a circular layer of active cells that grows leaving a central necrotic area. This type of tissue is almost dead and its metabolic functions should be nearly reduced to zero. The autoradiography shows that the center of the nodules absorbed less boron than the peripheral cells, as expected. Fig. 2.5 shows that the boron distribution accurately reproduces the circular structure of the adenocarcinoma metastases, proving that the surrounding normal parenchyma absorbed a relatively low concentration of ^{10}B.

The neutron authoradiography is also a powerful tool that we used in addition to α spectroscopy to determine the boron concentration in the samples. A lots

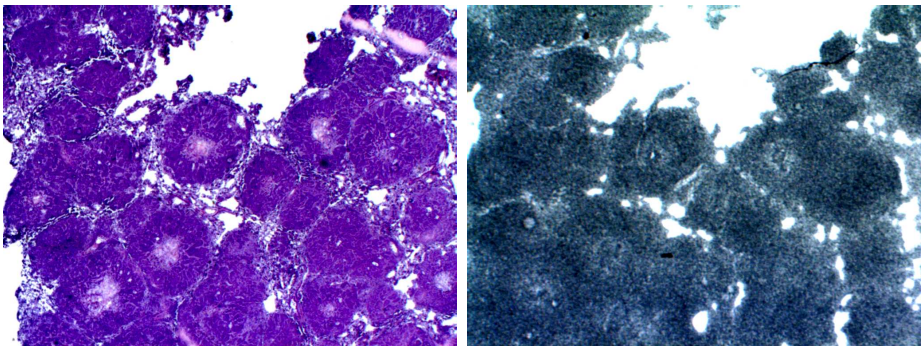

Figure 2.3: Enlargement (40 x) of some metastases in the histological preparation (left) and in the neutron autoradiography (right). The center of the metastases remains clearer in the neutronigraphy, because the center of the circular structure is necrotic, as can be seen in the histology, and absorb less boron than the peripheral and active cell layers.

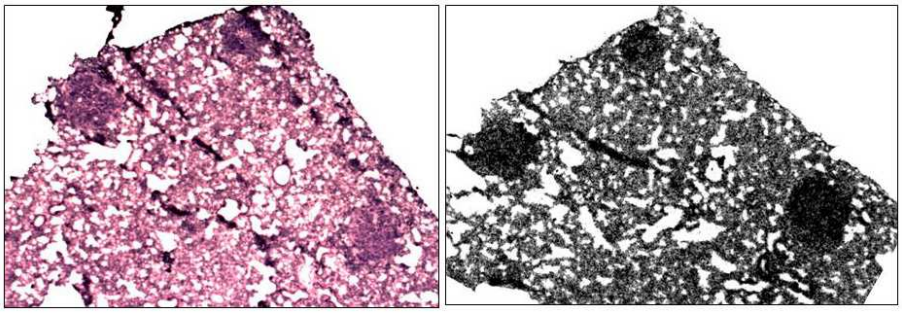

Figure 2.4: Another example of correspondence between the spatial distribution of the metastases and the zones of high boron concentration in the sample cut only 40 μm away.

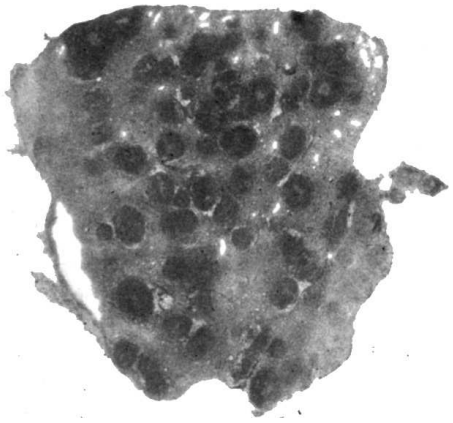

Figure 2.5: Image of the authoradiography of a lung tissue sample treated with BPA. The circular structure of the metastases is clearly visible and the difference in gray scale with the surrounding healthy parenchyma visualizes the selective uptake of ^{10}B in the tumour.

of methods have been developed for boron concentration measurement in tissues samples, such as Prompt Gamma Neutron Activation Analysis (PGNNA), Inductively Coupled Plasma Atomic Emission Spectrometry (ICP-AES), Inductively Coupled Plasma Mass Spectrometry (ICP-MS), and others. The main difficulty in interpreting the results of all these methods depends on the fact that the samples are not homogeneous. The measurements give the mean value of the boron concentration, that may vary in different zones of the same sample due to the different amount of tumour with respect to healthy tissue. For this reason an imaging method is needed to visualize the composition of the tissue that is being analyzed, in order to weight properly the contribution of the tumour and of the other kinds of tissues that may be present in the sample to the final concentration value. In the following section the use of neutron autoradiography in addition to α spectroscopy for the quantitative boron measurements in lungs is explained.

2.4 The ^{10}B concentration measurement by α spectrometry

The method applied in Pavia is a non destructive technique based on the determination of boron by the energy spectrum of the charged particles coming from the reaction ^{10}B(n,α)^{7}Li. To obtain these spectra, tissue samples treated with BPA are irradiated for 15 minutes in the Thermal Column, in a position where the thermal neutron flux is of the order of 10^9 cm^{-2} s^{-1}. The tissue slices thickness is 60 μm; even if they loose all their water content, the dry samples are still thicker comparing to the range of α particles in tissue. For this reason the obtained spectra are not Gaussian peaks and the determination of the boron concentration requires a deep analysis that involve information about the stopping power of α

Figure 2.6: A picture of the samples holder for irradiation in the Thermal Column.

particles in lung tissue. The original idea of this method described is reported in [43][44].

2.4.1 The experimental apparatus

As described before, frozen lungs were obtained after BPA administration to the rats affected by lung metastases from colon adenocarcinoma. The frozen samples were cut into slices using a Leyca cryostat, and the slices were deposited on mylar for the measurement, on films for neutron autoradiography and on glass for histology. Mylar disks with lung slices were prepared and positioned on a Teflon circular holder, equipped with 12 positions for sample irradiations and constructed to allow a series of measurements without shutting down the reactor (see Fig. 2.6). The first position of the holder is occupied by an empty mylar disk for background determination. The last position is occupied by a silicon sample with superficial implantation of ^{10}B; its spectrum gives the energy calibration of the acquisition system.

The other positions are occupied by the tissue samples. The Teflon holder is placed at the end of the Thermal Column, and it is remotely rotated to change the sample being analyzed from the laboratory. One sample at a time is irradiated facing a silicon detector, as illustrated in Fig. 2.7.

The detector sees the samples across a teflon collimator which function is to reduce the angular distribution of the incoming α particles.

When the tissue slice thickness is much smaller than the range of α particle, with a maximum energy of 1777 keV, the α spectrum would consist of two Gaussian peaks corresponding to the branches of the reaction: the first one centered at 1473 keV (94%) and the second one at 1777 keV (6%). This kind of spectrum is obtained by irradiation of the calibration sample, on which the boron atoms are implanted on the surface of the support. Fig. 2.8 shows a spectrum obtained from a 5 minutes irradiation of the calibration sample. The two α peaks are visible, and also the ^{7}Li peak with greater probability (maximum energy of 840 keV). The

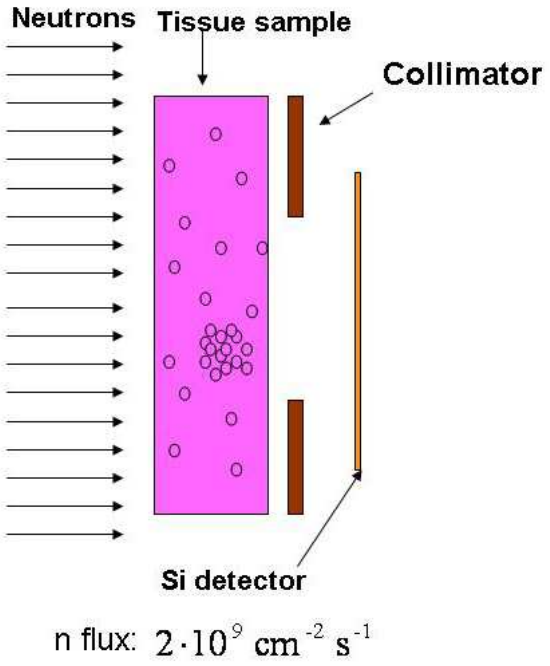

Figure 2.7: Sketch of the sample analysis by α spectrometry.

second lithium peak (1010 keV) is not visible due to the poor resolution of the detector energy. The peaks are fitted in order to determine the mean energy and provide the calibration factor.

2.4.2 The calibration sample

The sample for the energy calibration was built implanting ^{10}B atoms of 75 keV in a silicon support. The analysis of the experimental spectra showed that the α peak is a Gaussian that is slightly asymmetric, with the mean energy shifted to lower energy values. A Monte Carlo study was performed in order to understand and reproduce these spectra. In particular calculations were done to determine the boron profile distribution in the silicon sample. We used SRIM (Stopping and Range of Ions in Matter), a Monte Carlo code that transports ions through a slab of material supplied by the user [1]. The first step of this study was to simulate the process of ion implantation in the slab of silicon at the energy of 75 keV, as indicated by the producer. The outcome of the code was the depth distribution profile of the boron atoms in the silicon target, that is centered at 2420 $\dot{A}$, with a straggle of 658 $\dot{A}$, as shown in Fig. 2.9.

This distribution was used in a custom made Monte Carlo code to sample the depth of α and ^{7}Li ions emitted in the reaction ^{10}B(n,α)^{7}Li. The flight directions of these particles were also isotropically sampled and collected in an input file for a second SRIM run. Starting from this, we transported the α and ^{7}Li ions trough

[1] http://www.srim.org

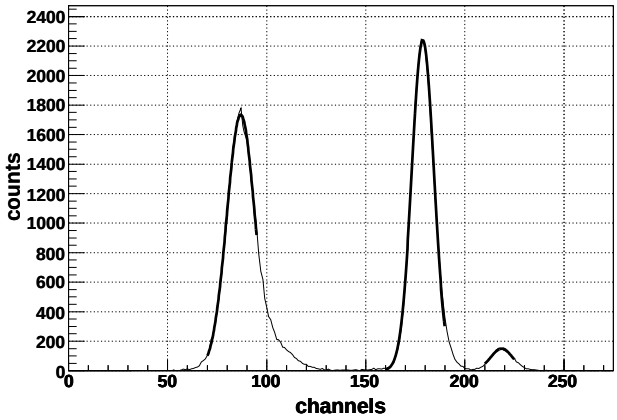

Figure 2.8: The spectrum obtained from irradiation of a calibration sample. The peaks are fitted in order to obtain a calibration factor (keV/channel) for analyzing the energy spectra of the tissue samples.

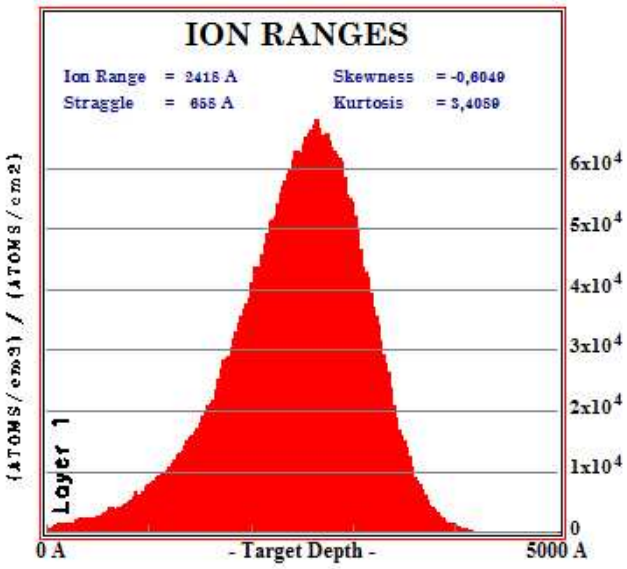

Figure 2.9: Depth distribution inside the Silicon support of the ^{10}B atoms obtained by a SRIM simulation using the implantation parameters given by the manifacturers.

Table 2.1: SRIM simulation of calibration spectrum: result after peaks fitting.

	α peak (keV)	σ (keV)	^{7}Li peak (keV)	σ (keV)
93%	1422.1	16.91	753.4	28.51
7%	1736.0	14.03	918.1	28.09

the same slab of silicon, and collected the residual energy of the particles coming out from the sample. The spectrum was then broadened with a Gaussian function to take into account the resolution of the detector (2.6% for the α peaks and 7.5% for the ^{7}Li peaks), and the results of the fit is listed in Table 2.1.

Comparing the mean energies with the theoretical values, there is a slight shift towards lower energies due to the fact that the boron atoms are not on the surface of the sample as demonstrated from the first SRIM calculation, and thus the energy is slightly absorbed and the spectra are shifted. These results were in perfect agreement with the experimental results, and the energy of the α peak used to calibrate the system was 1422 keV.

2.4.3 The tissue spectra

The spectra obtained from tissue samples are far more complex than the calibration spectrum. In fact the samples are thick compared with the range of charged particles emitted by boron and there is also a contribution from nitrogen which is present in tissue. According to ICRU and ICRP [47] the standard lung tissue components are listed in Table 2.2.

Table 2.2: Lung tissue composition provided by ICRU46.

element	H	C	N	O	Na	P	S	Cl	K
percentage by mass	10.3	10.5	3.1	74.9	0.2	0.2	0.3	0.3	0.2

The reactions that take place in the tissue samples are ^{14}N(n,p)^{14}C, with the production of 585 keV protons, and ^{1}H(n,γ)^{2}H, with the production of 2.2 MeV γ. The cross sections are σ =1.8 b for the neutron capture in nitrogen, and σ =0.322 b for the neutron capture in hydrogen. The γ coming from hydrogen cannot be detected by the system, but contributes to create a low energy background. On the contrary the range of 585 keV protons in the tissue is in the order of 10 μm, resulting in an additional peak in the spectrum obtained from the samples irradiation. Fig. 2.10 shows the spectrum obtained from the irradiation of a lung sample, taken from a control rat, which was healthy and not treated with BPA. The only peak in the histogram, located at 590 keV, is made up of the protons from the ^{14}N(n,p)^{14}C reaction, it is an absorbed spectrum due to the attenuation of the proton energy in the tissue slice.

Fig. 2.11 reports a typical spectrum from the irradiation of a tumoural lung sample taken from a rat treated with BPA infusion, before and after background subtraction. In this case the contributions of α and ^{7}Li are visible; the proton peak is superimposed to the lithium peak of lower energy.

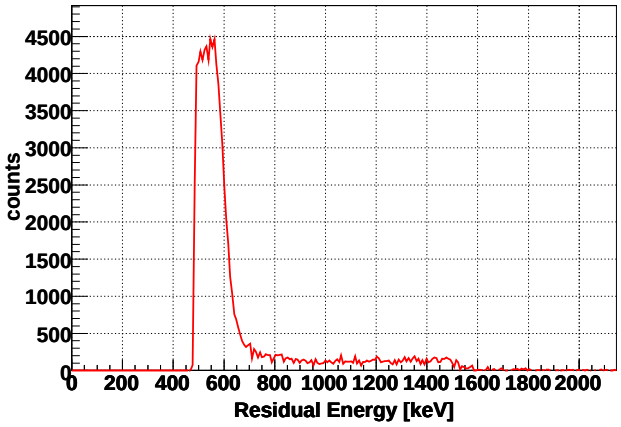

Figure 2.10: Spectrum obtained from irradiation of a control sample. The protons from the interaction of the thermal neutrons with nitrogen in the tissue are the peak at 590 keV.

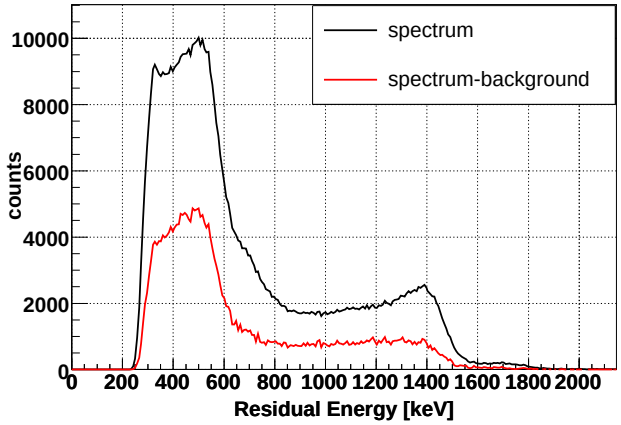

Figure 2.11: Spectrum obtained from irradiation of a tumoural sample. The blue curve one is the spectrum of the sample as it is collected by the system, and the red curve is the same spectrum after the background subtraction.

2.4.4 The spectrum analysis

The α component of the spectrum obtained from a tissue sample irradiation is a broad distribution, because the particles start at different depths in the tissue. Besides, the contributions of α and ^{7}Li are superimposed for some energy values. However, it is possible to select a zone in the histogram in which the collected events are only α. This interval could be the ΔE between 1100 keV and 1350 keV. The integral of the histogram in this interval is the number of particles that left the tissue sample with a residual energy between 1100 keV and 1350 keV. Using the relation between the α residual energy and the distance covered in lung tissue, the depths x1 and x2 corresponding to the residual energies 1100 keV and 1350 keV can be calculated. Thus the volume of the sample in which these particles originated can be calculated. The cross section of the neutron capture in boron and the geometrical efficiency of the apparatus allow to obtain the boron concentration in that sample volume. Assuming that boron is uniformly distributed in each analyzed sample, the concentration in the calculated sub-volume is equal to the concentration of the whole tissue slice.

To perform this kind of analysis requires more information about the irradiated samples. First of all, it was necessary to determine the experimental curve of the α residual energy as a function of the distance covered in lung tissue. Besides, the low thickness of the tissue slices prepared for the irradiation, makes the samples to loose their water content few minutes after the cutting. Under the assumption that the drying process happens without boron loss, the concentration value must be corrected for the original mass of the sample. The factor $\mathrm{m}_{dry}/\mathrm{m}_{fresh}$ was experimentally determined with a series of lung slices weighted just after the sampling (fresh) and some days after (dry).

Finally it was mandatory to determine the percentage of tumour in each sample we irradiated. In fact, to measure the boron concentration in tumour and in normal lung, the volume occupied by tumour with respect to the total sample volume has to be known. In the next subsections each step of the spectrum analysis is explained in detail.

2.4.5 The concentration calculus

Let us consider a tissue sample with a uniform boron distribution. With a uniform thermal neutron irradiation of the whole sample, α particles are uniformly emitted in all the directions from different depths in the tissue. In the following calculations only the particles moving parallel to the x-axis towards the negative values will be considered. This is illustrated in Fig. 2.12.

If E_0 is the initial energy of the particle, and x_1 the depth in the tissue where it was born, the residual energy E_{res} in the position in which the particle leaves the tissue and is detected is:

$$E_{res}(x_1) = E_0 - E_{diss}(0 \rightarrow x_1) = E_0 - \int_0^{x1} \frac{dE}{dx} dx \tag{2.1}$$

Similarly, if the particle comes form a depth $x_1 + \Delta x$, its residual energy will

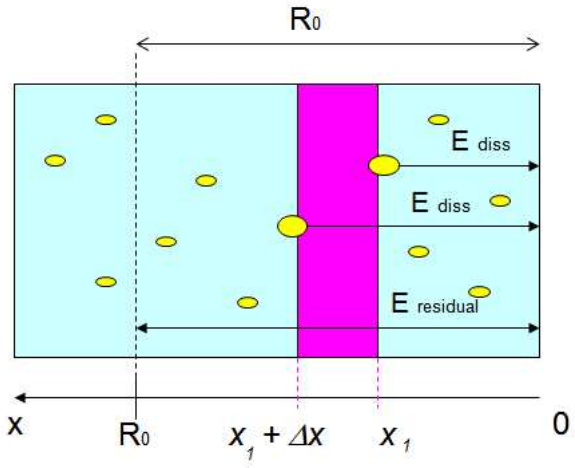

Figure 2.12: Representation of a transversal sample section, with the α particles coming from different depths and loosing different amount of energy in the tissue

be:

$$E_{res}(x_1 + \Delta x) = E_0 - E_{diss}(0 \rightarrow x_1 + \Delta x) = E_0 - \int_0^{x1+\Delta x} \frac{dE}{dx} dx \tag{2.2}$$

The interval of the residual energy of all the particles that come from the depth interval Δx is thus:

$$\Delta E_{res} = \int_{x_1}^{x_1+\Delta x} \frac{dE}{dx} dx \tag{2.3}$$

The number N of α events collected in the interval between $\mathrm{E}_{res}(\mathrm{x}_1)$ and $\mathrm{E}_{res}(\mathrm{x}_1+\Delta\mathrm{x}_1)$ depends on the number of reactions that took place in the depth interval Δx. Defining K as the number of events per unit time t and per energy interval unit:

$$K = \frac{N}{\Delta E \cdot \Delta t}, \tag{2.4}$$

the following relation holds:

$$\frac{K\Delta E}{\eta} = \frac{N}{\eta \Delta t} = \Sigma \Phi \Delta V = n\sigma\Phi S\Delta x \tag{2.5}$$

where:

- η is the detector efficiency;
- Σ is the macroscopic cross section of the boron neutron capture reaction;
- σ is the microscopic cross section of the boron neutron capture reaction;

- Φ is the neutron flux in $cm^{-2}s^{-1}$;
- n is the number of nuclei of ^{10}B per unit volume in the sample;
- S is the surface of the sample that the detector see through the collimator;
- V is the volume of the sample that the detector see through the collimator.

Starting from Eq. 2.5 and assuming no boron loss in the drying process, it can be demonstrated that:

$$(ppm)_F = \frac{K_D}{\eta\sigma\Phi S}\frac{\Delta E_D}{\Delta(\rho_D x_D)}\frac{A_W}{N_A}\frac{m_{TD}}{m_{TF}}, \tag{2.6}$$

where:

- $\frac{\Delta E_D}{\Delta(\rho_D x_D)}$ is the stopping power of α particles in dry lung tissue;
- A_W is the atomic weight;
- N_A is the Avogadro number;
- m_{TD}/m_{TF} is the dry:fresh sample mass ratio.

It is thus possible to calculate the boron concentration in the fresh tissue starting from quantities that are measured in the dry sample. Hence, the needed factors for this calculation are the curve $(\Delta E/\rho\Delta x)_D$ and the ratio m_D/m_F. These parameters depend on the type of the tissue and were experimentally measured for the lung. The first one was also computed by means of SRIM, as discussed in the following section.

2.4.6 The residual energy of α particles in lung tissue

The residual energy of α particles as a function of the distance travelled in tissue, allows to calculate the depth range Δx corresponding to the energy range ΔE selected in the spectrum. The curve that we use at present, to calculate the boron concentration, is obtained by SRIM range-energy tables.

Another way to determine the curve is to perform experimental measurements, using α particles from a radioactive source (^{241}Am). The main problem of SRIM calculations applied to biological tissues is that the slab of material programmed by the user is always uniform and has a homogeneous density. On the contrary, the biological tissue is highly non homogeneous, with zones of lower density or with holes.

The experimental set-up used to measure the α stopping power in pulmonary tissue, consists of a vacuum chamber in which an ^{241}Am source, the tissue sample and a semiconductor Si detector are placed (see Fig. 2.13).

The detector collects the residual energy of the collimated α particles, after crossing increasing thickness of pulmonary tissue. The tissue slices are deposited on mylar supports which are 23 μm thick, and reduces the energy of the particles from 5486 keV to 2210 keV. Thus the starting energy (E_0) of the α entering the

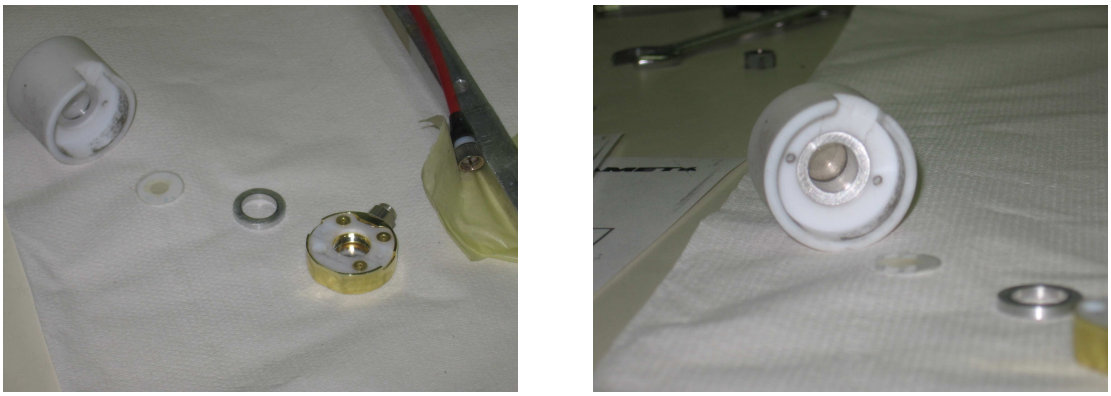

Figure 2.13: Pictures of the experimental set-up to measure the α residual energy as a function of the distance covered in the tissue. On the left, from left to right: Am source holder, tissue sample, circular support and silicon detector. On the right: enlargement of the Am source holder, where the collimator is visible.

tissue is 2210± 280 keV. This experimental set-up collects data about α energy loss in the energy range that we need for our purpose, as the maximum energy of the α from ^{10}B reaction is 1777 keV. Spectra of residual energy for slices thickness varying from 0 (only mylar) to 0.7 mg/cm^2 were built. In Fig. 2.14 we report the results of the analyzed samples compared to the SRIM curve. The difference between the experimental and calculated curve may depend on the difference between the uniform slab of material simulated in SRIM and the morphological structure of the real biological samples. This is also the reason why the experimental errors are so large: the energy error bar is the standard deviation of the Gaussian that fitted the spectra of each samples. As the thickness increased, the residual energy lowered and the straggling effect increased. This made the spectra broader with increasing sample thickness. Further measurements have been planned to increase the precision of the results. The boron concentration evaluation using the experimental data differ from the one using SRIM data by 5%. For this reason the calculations made for the pharmacokinetics curve (see Section 2.5) were made using SRIM energy-range data.

2.4.7 ^{10}B concentration measurement in tumoural samples

The procedure described up till now leads to a value for the ^{10}B concentration under the assumption that the boron is uniformly distributed in the samples that are analyzed. This is surely true when the sample is healthy. When the sample is tumoural, it is usually made up of different kinds of tissue. The tumour has a complex structure that often includes zones of active cells, necrotic areas, and mucus mixed with healthy tissue. In the case of metastases from colon adenocarcinoma the histology shows that the samples are far from being uniform, and the same holds for the boron distribution. Fig. 2.15 is an example of liver colon adenocarcinoma metastases: on the right the neutron radiography of a sample

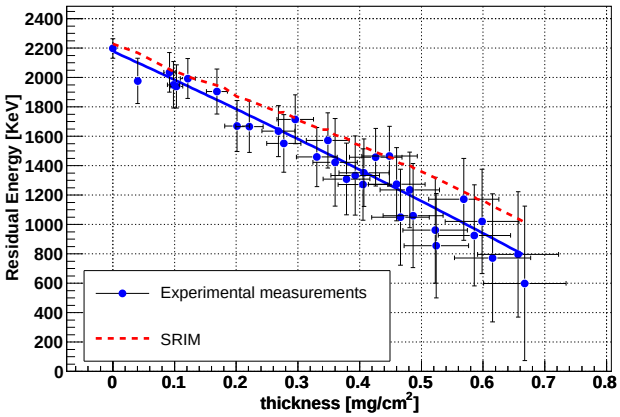

Figure 2.14: Comparison of the SRIM curve (red dashed line) and the experimental results of the residual energy as a function of the tissue thickness crossed (blue circles, the blue line is the fit result).

slice shows the boron distribution corresponding to the different structures shown in the histological preparation of a contiguous slice on the left. The darker areas, corresponding to a higher boron concentration, are active tumour cells, while the pale areas match with the necrotic zones. The healthy parenchyma absorbed an intermediate boron concentration.

The boron concentration value obtained would be a mean value strictly depending on the composition of the sample analyzed. If the same kind of measurement were performed on a series of tissue slices cut from the same lung sample, the obtained boron concentrations would vary a lot, resulting in a mean total value affected by an high error. To avoid this situation, the first step to be done is the concentration measurement of an healthy, homogeneous sample. Then the percentage of tumoural tissue inside each sample have to be determined. Finally, the concentration value in healthy tissue is used to correct the concentration value obtained in the mixed tumoural samples. If $\alpha = V_T/V_{tot}$ is the tumoural:total volume ratio for the sample inside the collimator, the concentration in the mixed sample (tumoural with zones of healthy tissue) is:

$$ppm_M = \alpha(ppm_T) + (1-\alpha)(ppm_H) \tag{2.7}$$

where ppm_T, ppm_H and ppm_M are the concentration in tumour, healthy tissue and the mean concentration in a mixed sample, respectively. The boron concentration in tumour is then evaluated from the measured mean concentration in the tumoural sample, the concentration in healthy tissue, and the ratio between tumoural area and total area of the sample:

$$ppm_T = \frac{ppm_H}{\alpha}\left(\frac{ppm_M}{ppm_H} - (1-\alpha)\right). \tag{2.8}$$

The α parameter is measured using the imaging system Leica Q500MC, consisting in a stereo-microscope with a digital Charge Coupled Device camera. With

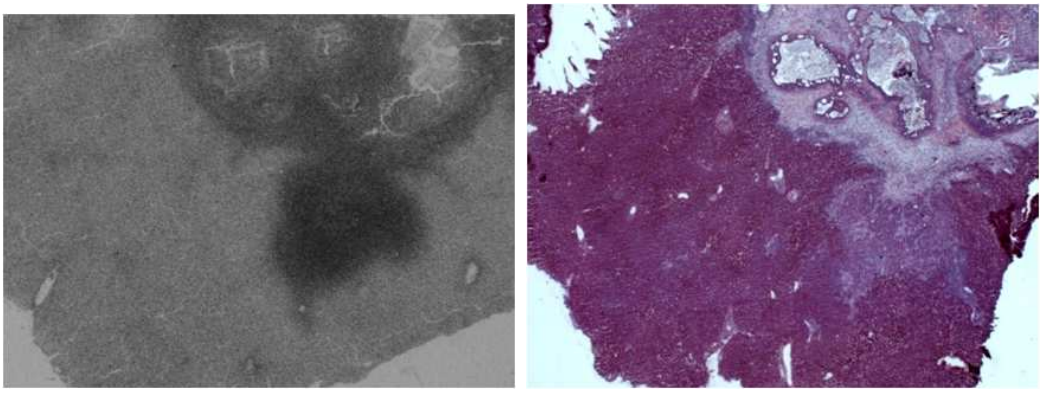

Figure 2.15: Pictures of the radiographic image of a tissue sample slice (left) and of the histological preparation of the subsequent slice (right). The different structures, as seen by the staining in the histologic glass, correspond to a different boron concentration as shown in the neutron autoradiography.

the imaging software the image can be visualized on the monitor, a region of interest can be selected and its area can be calculated.

To select the tumoural area the histological preparation that was cut after the irradiated sample is used. The neutron autoradiography of a third slice allows to compare the darker areas in the etched film and the tumoural zones. Then a collimator like the one used during the irradiation is put on the histological glass to delimit the maximum area of the sample (A_{tot}), and the tumoural areas are selected and calculated (A_T). As said before, neutron autoradiography is not only a tool for the imaging of the boron distribution in tissue, but it also helps to quantitatively determine the boron concentration in different kinds of tissues and thus to collect all the information needed to make the treatment plan.

2.4.8 SRIM and boron concentration

The boron concentration method was tested by means of a Monte Carlo calculation. The experimental spectra of the charged particles, obtained from neutron irradiation of healthy and tumoural lung samples, were reproduced using the SRIM code. Using the method described in the Appendix the starting points of emission of α, ^{7}Li and protons were extracted in the lung tissue samples. The flight directions were also sampled isotropically for each emitted particle and all these data were used as an input for SRIM. The element percentage in weight of the dry tissue sample simulated is reported in Tab.2.3. These values were obtained by analytical experimental methods based on combustion procedures.

After the transport calculations, SRIM provides the coordinates of the exit point, the final flight directions, and the residual energy of each transported particle. The flight directions were used to check if the particle would enter the detector due to the geometry of the sample-detector system, and thus if its residual energy could be collected. These data were then used to build the energy

Table 2.3: Concentration of the principal components of dry lung tissue.

Element	Mass Measured Percentage
N	9.50
C	48.00
H	7.30
O	30.34
Others	4.86

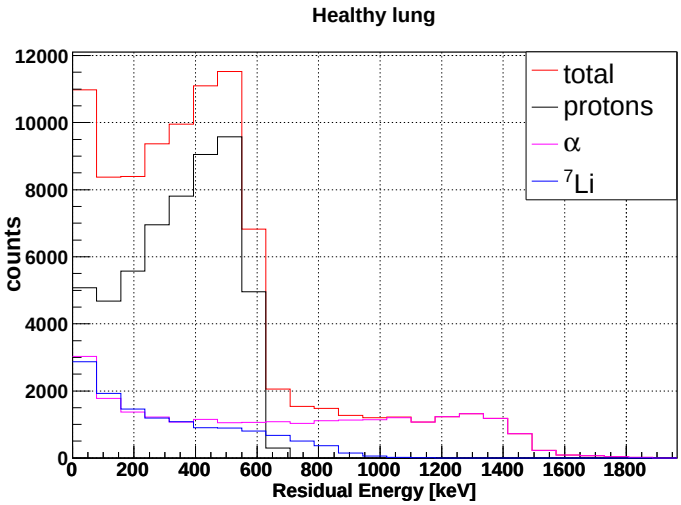

Figure 2.16: Histogram of the residual energy of the three radiation components due to thermal neutron interaction with the dry lung tissue: α component (purple),^{7}Li component (blue), protons (black), and total spectrum (red).

histograms to reproduce the experimental spectra. An example of this result is reported in Fig. 2.16 where the different components (α, ^{7}Li and protons) are indicated, together with the total spectrum.

Fig. 2.17 reports a scatterplot of the starting points of the particles (coordinate along the tissue depth) as a function of the residual energy. The three components are indicated with different colors.

In the Monte Carlo that was used to extract the particles, the boron concentration used could be changed to reproduce the experimental spectra. In Fig. 2.18 and 2.19 two examples are reported, for an healthy and a tumoural sample respectively. The boron concentration that was used equals the esperimental values, measured with the method described above. The results of the simulated and the experimental spectra for energies higher than 300 keV are in good agreement. Below this energy the experimental spectrum is cut by a threshold set in the aquisition system, to cut the electronic background.

The Monte Carlo code (as described in the Appendix) was also used to verify the precision of the boron concentration evaluation from the experimental spectra. Two effects were taken into account: the precision of the Δx corresponding to the particles with residual energy in the chosen ΔE, and the contamination of the

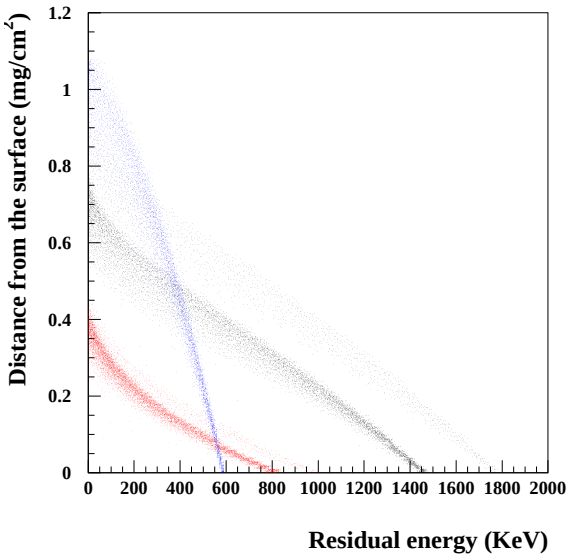

Figure 2.17: Scatter plot of the starting points along the tissue depth vs the residual energy of the three components of the spectrum: α (black), ^{7}Li (red) and protons (blue).

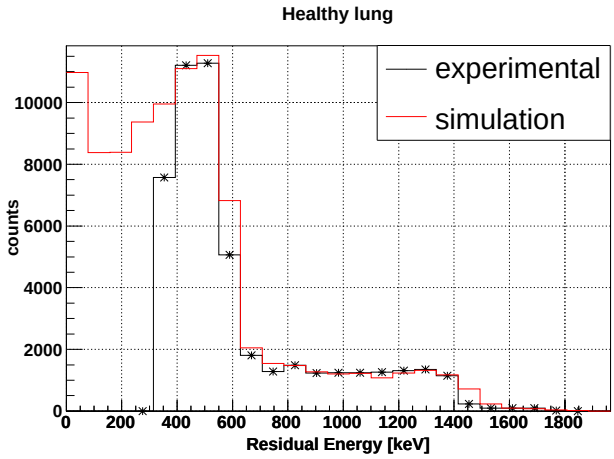

Figure 2.18: Comparison between the calculated (red) and experimental (black) spectra for a healthy sample with 4 ppm of ^{10}B.

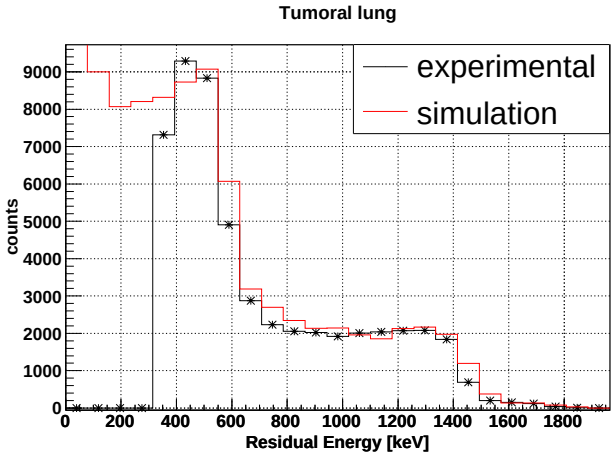

Figure 2.19: Comparison between the calculated (red) and experimental (black) spectra for a tumoural sample with 13.3 ppm of ^{10}B.

spectrum zone considered by the α of higher energy.

About the latter, Fig. 2.20 shows the separated components of the α of the two possible energies to the total spectrum (red and blue curves); the interval of energy used for the calculation of the boron concentration is indicated. The Δx corresponding to the two components that have residual energy in this ΔE are different, as clearly visible in Fig. 2.21. In the upper part the distribution of the starting points of the α with initial energy 1780 keV is shown. In the middle the same distribution is reported for the α with initial energy equal to 1470 keV. The last distribution is the total one.

The correct procedure would thus consist in subtracting the events with higher initial energy from the integral of the spectrum in the chosen interval (N), and correcting the number of reactions for the branching ratio 0.94. The percentage of the events that should be subtracted is 5.5%. At this point the number of events obtained must be lowered by a factor 0.94 (branching ratio). If these correction factors are not taken into account the result is overestimated with 0.5%.

The other effect that should be considered in the evaluation of the depth interval Δx is represented by the resolution of the detector, that broadens the energy histograms of the collected particles. This effect is propagated to the Δx calculation and could impair the precision of the evaluation. Besides, the particles that are emitted from the different points in the tissue have isotropic flight directions, and the angles allowed by the geometry of the set-up are from 0 to 45 degrees. The particles that travel with a bigger angle with respect to the perpendicular flight direction, cover a longer distance in the tissue and may be detected with residual energy between the chosen limits. The amount of particles that started from another Δx but lost more energy in the path affects the results of concentration evaluation.

To check the effect of the detector resolution and the flight direction angle we used the simulated spectrum obtained from a lung tissue slice with 13.3 ppm of

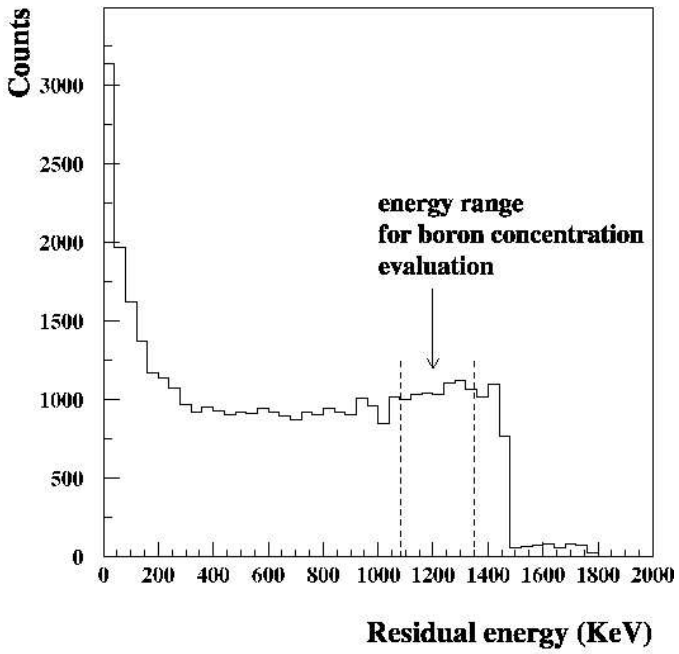

Figure 2.20: Histograms of the simulated α spectra. The black one is the total spectrum, the red is the spectrum of the α with higher energy (6%) and the blue one is the spectrum of the α with lower energy (94%). The energy limits chosen for the evaluation of the number of boron reactions are shown.

^{10}B. The total histogram is the sum of the contributions of protons, α and ^{7}Li, with and without the detector resolution broadening. If we focus on the energy interval from 1100 keV to 1350 keV, the corresponding Δx is calculated using the SRIM energy-range tables in the interval between 0.064 and 0.229 mg/cm^2. The simulated spectra allow to calculate the number of particles with starting energy 1470 keV, that started from this depth interval. This calculation, corrected by the factor 0.94, gives nearly the correct boron concentration (13.60 ppm), as we expected whether the Monte Carlo code was correctly implemented. The same procedure that we would use on an experimental spectrum was then applied both to the total spectrum without the detector resolution effect and to the broadened one. The result of the boron concentration evaluation on the first spectrum, integrated between 1100 keV and 1350 keV, is 14.18 ppm. This overestimation (of 6.6 %) depends on the angle distribution of the α flight directions, that makes more events entering in the chosen energy range. The error associated with the caluclation using the broadened spectrum increases to 7.7%. This means that the resolution of the silicon detector that was used, does not affect much the results. The most important source of uncertainty is the number of events that started from a different Δx but have a residual energy in the chosen interval.

Fig. 2.22 shows in black the broadened spectrum used for the concentration evaluation and in red the number of α particles coming from the calculated Δx that should be counted instead. The percentage of the red spectrum that lies outside

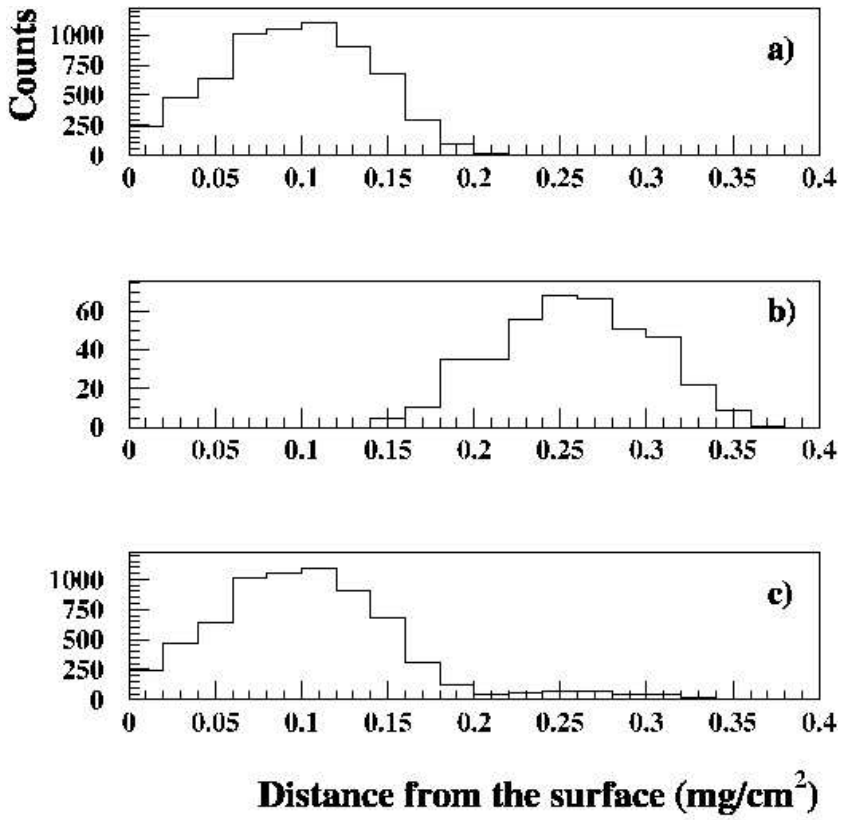

Figure 2.21: Histograms of the distance from the sample surface where the α particles with residual energy between 1082.5 keV and 1384 keV started. (a) α of 1470 keV, (b) α of 1780 keV, (c) total.

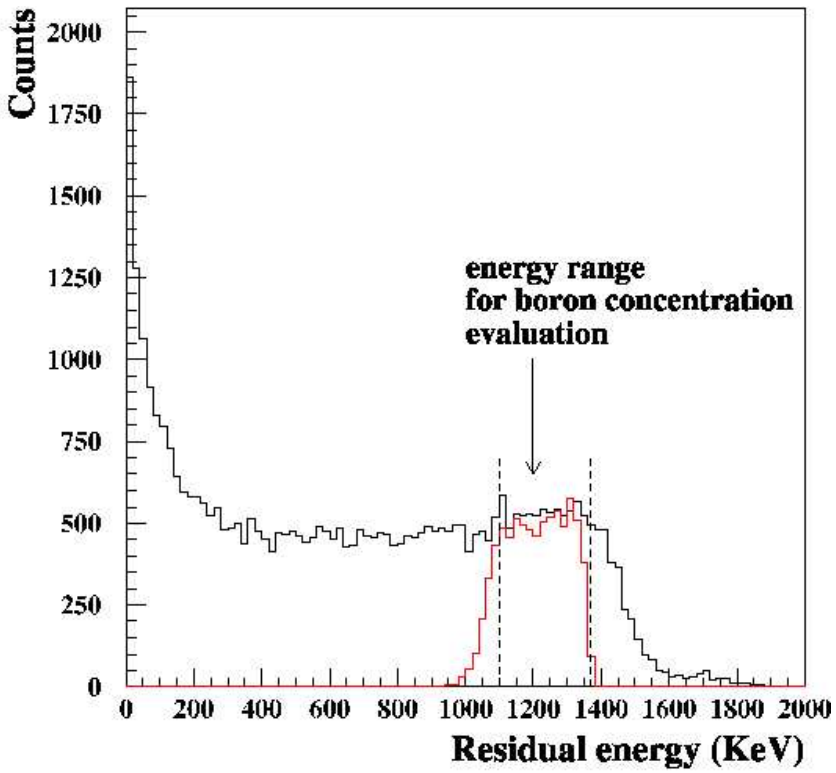

Figure 2.22: Simulated spectrum broadened with the detector resolution (black) and α events coming from the calculated Δx (red). These events should be counted to calculate the boron concentration, while in the experimental situation the integral of the total spectrum is done between the indicated limits (vertical dashed lines). The error associated with this procedure is determined by the portion of the red spectrum that lies outside the marked limits (7%).

the energy limits represents particles that are lost in the calculation. However, there is a small compensation due to particles that should not be counted but that fall between the limits. The error associated with the whole procedure that propagates to the final concentration result is 7%.

2.5 Results of the pharmacokinetics study in lung tissues

Following the described techniques a lot of samples were irradiated and analyzed. Before studying the boron concentration in tumour and in normal pulmonary tissue obtained with the BPA administration, we made some control measurements to determine the background boron concentration in the lung. The results were compatible to the control measurements made in rat liver being less than 0.5 ppm. To study the BPA pharmacokinetics, 40 rats have been treated to date, both healthy and tumoural. The animals were sacrificed at different intervals

of time after the drug infusion. In particular the measures were performed at t=1,2,4,6,8 hours to obtain values for $C_T(t)$ and $C_H(t)$ (^{10}B concentration in tumoural and healthy tissue) and to calculate $T(t) = C_T(t)/C_H(t)$. The goal is to find the optimal interval of time between the BPA administration and thermal neutron irradiation, as the ratio of concentration between tumour and normal lung should be maximum. Of all the treated rats, 16 have been analyzed for the boron concentration measurement. In Fig. 2.23 the first results of the study of BPA pharmacokinetics are reported. An improvement of the statistics is scheduled: more rats will be treated and analyzed for each of the above described time intervals.

Fig. 2.24 shows the behaviour of the ratio T(t): at 4 hours after BPA infusion the ratio between the concentrations in tumour and normal lung is 4.5. This value is of the same order as the one obtained in the liver metastases studies. In principle this ratio is high enough to make the treatment feasible.

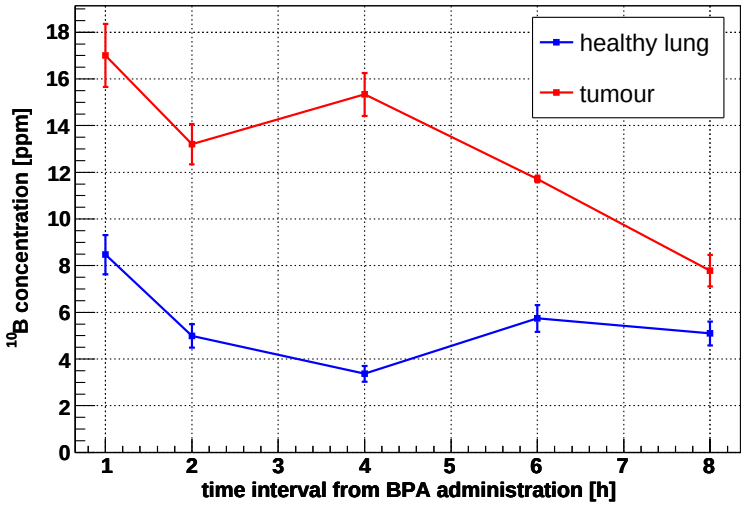

Figure 2.23: Behaviour of the boron concentration in normal lung and in tumour as a function of the time after BPA infusion.

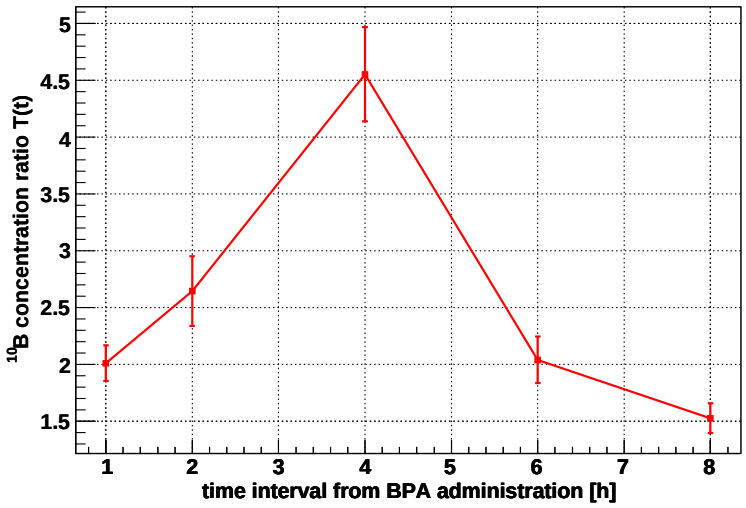

Figure 2.24: ^{10}B concentration ratio between healthy and tumoural tissue as a function of the time after BPA infusion.

Chapter 3

BNCT of Lung Tumours: simulations of the dose distribution in the thorax

3.1 Introduction

The selective boron uptake in the lung metastases comparing to normal tissue makes BNCT a potentially advantageous technique, especially if the whole organ has to be treated. The Pavia lung project wants to explore the possibility to irradiate the entire lung using external collimated epithermal neutron beams and using BPA as boron carrier. With respect to the past experience, it is the first time that the feasibility of an external neutron irradiation beam is studied in Pavia. The advantages of external irradiation are that the patient would not undergo a complicate and invasive procedure and that the neutrons, thermalized in the first layers of tissues, would not be attenuated a lot due to the low density of the lung (about 0.3 g/cm^3). In this case, using two opposite beams, it would be possible to obtain a flat thermal neutron flux distribution inside the whole organ. The aim of this simulation study was to verify if a proper dose distribution can be obtained in the lung and check if the surrounding sensitive organs can be spared from a severe damaging dose. The first study was conducted simulating the irradiation with two ideal neutron beams, mono-energetic and perfectly collimated [25]. In this chapter the results of this first study are presented.

3.2 Materials and methods

The simulations were done using MCNP, version 4C [23], and the anthropomorphic model named ADAM [48], kindly provided by ENEA Bologna [49][50]. The phantom ADAM is an improvement of the MIRD (Medical Internal Radiation Dose Committee) phantom [51], that was the basis for various anthropomorphic models representing the two genders of various age. MIRD phantoms had 35 separate organs and tissues and 3 materials: lung, skeletal tissue and soft tissue. This kind of

Table 3.1: Lung composition in mass percentages from ICRU 46 and applied in the Adam phantom.

Lung Elements	ADAM	ICRU 46
H	10	10.3
C	10	10.5
N	2.8	3.1
O	76	74.9
^{23}Na	0.19	0.2
Mg	0.0074	-
^{31}P	0.081	0.2
^{32}S	0.23	0.3
Cl	0.27	0.3
K	0.2	0.2
Ca	0.007	-
Fe	0.037	-
Pb	0.000041	-

phantom have been used to calculate organ and tissue equivalent doses. ADAM, and its female correspondent EVE, were introduced by Kramer et al. [48], and were used at GSF (Nuernberg, Germany) to calculate kerma-approximated conversion coefficients for external exposure to photons. Their organs are described by mathematical expressions such as planes, circular and elliptical cylinders, spheres etc. Organ, masses, body weights and body heights correspond to the anatomical data for adults males and females recommended in the first ICRP Reference Man Report, ICRP publication 23 [52]. The phantom that was used for this study is an input for MCNP, and is described using 4 materials: lung, bone, skin, and soft tissue. These material compositions were compared to ICRU 46 recommendations, and a comparison between the lung elements percentages in ADAM and in ICRU 46 is reported in Tab. 3.1.

Using the MCNP capability of the repeated structures, Adam's thorax and its organs were voxelized. In this a mesh of 1 cm^3 voxels was obtained, in which the tallies[1] were defined (see Fig. 3.1). The tallies obtained in each voxel were corrected for the real volume of the voxel, calculated using the statistical method, as explained in the MCNP manual.

The simulated irradiation source consists of two neutron beams which are mono-energetic and collimated, with dimensions of 11 x 26 cm^2, chosen to cover the whole lung volume. The lung is irradiated from two opposite directions: antero-posterior and postero-anterior, as shown in Fig. 3.2. In MCNP this source was obtained building two planar source from which the neutrons were sampled with uniform probability. In the real treatment only one beam would be used, and the patient would be turned halfway through the irradiation time.

For each of the calculations that were performed, three transversal sections

[1] a *tally* is the quantity that is scored by MCNP, defined by the user (i.e. the neutron flux in a cell or the current across a surface).

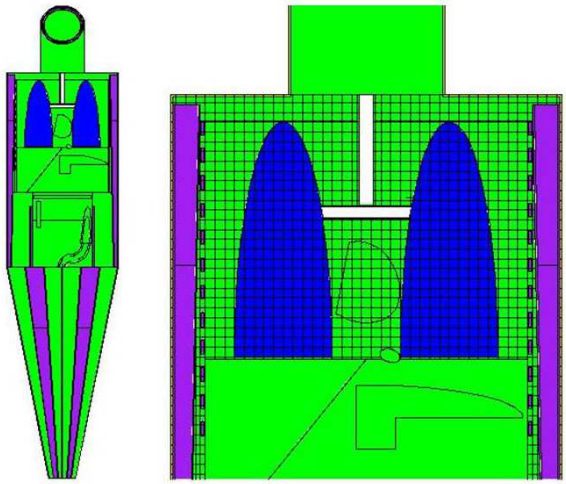

Figure 3.1: The ADAM model with an enlargement of the thorax in which the 1 cm^3 voxels can be seen.

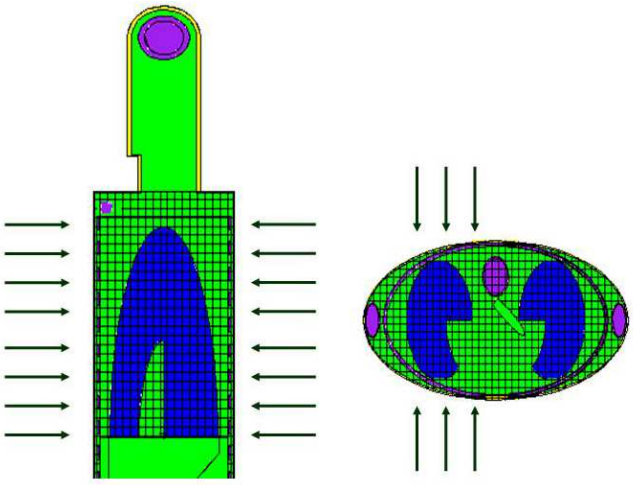

Figure 3.2: Lateral view of the collimated neutron sources that irradiated the lung.

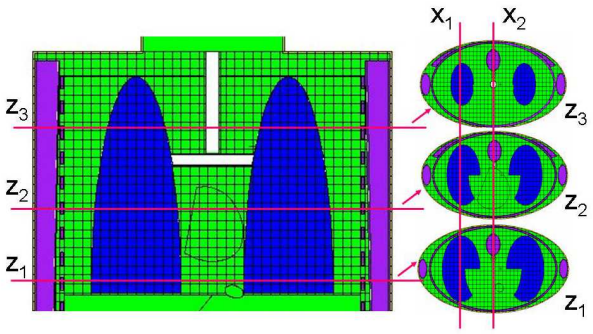

Figure 3.3: Positions of the profiles chosen to analyze the dose and flux distributions in ADAM's thorax.

(z1, z2 and z3) at different heights from the base of the lungs were considered. two antero-posterior axis (x1, x2) were fixed for each section, where the profiles of dose and flux distribution were built. x1 is an in-beam profile, located at the center of the right lung and x2 is an out-of-beam profile, crossing the spinal cord in the center of the thorax. Fig. 3.3 shows these axis and the transversal sections chosen to analyze the dose distribution.

The thermal neutron flux distribution was obtained using the F4 tally, with an upper thermal energy threshold set at 0.2 eV.

The dose distribution in the tissues was studied separating the different components of the total absorbed dose. Two tally types were used to calculate the dose: F6 tally and F4 tally, in mode:n,p runs. F6 is a cell heating tally, its units are MeV/g, and it is equivalent to an F4 tally (cell flux tally) multiplied for an energy dependent multiplier (FM card) whenever there is a Charged Particles Equilibrium (CPE). The FM card is used to calculate any quantity of the form:

$$C \int \Phi(E) R_m(E) dE, \tag{3.1}$$

where $\Phi(E)$ is the energy-dependent fluence (particles/cm^2),and R_m(E) is an operator of additive and/or multiplicative response functions from the MCNP cross sections libraries or specially designed quantities. The constant C is a normalization quantity (see the MCNP manual, version 4c [23]). In the dose calculations with the F4 tally the energy deposition is due to the reactions: ^{1}H(n,γ)^{2}H, ^{14}N(n,p)^{14}C, ^{1}H(n,n)^{1}H', ^{10}B(n,α)^{7}Li. These processes correspond to the ENDF/B reaction numbers: 102, 103, 2 -4, 107. The normalization constant was the quantity $(\rho_a/\rho_g) \cdot 10^{-24}$, that produced tallies results in number of reactions/g units; the dose was calculated multiplying with the Q-value of the reaction. The sum of the dose contribution calculated using F4 tally with FM card was identical to the F6 tally result. This result gives an indication of the energy deposition of the secondary particles and that there is CPE.

The γ dose was obtained with an F6 tally for photons, in a mode n+p run. In this case the γ energy was deposited by MCNP in the point where the photons were created, being an overestimation of the γ dose especially in the points where

there is not CPE.

3.3 The energy of the source

The first simulations were performed to choose such a source energy that creates a uniform thermal neutron flux distribution inside the lung. We started with thermal neutrons and then increased the energy until 1 keV. In Fig. 3.4 the thermal neutron flux inside ADAM's thorax is shown, comparing the results obtained with a thermal source (E_n = 0.0253 eV) and with a 1 keV neutron source. The first figure (up) refers to the in-beam profile, named x1, while the second (down) refers to x2, the out-of-beam axis. Both the profiles are taken in the middle of the lung, that is the plane named z2 in Fig. 3.3. In all the plots reported in this section, the x axis represents one of the two defined profiles across ADAM's thorax, the distance is expressed in cm. The center of the x axis is the center of the lung: in these profiles built in the z2 plane along x1 axis, the lung edges are in x=-7 and in x=7.

The thermal neutron flux profile along x1 in the middle of the thorax demonstrates that a thermal external beam would not be suitable for lung irradiation. The flux value in the skin (x=-9) is about two times higher than its value in the lung surface (x=-7) and 4 times higher than in the middle of the lung (x=0). This would mean a higher dose delivered to the skin and to the first layers of tissues comparing to the therapeutic dose that would be delivered to the lung tumour. On the contrary, using a 1 keV neutron beam, the neutrons are thermalized before reaching the lung, and the thermal neutron flux values would be three times higher along the lung axis than in the surrounding structures (skin, bones, soft tissues). Besides, using two opposite neutron beams it is possible to obtain a very homogeneous thermal neutron flux distribution, due to the low density of the lung when it is inside the thorax (0.3 g/cm^3). This condition is important in BNCT to better exploit the selective boron uptake in the tumour. In fact, the irradiation time is chosen to spare the normal tissue and to deliver a potentially therapeutic dose to the tumour; if there are peaks of the thermal neutron flux in healthy zones, the irradiation should be shorter, thus delivering a lower dose to the tumour. The results obtained using a 0.5 keV neutron source are very similar to the ones obtained with the epithermal source of 1 keV, and are therefore not shown here.

3.4 The dose distribution in the thorax

Setting the energy of the neutron source to 1 keV, the dose distribution profile were calculated along the chosen axis in the three transversal planes. Figure 3.5 shows the dose components in the central section z2 for the in-beam axis x1 and the out-of beam axis x2 respectively, the units are Gy per source neutron. The charged particles total dose is defined as the sum of the contributions coming from the reactions with boron, with nitrogen and from the elastic scattering on

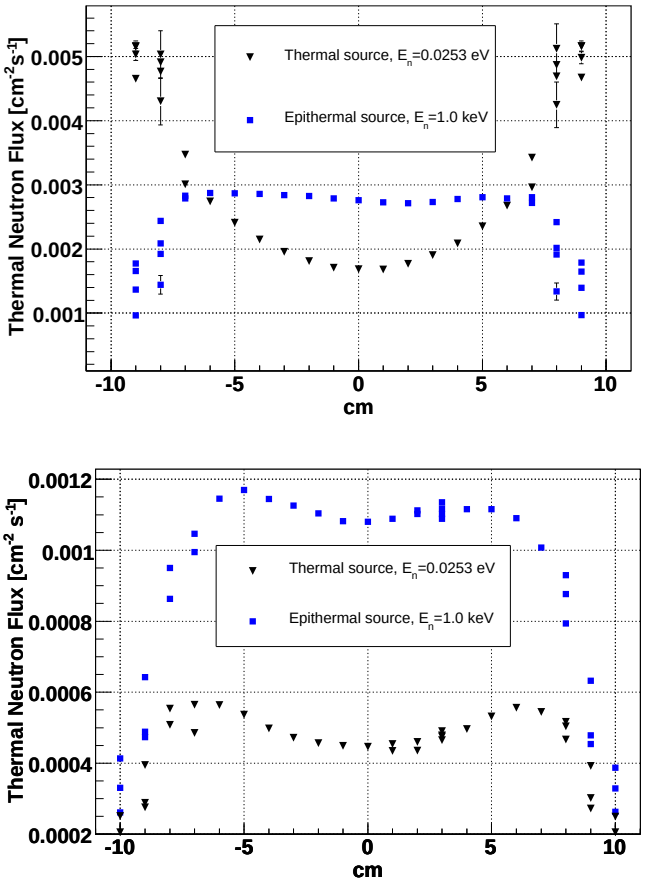

Figure 3.4: Thermal neutron flux ($E_n < 0.2$ eV) profile along x1 (up) and x2 (down) in the z2 plane at half the height of the thorax (in-beam profile). The center of x axis is placed in the center of the lung.

hydrogen.

These calculations were made for 1 ppm of ^{10}B in all the tissues, while the nitrogen and hydrogen percentage for each ADAM material is reported in Tab. 3.2.

Table 3.2: Hydrogen and Nitrogen mass percentages in ADAM materials

Tissue	Nitrogen %	Hidrogen %
Soft tissue: heart, trachea, esophagus...	2.3	10
Lung	2.8	10
Skeletal tissue: rib cage, spine	3.9	7
Skin	4.26	10.2

The same dose profiles are reported for x1 and x2 axis in the z1 and z3 planes (see Fig. 3.3), at the base of the lung and in the upper part of which the profile are shown in Fig. 3.6 and 3.7 respectively.

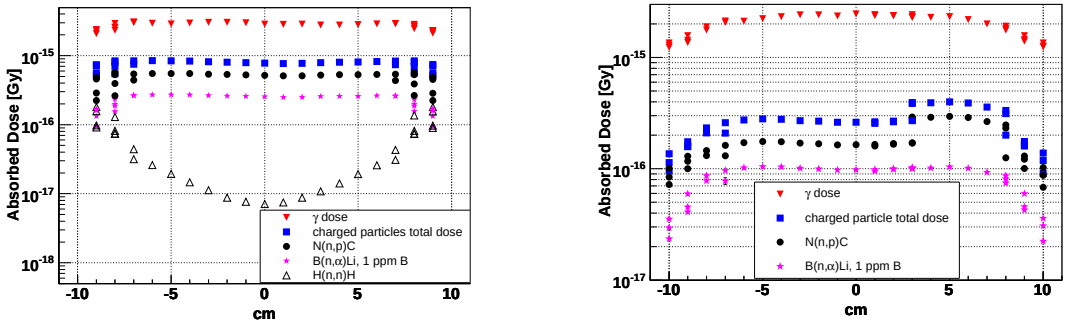

Figure 3.5: Dose components profiles along x1 (left) and x2 (right) in the central section z2. The H(n,n)H is absent in the right figure as the contribution is negligible. Note: the scale of the two plots is different.

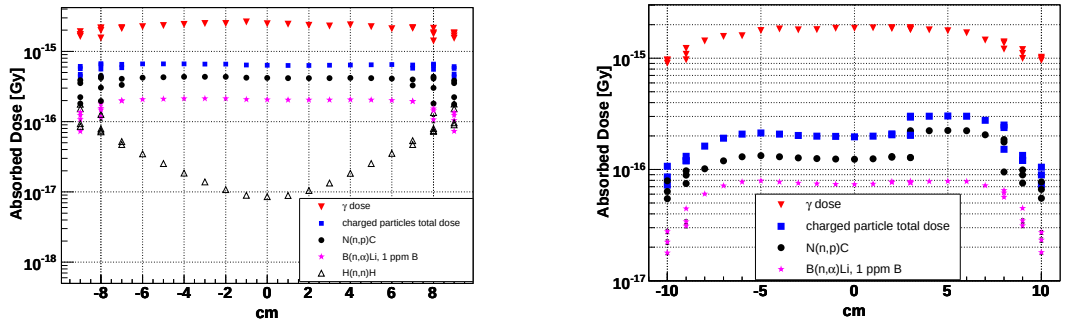

Figure 3.6: Dose components profiles along x1 (left) and x2 (right) in the base section z1.

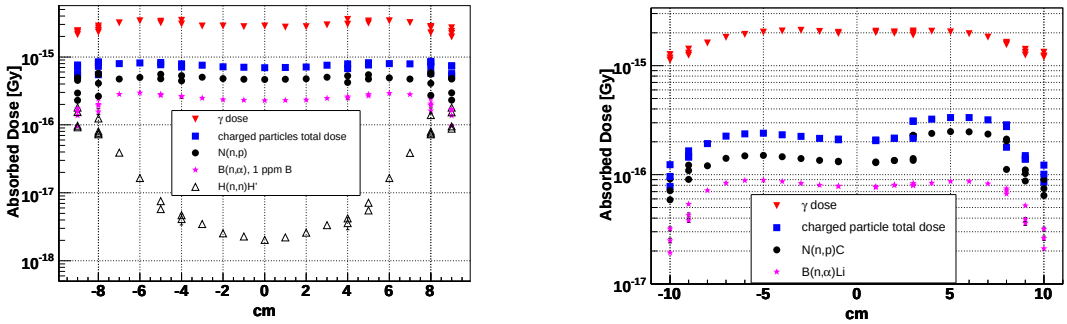

Figure 3.7: Dose components profiles along x1 (left) and x2 (right) in the upper section z3.

The contribution due to elastic scattering with hydrogen (void triangles) is absent in the profiles along x2, because the epithermal flux component in the out-of-beam position is negligible. The step increase of the charged particles contribution to the absorbed dose (blue squares) at x=3 cm in the eight plots is at the location of the spine, and it is determined by the higher nitrogen percentage in the skeletal tissue material (see Tab. 3.2). The γ contribution from the neu-

Table 3.3: ^{10}B concentration in ppm used to calculate the total dose in the thorax of ADAM.

Tissue	^{10}B concentration (ppm)
Soft tissue: heart, trachea, esophagus...	5
Lung	5
Skeletal tissue: rib cage, spine	5
Skin	7.5

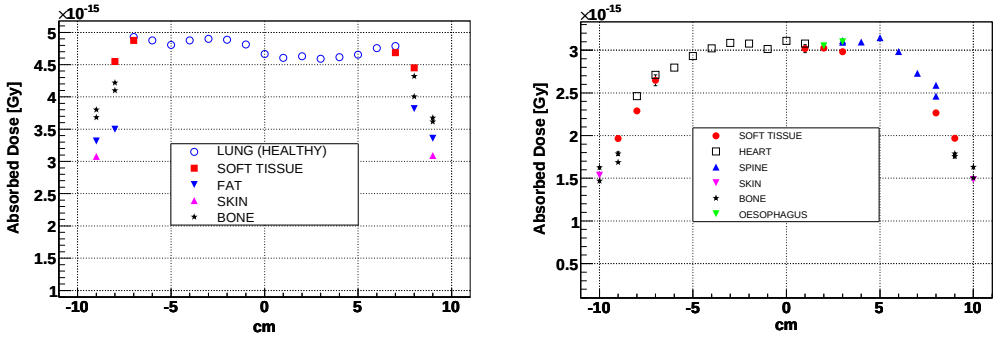

Figure 3.8: Total dose profiles along x1 (left) and x2 (right) in the central section z2. Note: the scales in the two plots are different.

tron capture in hydrogen (red filled triangles in the plots) is of the same order along the axis crossing the lung and along the axis crossing the spine, and it is considerably higher than the charged particles total contribution (blue squares). The cross section of the reaction ^{1}H(n,γ)^{2}H is 0.322 b, which is low compared to the cross section of ^{14}N(n,p)^{14}C (1.8 b), but the mass percentage of hydrogen in tissues is already higher (see Tab. 3.2)[2]. On the other hand the charged particles contribution to the absorbed dose is two times higher along the in-beam axis than along the out-of-beam one.

Starting from these data we calculated the total dose distribution (γ and charged particles contributions) in the different organs, using the boron concentration in the different tissues reported in Tab. 3.3. The concentration in healthy lung came from the experimental results in the animal study, described in the Chapter 2 and published in [24]. The ^{10}B concentration values in the other tissues were taken from Coderre et al. [53].

In Fig. 3.8, the profile of the total absorbed dose is reported, for the central section z2, along the two axis x1 and x2 (up and down respectively).

If a boron concentration ratio between healthy tissues and lung tumour of 5 is assumed to be obtained with the BPA administration, the ratio between the physical absorbed dose in the tumor and in the lung is about 2, as shown in Fig. 3.9.

The profiles of physical total dose (γ and charged particles contribution) for the x1 axis in the section z1 and z3 are also reported (Fig. 3.10 and 3.11 respectively).

The ratio of 2 is mainly due to the relative high γ contribution in the total

[2]The atomic percentage difference is even larger.

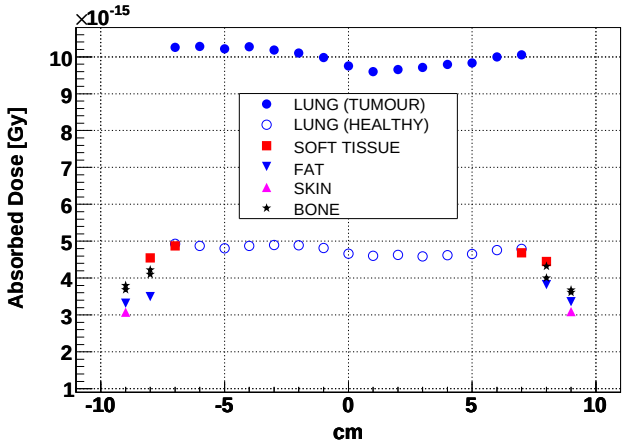

Figure 3.9: Total dose profiles along x1 in the central section z2, for the normal lung with 5 ppm of ^{10}B (open circles), and for the tumour with 25 ppm (blue circles). The ratio of the dose delivered to the metastases and to the lung is about 2.

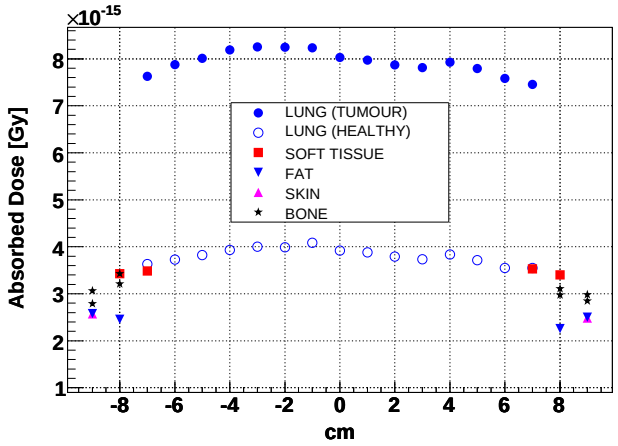

Figure 3.10: Total dose profiles along x1 in the base section z1, for the normal lung with 5 ppm of ^{10}B (open circles), and for the tumour with 25 ppm (blue circles).

dose, as shown in the precedent plots. If only the charged particles contribution to the total absorbed dose is taken into account, the ratio is higher. Fig. 3.12 reports the dose profiles along x1 and x2 in the central section of the lung, subtracted from γ contribution. Fig. 3.13 shows that the ratio of the absorbed dose is about 3.5 when only the charged particles contribution is taken into account.

The tumour:normal tissue dose ratio increases when wheighting each component of the dose for biological factors. These factors are the RBE (Relative Biologic Efficacy) of the charged particles with respect to γ, and the CBE factors (Compound Biological Effectiveness factor) that depend on BPA biodistribution in tissues [54]. The Compound factors used in this calculations were taken from the table III in [53], for the skin and the tumour; and from [26] for the normal

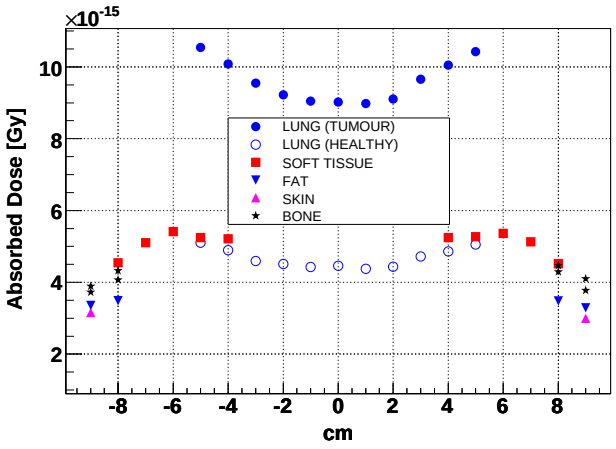

Figure 3.11: Total dose profiles along x1 in the upper section z3, for the normal lung with 5 ppm of ^{10}B (open circles), and for the tumour with 25 ppm (blue circles).

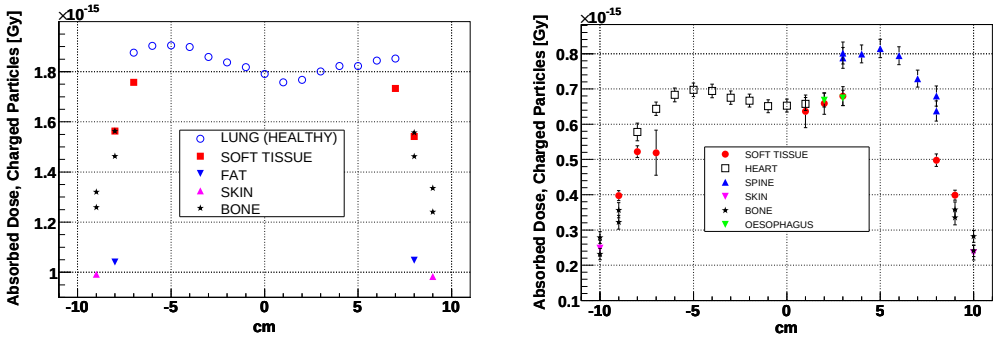

Figure 3.12: Dose profiles from charged particles along x1 (left) and x2 (right) in the central section z2.

tissue. Tab. 3.4 reports a summary of the CBE factors that is used to weight the boron dose components. The RBE value for the high-LET components of the neutron dose (^{14}N(n,p)^{14}C and H(n,n)H') was assumed to be 2.2 as measured by Kiger et al in [26]. The CBE factor used for the tumour was assumed to be equal to the one measured by Coderre for the 9L gliosarcoma cell line [55]. This assumption could be justified at least by the radiobiological study conducted on the DHD/K12/TRb cell line in Pavia, used to induce liver and pulmonary metastases in our present rat model. The dose-effect curve relative to the adenocarcinoma cells survival and the curve reported in the cited paper [55] had the same behaviour. This result confirmed that the efficiency of BNCT irradiation in killing the cells of the two lines, using BPA as boron carrier was identical. This justifies the employ of the CBE factor calculated for brain tumours.

Using these factors, a plot of the biological total weighted dose (γ and charged particles weighted contribution) in the tumour and in the normal lung was realized (Fig. 3.14). The ratio of the dose delivered to the tumour and to normal lung tissue is 5. The overall outcome can be compared to the doses delivered to the

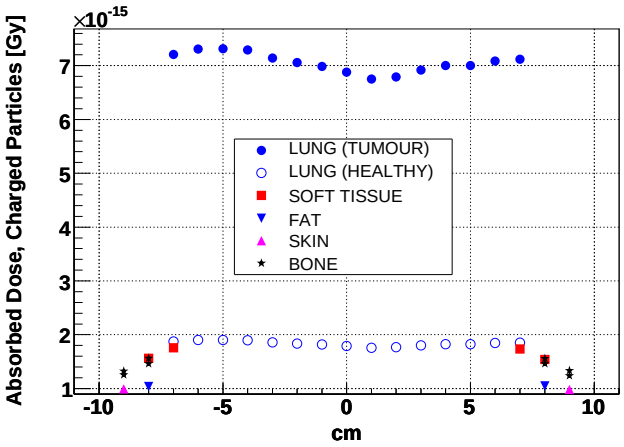

Figure 3.13: Total dose profiles along x1 in the central section z2, for the normal lung with 5 ppm of ^{10}B (open circles), and for the tumour with 25 ppm (blue circles). The ratio of the dose delivered to the metastases and to the healthy lung is about 2.

Table 3.4: ^{10}B concentration ratio with respect to the concentration measured in normal lung (ppm), and CBE factor used to calculate the total biological dose in the tissues. The value of the boron concentration ratio for the tumour was taken from the past experience in the liver BNCT, and from the suggested results of the animal experimental phase in the lung research.

Tissue	^{10}B concentration ratio	CBE factor
Normal tissue	measured directly	1.2
Skin	1.5· Value in normal tissue	2.5
Tumour	5· Value in normal tissue	3.8

livers of the patients treated in Pavia [45].

In Komg et al. [56] a dose escalation study was carried out with γ fractionated radiotherapy (2 Gy/fraction), on 103 patients with non-small-cell lung cancer and a long time follow up is described. The toxic effects that were assumed as end points were pneumonia (early effect) and fibrosis (late effect). The results reported indicate that a dose larger than a Mean Lung Dose (MLD) of 20 Gy can be delivered to patients with this pathology, if the treated lung volume is limited. For whole-lung irradiations, the lung tolerance dose decreases with increasing dose after 8.2 Gy in a single fraction, or after 26.5 Gy in 20 fractions. The dose delivered to normal lung with an irradiation of 15 minutes with a neutron flux of $1.75 \cdot 10^9$ would be 4 Gy-Eq in the central section of the lung, which is highly compatible with the prescriptions of the study of Kong et al. In [21] a dosimetric study on BNCT lung irradiation by simulating two epithermal neutron beams is described. The mean dose delivered to healthy tissue is 3.5-4.2 Gy-Eq. The biologically weighted dose on the organs and tissues surrounding the lung was not calculated due to the lack of CBE factors in the literature. We used the same CBE of the normal lung in the plot of biological weighted dose, but we intend

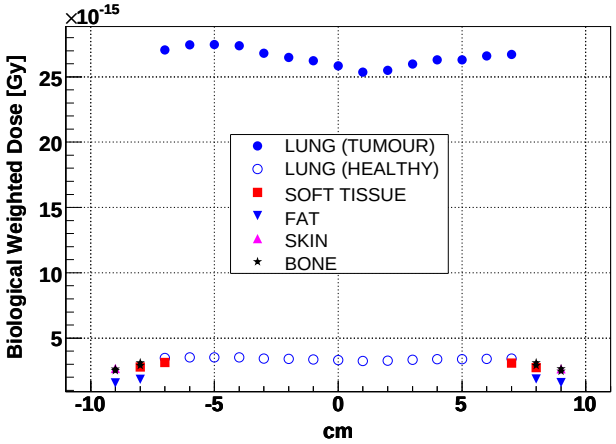

Figure 3.14: Total weighted dose profiles along x1 in the central section z2, for the normal lung with 5 ppm of ^{10}B (open circles), and for the tumour with 25 ppm (blue circles). The ratio of the dose delivered to the metastases and to the lung is about 5.

to perform an accurate experimental study of boron biodistribution in the thorax tissues other than in the lung. To this goal a Prompt Gamma Neutron Activation Analysis (PGNAA) [57] facility is being projected. In fact the α spectrometry method described in Section 2.5 is suitable only for solid samples, which can be measured under vacuum, while PGNAA could be used also for blood and other samples which are impossible to cut into thin slices.

These preliminary results obtained with an ideal beam provide optimistic indications about the possibility to irradiate lung tumours using multiple external epithermal neutron beams. The low density of the lung allows a quite uniform dose distribution in the whole organ when irradiating with two opposite beams. The next step to confirm the feasibility of the irradiation is to repeat the simulation using a real beam constructed at the TAPIRO reactor in Rome.

3.5 Future simulations

At the TAPIRO reactor, in Casaccia, Rome, an epithermal facility to treat brain gliomas was realized [58]. The beam section is 12x12 cm^2, and it could be used to irradiate a large portion of the lung. Simulations with ADAM positioned in front of the beam port are performed. An MCNP view of the geometry of the reactor with the phantom in the irradiation position is shown in Fig. 3.15. this plot is taken from the lung and therefore the head of ADAM is not visible.

The aim of this set of simulations is to compare the ideal situation presented in this chapter with a more realistic beam using the same phantom. The calculations for each axis chosen for the dose profiles plotting is investigated at present. We report here only a comparison between the profiles obtained irradiating with an ideal antero-posterior beam and with the TAPIRO beam, with ADAM positioned in front of it. In Fig. 3.16 the profiles of the different dose components are shown

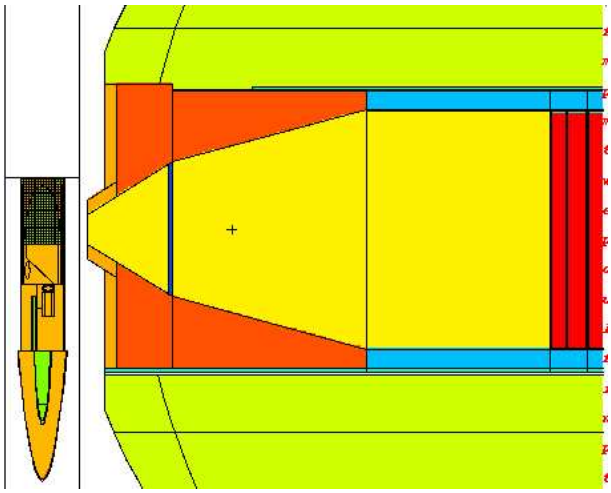

Figure 3.15: MCNP view of the TAPIRO reactor geometry with the ADAM model positioned in front of the irradiation port.

for the two cases: the ideal neutron source on the left and TAPIRO beam on the right. The position in the phantom is the section z1 at the base of the lung along x1, crossing the organ.

The behaviour of the dose components is similar in the two cases, supporting the possibility to create a uniform thermal neutron field inside the lung, when the phantom would be irradiated also with the postero-anterior beam. The existing difference in the profiles is caused by the elastic scattering; the TAPIRO beam energy spectrum contains a fast component that in the ideal beam was not present. To quantitatively compare the two situation the neutron flux has to be taken into account. As previously stated, to deliver 4 Gy to the normal tissue the flux of the ideal source would be $1.75 \cdot 10^{9}$ cm^{-2} s^{-1}. With TAPIRO working at 5 KW, thus emitting $4.23 \cdot 10^{14}$ neutrons per second, an irradiation of about 3 hours would be needed to deliver the same dose to the normal tissue. Obviously this is only an estimation of the irradiation time, as this study is preliminary. The dose distribution has to be calculated summing the results of the irradiation of both sides of the patient. Nevertheless this evaluation of the order of magnitude of the times that would be scheduled is an indication of the feasibility of the neutron irradiation using a real epithermal beam.

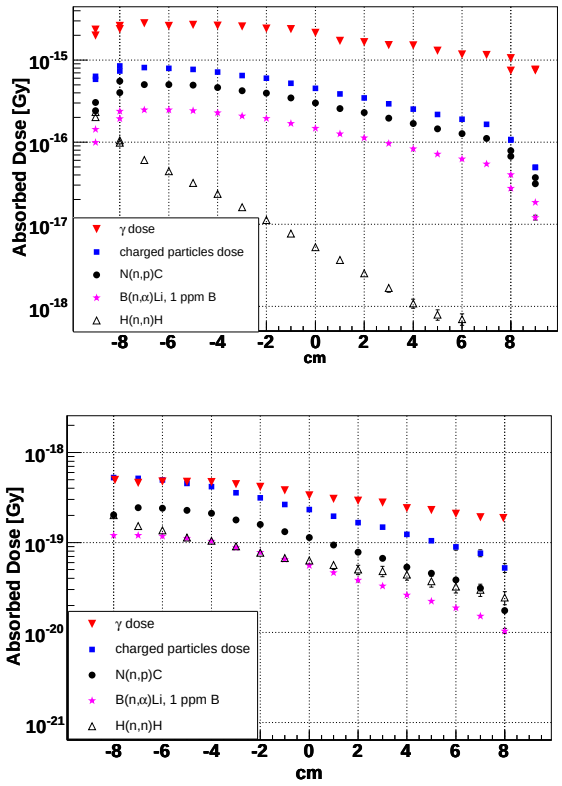

Figure 3.16: Dose components profiles along the in-beam x1 axis in section z1, at lung base, for 1 keV case (up) and TAPIRO (down). Note: the scales of the two plots are different.

Chapter 4

BNCT of liver metastases employing the autotransplantation technique

4.1 Introduction

As described in Chapter 1, the first stages of BNCT research in Pavia involved the development of the autotransplantation method for livers. The research work involved physicists, medical doctors and biologists, and two patients were treated in 2001 and 2003.

In the first section of this chapter the experimental measurements and the Monte Carlo calculations used to study a new concept of an organ irradiation facility are described. These methods afforded a highly uniform irradiation field inside the explanted liver. Furthermore, the set-up would be easy to assemble as there are more advantages compared to the existing facility. The other sections are dedicated to the studies undertaken in collaboration with some groups in Europe and Argentina, that are planning to apply BNCT to the treatment of liver metastases employing the autotransplantation technique.

A research agreement was signed between the Universities of Pavia and Mainz (Germany). The plan is to modify the thermal column of the TRIGA reactor in Mainz, characterize it and to begin the boron biodistribution studies in human liver. Section 4.4 reports the results of the measurements and the simulations that have been performed to date.

The other project is in progress in Italy, at ENEA Casaccia (Rome). Future plans involve the modification of the TRIGA Casaccia Reactor. MCNP calculations are being performed to find the best configuration for the liver irradiation. Presently the MCNP results obtained for the TRIGA Pavia Reactor and the the TRIGA Casaccia Reactor are being compared. The possibility to implement at TRIGA Casaccia the new column configuration that was tested in Pavia is being taken into account. The structural differences between the two reactors cause the flux distributions and their values inside the phantom to differ between the two

calculations. The aim of the work in progress is to understand these differences and to plan the most advantageous strategy for the column modifications. In section 4.5 this work is presented.

The last section of this chapter is dedicated to the BNCT project in Argentina, where the author spent two months in 2007 to work in collaboration with the group of physicists at the reactor RA-3 (Buenos Aires). During this period MCNP simulations of the reactor and thermal neutron flux measurements in a phantom were made. In section 4.6 the BNCT project, the present status and the future developments are described. In particular the new methodology for BNCT of the explanted liver proposed by the medical doctors of Angel H. Roffo Institute of Oncology (Buenos Aires) and under study at the National Atomic Energy Commission in collaboration with Angel H. Roffo Institute, is presented.

4.2 The new concept of the liver irradiation facility in Pavia

One of the tasks involved in the application of BNCT to explantable organs, is to design and construct an adequate irradiation facility that, most importantly, will provide a high and uniform thermal neutron flux distribution inside the organ. The high intensity guarantees a short irradiation time, and the uniformity improves the advantage conferred by ^{10}B selectivity in the tumour. The treatment plan for the irradiation of an explanted organ must deliver a lethal dose to the tumour regardless of its spatial distribution, keeping the dose absorbed by normal tissue as low as possible, or at least below the tolerance level. The thermal neutron irradiation must also destroy the micrometastases that cannot be identified before the treatment. For this reason, the irradiation time is calculated assuming the presence of a small tumour at the point in the liver where the flux is minimum, and considering that the delivered neutron fluence must ensure a dose that is sufficient to destroy this tumour. Based on this assumption, the tumour will absorb a lethal therapeutic dose whenever it is located inside the organ. The total dose absorbed by normal tissue is thus minimal near the point of minimum flux, but increases at the points where the thermal neutron flux is higher. This is the reason why a uniform thermal neutron flux distribution would be a benefit for the treatment. Besides, the irradiation time established to deliver a lethal dose to the tumour depends on the minimum value of the thermal neutron flux inside the organ, while the minimum dose delivered to normal tissues depends on the boron concentration ratio between tumour an healthy liver. Hence, as the uniformity of the thermal flux distribution increases, lower boron concentration ratios between tumour and normal tissues will be acceptable for explanted organ treatment. For these reasons a considerable effort has been dedicated to design a new graphite configuration in order to ensure a more uniform neutron flux distribution in the explanted liver.

The original configuration of the thermal column, designed and used to treat the explanted liver, was a 40 x 20 cm^2 channel of 1 meter long, surrounded by

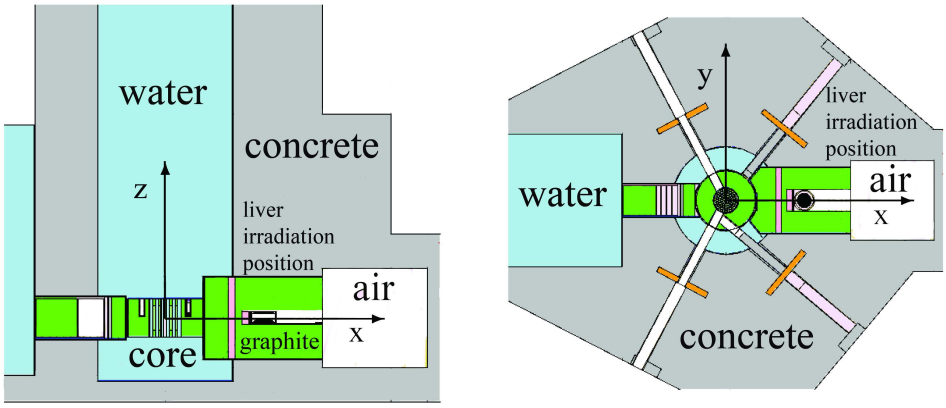

Figure 4.1: Vertical (left) and horizontal (right) section of the MCNP simulation of the TRIGA Mark II, University of Pavia.

graphite blocks. The facility was shielded with two bismuth screens of 10 cm thick, to attenuate the γ radiation from the core. This facility was simulated and experimentally characterized. The thermal neutron flux distribution obtained in the two treated livers allowed for the elimination of the metastases without damaging the healthy tissue employing an irradiation time of 10 minutes [45].

A simulation study to design a new Thermal Column configuration, in order to improve the uniformity of the flux inside the explanted organ, began 4 years ago. Different solutions have been evaluated to change the graphite geometry around the irradiation position. In [59] the best configurations that were tested and the thermal neutron flux distribution obtained are described in detail. In the first section of this chapter we summarize the experimental and Monte Carlo methods used for this study. We obtained a configuration of the thermal column that would ensure a highly uniform irradiation field inside the organ with a set-up that is easy to construct.

The Pavia reactor (TRIGA Mark II, 250 KW) was simulated with the MCNP neutron transport code, using the information on the geometry and materials reported in the Final Safety Report [60]. Fig. 4.1 shows a vertical and a horizontal section of the MCNP geometry; the origin of the coordinate system was placed in the center of the reactor core.

The reactor core was simulated using repeated structures and each fuel element was described in detail. The neutron source was simulated by sampling the neutrons with a uniform distribution in the volume of each fuel element, with the energy distributed as the Watt spectrum [61]. The sampling was also uniform for the overall distribution of the elements in the core. These simplifications conceivably led to some discrepancies between calculations and measurements because the real distribution has a maximum in the core central zone. Nevertheless the agreement between the calculations results and a number of experimental mea-

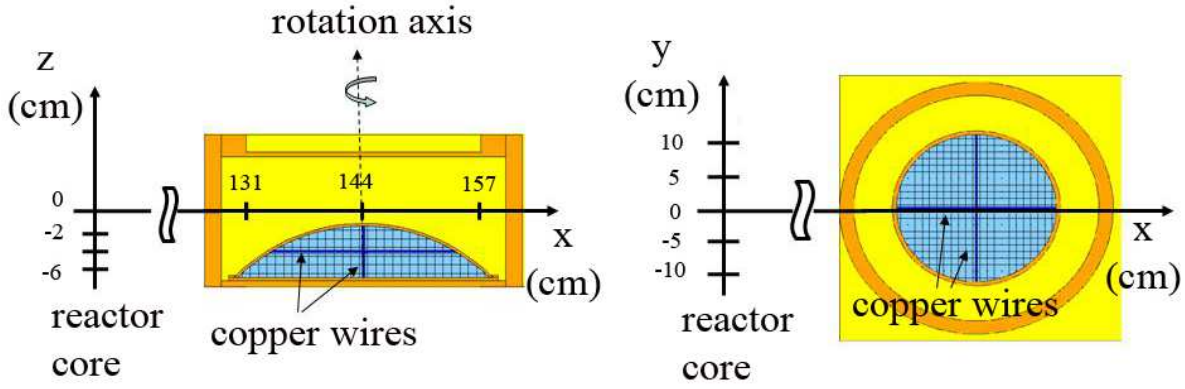

Figure 4.2: MCNP geometry of the liver phantom inside the teflon holder, vertical (left) and horizontal (right) sections. The copper wires were used for experimental measurement of the thermal neutron flux by the activation method.

surements made in different irradiation positions in the reactor was enough good. MCNP tallies were normalized to the reactor power using the factor $1.9 \cdot 10^{16}$ s^{-1}, which is the number of neutrons emitted per second from a reactor core working at 250 KW. The explanted human liver was modeled on the basis of the experimental phantom, as a spherical segment, 6 cm high and with a base radius of 15 cm. The phantom volume was divided into cubic voxels of 1 cm^3 in volume. In this way 5 meshes of voxels were obtained starting at 0.5 cm from the base, located at z=-6,-5,-4,-3,-2 cm from the center of the coordinate system, at the center of the reactor core (Fig. 4.2). The fluxes were obtained from the F4 tallies in the voxels, and were analyzed by building the profile of the fluxes along the central axis of the meshes. All real voxel volumes were obtained using the stochastic method, as described in the MCNP manual. The energy thresholds fixed in the calculations were a thermal bin ($E_n < 0.2$ eV), and one in the energy range between 0.2 eV and 0.5 MeV. Above this energy, previous calculations demonstrated that the neutron flux is at least 4 orders of magnitude lower than the thermal one.

The first step of the characterization was the validation of the code using the experimental results, obtained in the phantom with the thin foil activation method [62]. The experimental phantom consisted in a spherical teflon segment, with 3 mm thick walls. To study the neutron flux distribution in the liver, an hepatic-equivalent water solution was constructed and used to fill the teflon phantom. The composition and elemental percentages by weight of the hepatic solution are reported in Tab. 4.1 and 4.2. The elemental composition is similar to the liver composition reported in ICRU 46 [47], the only significant differences corresponded to the percentages of carbon and oxygen. Nevertheless, the sum of these two element percentages equals the sum of the same element percentages in the ICRU recommendation. This makes the solution suitable for liver simulation, because the cross sections of carbon and oxygen are very similar, at least up to 20 MeV [62].

Table 4.1: Compounds used for the hepatic-equivalent solution with 50 ppm of ^{10}B added.

compound	H_2O	CH_4N_20	$NaHSO_4$	KCl	H_3PO_4	H_3BO_3	Total
mass (g)	909.2	64.3	11.2	4.2	9.5	1.6	1000

Table 4.2: Elemental composition (percentages by weight) of the hepatic-equivalent solution compared to ICRU 46 liver composition [47]

Element	O	C	H	N	P	K	S	Cl	Na
Liver ICRU 46	71.6	13.9	10.2	3.0	0.3	0.3	0.3	0.2	0.2
Hepatic Solution	83.86	1.29	10.6	3.0	0.3	0.22	0.3	0.2	0.22

The Teflon phantom was equipped with thin copper wires along the x,y and z axis, as shown in Fig. 4.2, and was irradiated in the liver position. After the irradiation, the copper wires were cut into pieces 0.5 cm long and the ^{64}Cu activity produced by the reaction ^{63}Cu(n,γ)^{64}Cu was measured by a Ge detector. The thermal neutron flux was then calculated from the activity using the Wetscott formalism [63] [64].

4.2.1 Monte Carlo validation results

The measured values of the thermal neutron flux were compared to those obtained in the simulation of the phantom irradiated in the original facility (Fig. 4.3).

The first validation was made in air, irradiating the empty phantom and comparing with a calculation performed replacing the hepatic solution inside the model with air. The results are shown in Fig. 4.4.

The distribution along the x-axis, which is the longitudinal axis of the column, linearly decreases with the distance from the core (Fig. 4.4(a)), while along the other directions the distribution is uniform.

The second step consisted in studying the distortions caused by the liver tissue to the neutron flux distribution. The Teflon phantom was filled with the solution and irradiated in the Thermal Column. The results of the simulation in the same conditions were compared to the measured data. The thermal neutron profiles, both simulated and measured along the three principal axis, are reported in Fig. 4.5.

The MCNP simulations and experimental measurements are in good agreement, but the introduction of the hepatic solution drastically changes the neutron flux behaviour, mainly along the longitudinal direction. The ratio between the maximum and minimum flux values is Φ_{max}/Φ_{min}=4. To make the flux distribution more uniform, the organ can be rotated by 180^o halfway through the irradiation time. The effects of the rotation are shown in Fig. 4.6, in which the thermal neutron flux profiles are reported for the x-axis for each mesh from 1 to 5 cm from the base. Given the symmetry of the spherical segment around the z axis, the MCNP calculation would have produced exactly the same results if the phantom had been rotated. For this reason the distributions shown in this chapter

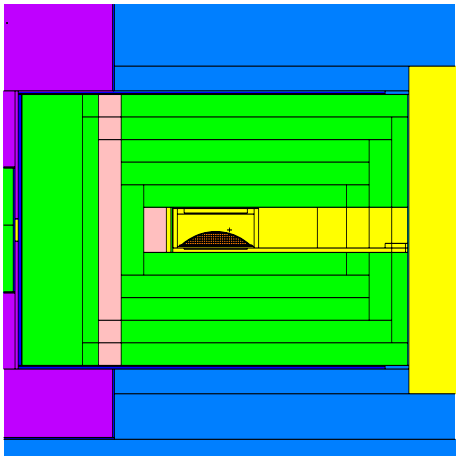

Figure 4.3: MCNP geometry of the original configuration of the Thermal Column with the phantom positioned for the irradiation.

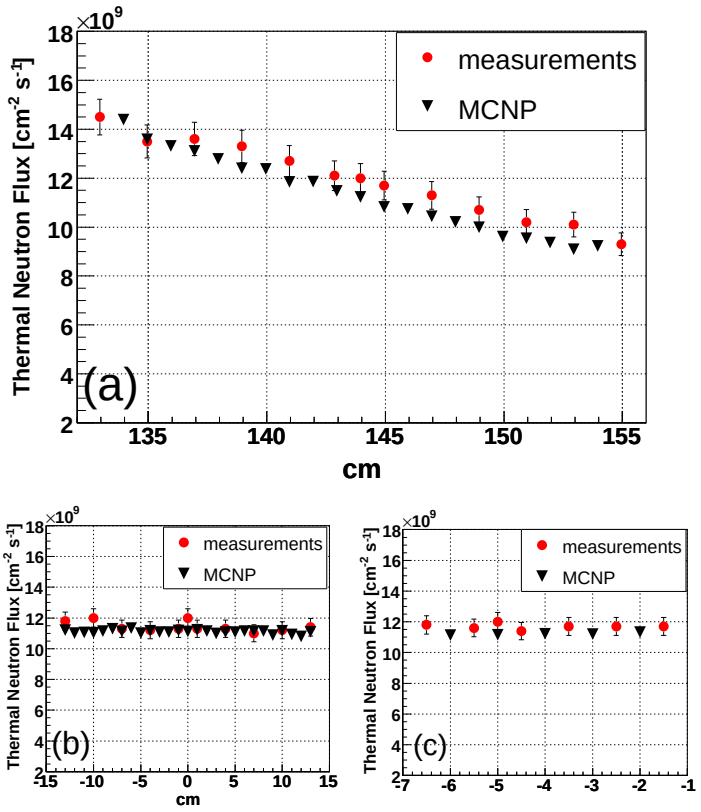

Figure 4.4: Thermal neutron flux distributions in the phantom filled with air along x (a), y (b) and z (c) axis. The triangles are the MCNP results, the red squares are experimental values. The center of the coordinate system is at the center of the reactor core, so the x axis in the picture (a) is the distance from the core.

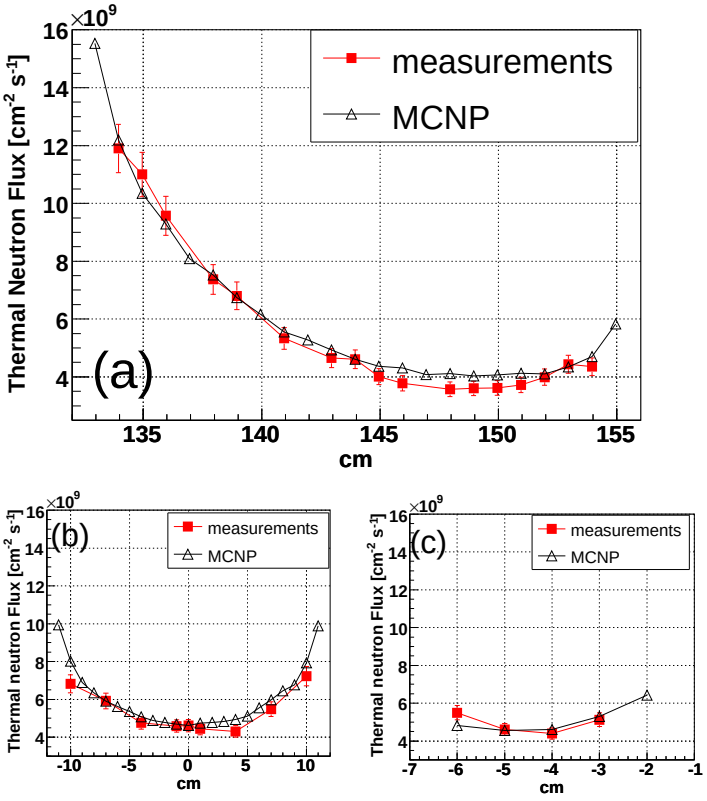

Figure 4.5: Thermal neutron flux distribution in the phantom filled with the hepatic solution along x (a), y (b) and z (c) axis, see Fig. 4.2. The triangles are MCNP results, the red squares are experimental values. The coordinate system is the same as in Fig. 4.4.

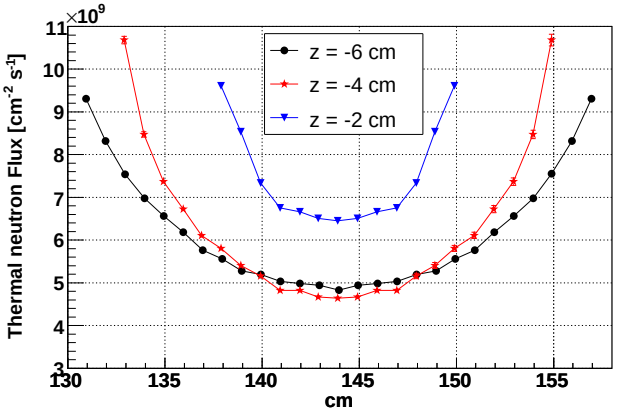

Figure 4.6: Calculated thermal neutron flux distribution along the longitudinal x axis after rotation of 180^o, see Fig. 4.2, at different positions along z-axis. The x-axis represents the distance from the reactor core.

were obtained by inverting and adding the Monte Carlo results along x axis, to simulate the effect of the organ rotation. After that, the outcome was divided by 2. As a result, the ratio Φ_{max}/Φ_{min} was lowered to 2.31.

4.2.2 The new design of the irradiation facility

Based on this validation, a number of new configurations of the Thermal Column were tested to lower the ratio between the maximum and the minimum flux values inside the organ. The goal was to improve the uniformity avoiding the organ rotation, to eliminate a possible source of problems during the irradiation procedure. The best solution was obtained by removing some graphite blocks from around the irradiation position, yielding a bigger irradiation compartment. In fact, in the original configuration, the thermal neutron flux was higher in the region of the liver facing the core. Therefore, attempts to lower these values by increasing the distance between the graphite and the anterior parts of the liver were made. As this change was not sufficient to avoid the rotation (although the ratio between maximum and minimum flux was reduced to 1.83), a layer of a neutron absorbing material was placed around the Teflon holder, on the surface facing the core. Fig. 4.7 shows the new configuration of the graphite inside the column and the absorber (in purple) around the liver holder.

The neutron absorber reduces the flux in the parts of the liver where it would be higher. The ideal candidate as an absorber would be a solid material containing small amounts of ^{6}Li, because it does not produce γ radiation. The simulations were performed placing a 1 mm thick LiF foil in the indicated position. The results of this run, without rotating the organ, are shown in Fig. 4.8.

The new configuration was compared to the existing one from the point of view of the dose distribution, using the Dose Volume Histogram (DVH). Boron concentrations in the normal liver and in the tumour, and a neutron reference

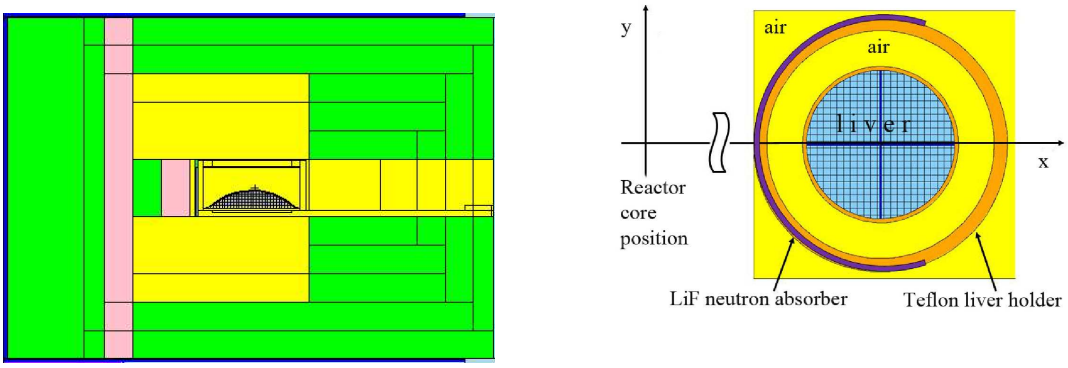

Figure 4.7: Open graphite configuration of the irradiation facility and the neutron absorber positioned around the external surface of the liver holder (enhanced thickness).

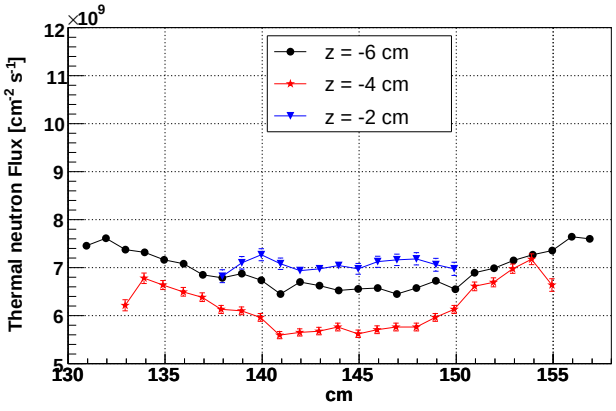

Figure 4.8: Thermal neutron flux distribution along the longitudinal axis for the different meshes, in the modified Thermal Column and with the neutron absorber. This result was obtained with no 180^o rotation.

fluence were assumed according to the treatment plan of the two treated patients. These values are 8 ppm, 50 ppm and $4 \cdot 10^{12}$ cm^{-2}, respectively. The irradiation time was fixed to deliver at least the reference dose to the tumour, assuming that the tumour was located in the points of minimum thermal neutron flux. Using the thermal neutron flux values in the phantom voxels, the contributions to the total absorbed dose from neutron capture reactions with nitrogen and boron were calculated. The epithermal and fast neutron dose contribution from the elastic scattering with hydrogen was neglected because it was evaluated to be at least one order of magnitude lower than the contribution from nitrogen. The absorbed dose due to charged particles was calculated for each voxel of the phantom (D_{vox_i}), using the following expression:

$$D_{vox_i} = (D_{Ni} + D_{Bi} \cdot C_H) \cdot \Phi_{vox_i} \cdot T_{irr}; \tag{4.1}$$

where D_{Ni} is the contribution of nitrogen (3% in weight) per unit of neutron fluence, and D_{Bi} is the contribution of boron per unit of concentration and of neutron fluence. C_H is the boron concentration in healthy tissues, assumed to be 8 ppm and Φ_{vox_i} is the thermal neutron flux of the ith voxel . The irradiation time $T_{irr} = 4 \cdot 10^{12}/\Phi_{min}$ was assumed to give a neutron fluence of $4 \cdot 10^{12}$ cm^{-2} at the voxel in the liver where the neutron flux is minimum. The dose components were calculated adding an FM card to the F4 flux tallies, as previously explained for the calculations in the phantom ADAM (Chapter 3, section 3.2). Finally the absorbed dose in each voxel was weighted by the factor $w_i = Vol_{vox_i}/Vol_{liver}$, to build the histograms of the volume-weighted absorbed dose (differential DVH), due to charged particles contribution. The cumulative function of these histograms is the integral DVH, representing the percentage of the organ volume that absorbed more than a certain dose value. The results are shown in Fig. 4.9. The upper graph shows the differential DVH, for the original column configuration (red line) and for the new configuration with broader irradiation space and the neutron absorber around the holder (black dashed line). The improvement is illustrated by a sharper distribution, centered on a mean dose around 4 Gy. The lower graph shows the integral DVH of the two configurations: the steepness of the graph shows that in the new Thermal Column a smaller amount of the total volume would absorb higher dose values.

The solution proposed is advantageous compared to the existing one, because of the improvement in neutron flux uniformity inside the liver, which results in a better DVH and a lower mean dose absorbed by the healthy liver. Besides, it would be straightforward to implement in terms of both the graphite configuration and the positioning of the LiF foil around the Teflon holder. Based on these considerations, we suggested that other BNCT research groups interested in performing a feasibility study prior to the treatment of liver metastases employing the autotransplantation method in TRIGA reactors, use the irradiation facility as proposed in this work. We began collaborating with the University of Mainz, Germany, and with ENEA. The ENEA group planned to modify the Thermal Column of its TRIGA reactor at Casaccia, Rome.

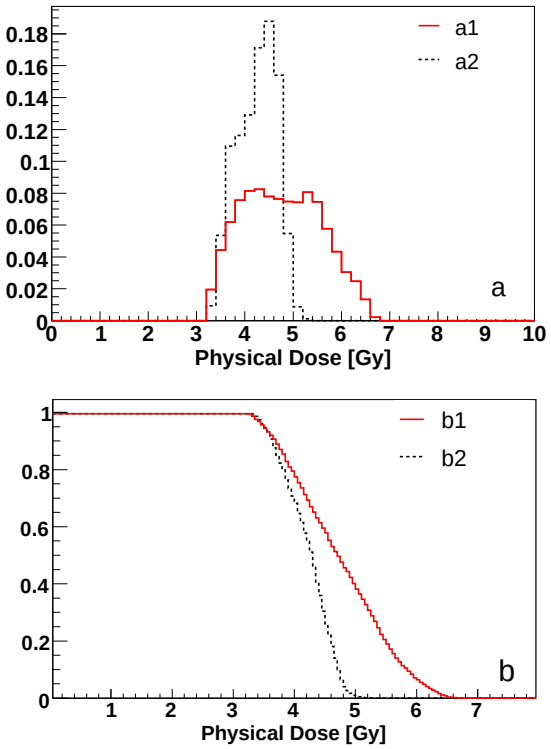

Figure 4.9: Up: Differential Dose Volume Histogram and down: Integral Dose Volume Histogram. red line: original facility and black dashed line: new configuration with the LiF absorber around the liver holder.

4.3 The TRIGA reactor in Mainz

The TRIGA reactor in Mainz is located at the Nuclear Chemistry Institute, Johannes Gutemberg University. Its structure is the same as that of the Pavia reactor, but the maximum power is lower: at stationary regime it can reach 100 kW. It also works in pulse mode, reaching a maximum power of 100 MW. A collaboration was signed between the Universitites of Pavia and Mainz to export the autotransplantation method for the treatment of human liver metastases to the Mainz facility, that could be performed by the transplantation unit located at the University hospital in the vicinity of the reactor.

In order to design the most advantageous modification for the definitive irradiation facility, many simulations were performed and validated for the present configuration of the Thermal Column. In this type of reactors some graphite bars can be extracted from the column in such a way that a channel arises with a cross section of 10 x 10 cm^2 and 1 meter long is obtained in the center. Inside this channel the thermal neutron flux distribution could be measured and calculated with Monte Carlo techniques and a deterministic evaluation. The simulation of the TRIGA reactor was performed using both MCNP, versions 5 and 4c, and ATTILA [66]. ATTILA was developed during 1995 at Los Alamos National Laboratories for solving 3-D steady-state coupled neutron and charged particle transport. It is a 3D multi-group Discrete Ordinate particle transport code, also used to calculate eigenvalues for critical systems. ATTILA solves the linearized Boltzmann transport equation and the applications for which it is suitable are burn-up, shielding, criticality, radiation protection, dosimetry, radiography and medical physics.

The first calculations were made to validate the codes, comparing the results to the experimental measurements performed along the channel obtained in the column by extracting the central bar. A Teflon bar was constructed to house TLDs and gold foils for neutron flux measurement by the thin foil activation method. The Teflon bar was inserted inside the channel with the gold foils in fixed positions, in order to build the thermal neutron profile. The same geometry was reproduced with the two neutron transport codes: Fig. 4.10 shows an MCNP section of the column with the channel and the positions where the flux was measured. The ATTILA simulations and some MCNP calculations were performed in Mainz. In Pavia some more detailed MCNP calculations were made, using a model of the whole reactor geometry. The core, smaller than the one in Pavia, was simulated with the same technique used for the TRIGA Pavia, using the repeated structures. The neutron source was built by sampling the neutrons uniformly in the volume of each fuel bar and globally in the whole core structure. The tallies were normalized to the reactor power (100 kW) by a factor of $7.6 \cdot 10^{15}$ s^{-1}, which is the number of neutrons emitted per second from a reactor core working at 100 kW.

The results of the comparison between ATTILA, MCNP and experimental measurements are shown in Fig. 4.11, where the MCNP tallies have been divided by a factor 1.25. This normalization depends on the simplification of the reactor source and/or on some changes in the reactor structures that may not be taken into account in the simulations performed in Pavia. Nevertheless, the flux behaviour inside the Thermal Column is perfectly reproducible and the codes were

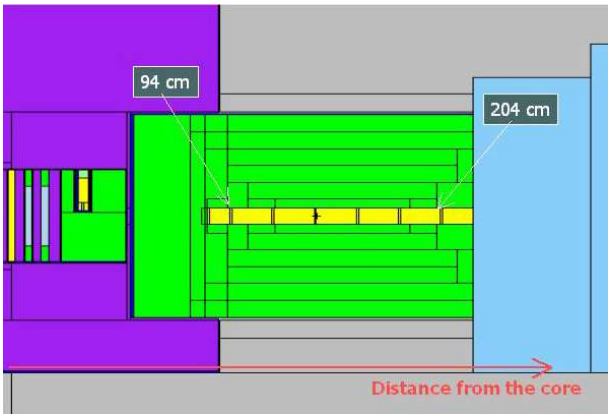

Figure 4.10: A transversal section of the Thermal Column in Mainz with the extracted graphite bars. The small sections in the channel are the points in which the neutron flux was measured.

validated for further simulations, in particular to test the effects of further column modifications.

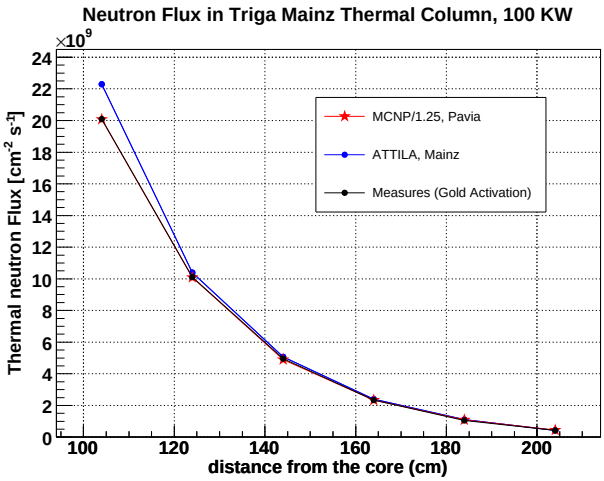

Figure 4.11: Comparison between the total neutron flux values obtained along the channel by ATTILA, MCNP and experimental measurements by gold foil activation.

After these preliminary studies the Thermal Column of the reactor geometry was modified to reproduce the Pavia configuration used for the patients' treatment. A larger channel was built and the bismuth screens were put in place (Fig. 4.12). The Teflon phantom with the hepatic solution was positioned in the same way to simulate neutron irradiation. The results are shown in Fig. 4.13, and represent the thermal neutron flux distribution (energy threshold: 0.2 eV) after the rotation of the organ. The voxel mesh that we used in this calculation is shifted towards the phantom base of 0.5 cm in reference to the previous calculation. This allowed

the use of all the phantom volume obtaining one more voxel row for the flux characterization.

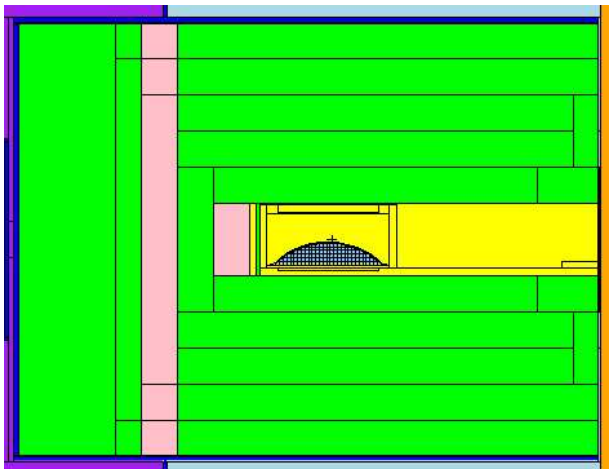

Figure 4.12: Modification of Mainz Thermal Column to yield a channel similar to the one constructed in Pavia.

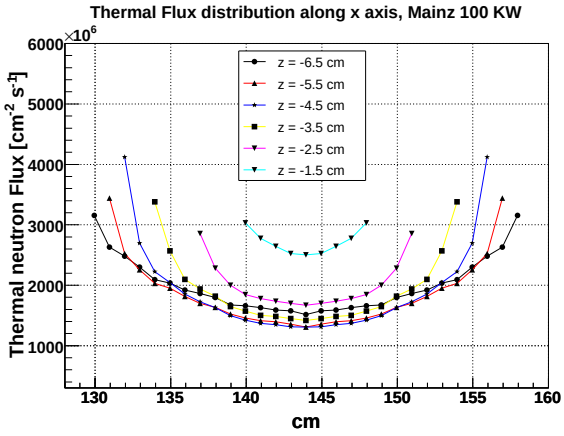

Figure 4.13: Thermal neutron flux distribution in the liver phantom in the column configuration of Fig. 4.12.

Fig. 4.14 shows two phantom planes, at -6.5 cm (left) and -5.5 cm (right) from the origin of the coordinate system, which is set at the center of the reactor.

The difference between the flux values could be explained by the differences in structure between the reactors, such as the core configuration and the position of the horizontal channels in reference to the core and the column. In addition to the absence of a thermalizing column, the TRIGA Pavia has three lateral channels that penetrate the graphite reflector, while in Mainz only one of the four enters the reflector. These differences can be seen in Fig. 4.15, where a section of the MCNP model of the Mainz reactor is shown on the left, and its counterpart at the Pavia reactor is shown on the right. Nevertheless the behaviour of the thermal

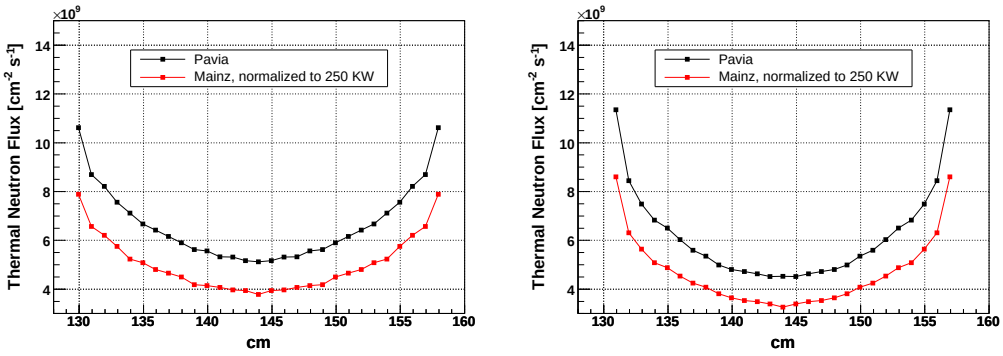

Figure 4.14: Comparison between thermal neutron flux profiles along 2 planes of the phantom in the Mainz and in the Pavia columns. Left: -6.5 cm, right: -5.5 cm from the center of the core.

neutron flux is identical for both sets of calculations, revealing that the strategy to obtain a more uniform thermal neutron flux distribution could be the same at both the reactors.

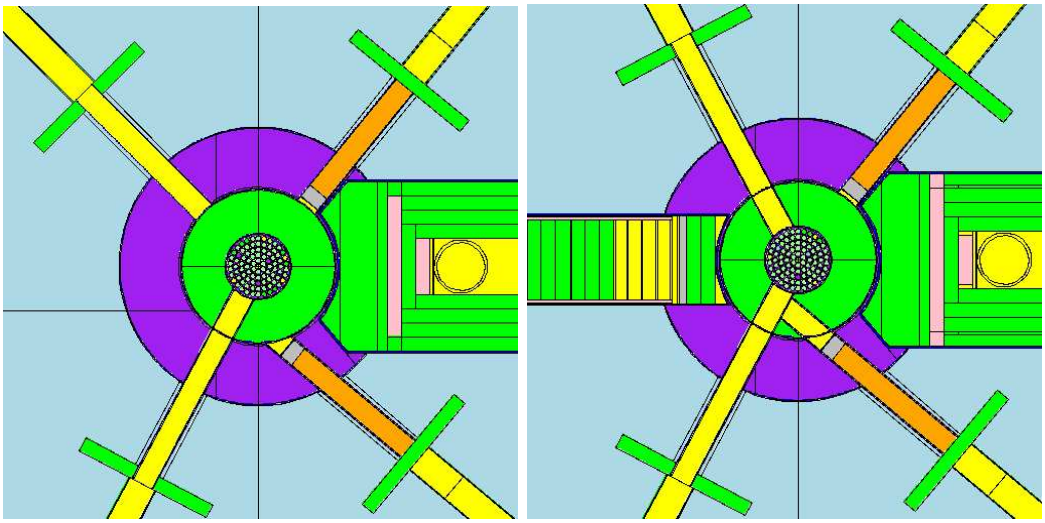

Figure 4.15: Comparison between the configuration of the lateral channels in Mainz (left) and Pavia (right) (sections at z=-7.5 cm from the core center).

Finally, the modified Thermal Column set-up was also tested for the TRIGA Mainz, opening the channel in the part of the column closer to the reactor core and placing a neutron absorber around the Teflon holder (Fig. 4.16). The thermal neutron flux distribution inside the phantom is shown in Fig. 4.17. This result is without the 180^o organ rotation. As can be seen when comparing the Figures 4.13 and 4.17, this Thermal Column configuration would also be advantageous in the Mainz reactor. In these two sets of calculations the results were divided by a factor 1.25 that resulted from the code validation as described.

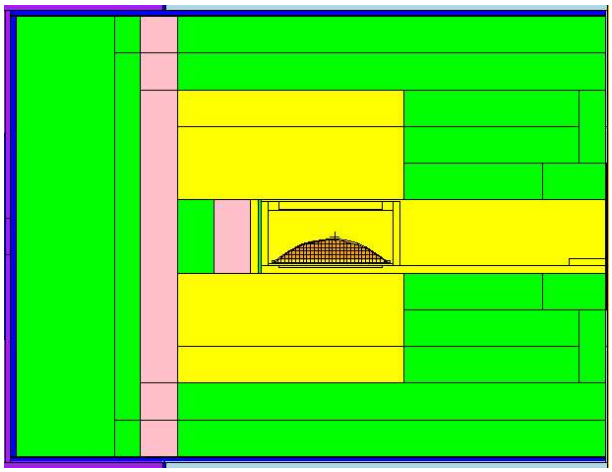

Figure 4.16: Modification of Mainz Thermal Column.

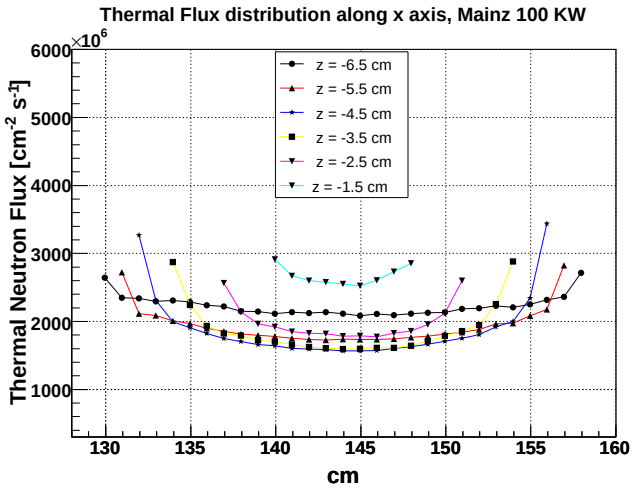

Figure 4.17: Thermal neutron flux distribution in the liver phantom positioned in the modified Thermal Column shown in Fig. 4.16.

As shown in Fig. 4.17, the uniformity gained in Mainz is worse than that obtained for the Pavia column. The ratio between the maximum and the minimum flux values is 2.1 in Mainz, while in Pavia it is 1.3; both these values were obtained without rotation. Nevertheless, the ratio is better in the open configuration with the neutron absorber than in the column configuration shown in Fig. 4.12. In fact, in this configuration the ratio would be 3.4, obtained by turning the organ by 180^o. Once again, the discrepancy between Mainz and Pavia results could be caused by the differences in reactor structure. In order to optimize the results, further calculations should be performed for the Mainz reactor, changing the absorber position, its thickness or its extension on the liver holder surface, as was previously done for the TRIGA in Pavia.

The BNCT project in Mainz is progressing as eactor configuration studies are

almost finished and authorization has been requested to perform boron concentration measurements in human liver samples. In the near future the Thermal Column will be modified and the facility for the liver irradiation will be built. When this is ready, the neutron and γ fluxes will be measured in air and in the phantoms to characterize and validate the BNCT irradiation field.

4.4 The TRIGA reactor in Rome

The TRIGA Mark II nuclear reactor, named RC-1 (Reactor Casaccia 1), was built in the early sixties by General Atomics, with an original power of 100 kW, and increased by ENEA staff to 1 MW in 1966. It is a pool thermal reactor whose core is contained in an aluminium vessel inside a cylindrical graphite reflector, surrounded by lead shielding. Demineralized water filling the vessel, ensures the moderation of neutrons, cools and acts as the first biological shield. Reactor control is ensured by four rods: two shims, one safety fuelled follower rod and one regulation rod. The produced thermal power is removed by natural circulation of water through a suitable thermohydraulic loop comprising heat exchangers and cooling towers. The core, surrounded by the graphite reflector, like the TRIGA in Pavia, is a lattice of fuel elements, graphite dummy elements, control and regulation rods, but it is bigger than the core of the Pavia reactor. It has 127 channels divided in seven concentric rings. One channel houses the start-up Am-Be source, and two channels are available as irradiation positions.

The Thermal Column will be modified for BNCT cancer treatment of explanted human liver (see Fig. 4.18). The objective is to find a graphite configuration that would ensure a uniform dose distribution in the explanted organ, eliminating the need for a 180^o rotation of the liver half-way during the irradiation. For this reason, the set-up that we tested for the TRIGA Pavia, was considered for the Casaccia reactor, and calculations were performed to check the validity of this solution in the RC-1.

The geometry of the open channel, the liver model inside the Teflon container and the neutron absorber were modeled into the MCNP simulation of the RC-1 (Fig. 4.19). We accurately considered all the differences between the simulations of the two reactors, that could cause important differences between the results of the calculations.

The main difference between the simulations of the two reactors is the model of the neutron source. While in Pavia the neutrons were sampled uniformly in the core geometry, the RC-1 source was calculated using the card KCODE, that generated a fission neutron distribution used in the following runs as a fixed neutron source. This is a more precise way to model a neutron source that originates in fission reactions in a reactor core. In fact this modeling procedure results in a neutron distribution that peaks at the center of the core, as in reality. Another important parameter to consider is the graphite density value. The density of the nuclear graphite is reported to be 1.7 g/cm^3 and is the value used in the ENEA simulations. However, in the calculations for the Pavia reactor this value was assumed to be 2.25 g/cm^3. This value is used in some cases to take into account

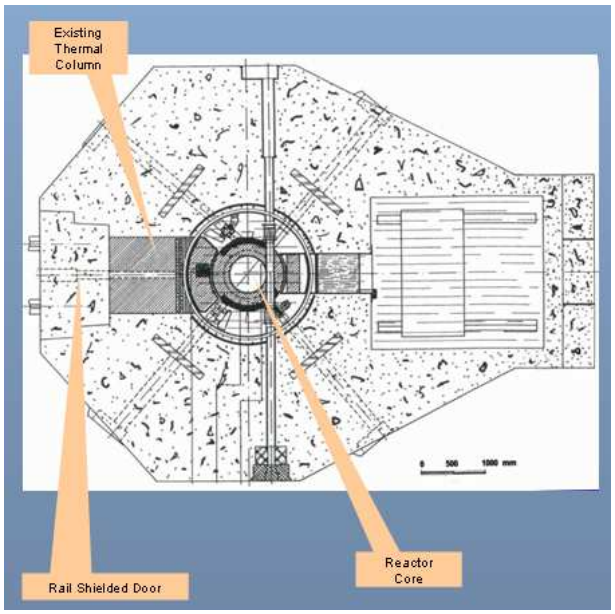

Figure 4.18: A section of RC-1, the position of the Thermal Column is indicated.

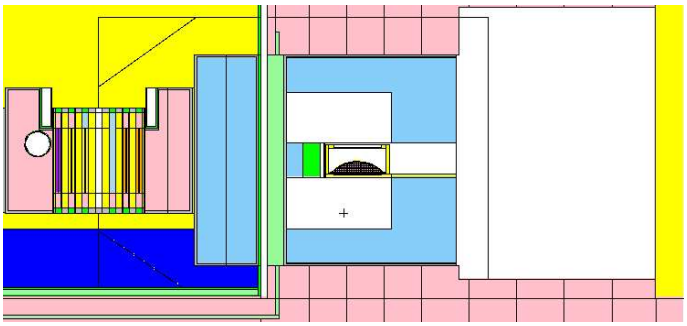

Figure 4.19: MCNP simulation of the RC-1, transversal view of the modified Thermal Column with the liver model in the irradiation position.

the graphite impurities that can change the total cross section of the thermal neutron interactions with graphite (see appendix II, Table II.3 in [65]). However, the values of the graphite density are justified by the validations performed by comparing against experimental data in both reactors (Fig. 4.4 and 4.5 for the Pavia reactor). An example is shown in Fig. 4.20, that shows the difference in the thermal neutron flux profile in the Pavia reactor model, using the two density values. In both cases the simulated profile is compared to a measurement performed inside the Teflon experimental phantom, showing that the lower graphite value could not be used in this reactor model.

More important are the structural differences between the two reactors. In the original Thermal Column of RC-1 two lead screens are placed as γ radiation shields, instead of the two bismuth walls in the Thermal Column of the Pavia reactor. Besides, the core is bigger at RC-1 and the phantom is placed 8 cm

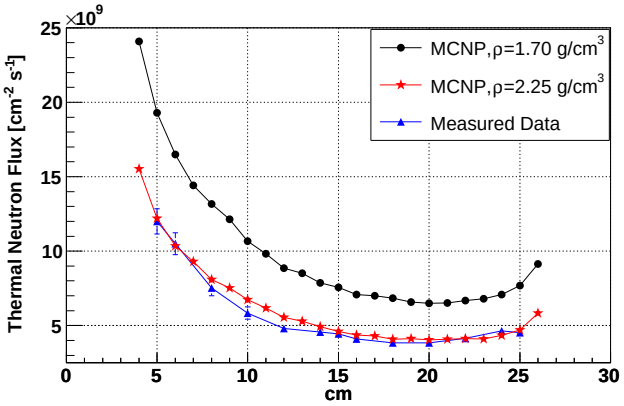

Figure 4.20: Comparison between a simulation using 2.25 g/cm^3 (red stars) and 1.7 g/cm^3 (black circles) as the graphite density value. The blue triangles represent the measured data inside the phantom. The agreement between MCNP and the measurements confirm that the first value should be used in the Pavia reactor model.

further away from the core compared to Pavia. In fact, between the lead screen and the end of the column towards the core there is 40.5 cm of graphite in RC-1, while in the TRIGA Pavia the graphite wall is only 34 cm thick. The two Thermal Columns have different sizes, and even if the irradiation compartments were modeled with the same volume, the structural differences might change the final result. To compare the two columns we show a view of the two geometries in Fig. 4.21.

Another important difference, that surely affects the thermal flux distribution in the phantom, is the presence of a layer of Masonite between the lead screen and the tank in the Thermal Column of RC-1, followed by a zone of air, that can be seen in the picture on the right in Fig. 4.21, and is indicated as a green and a white zone between the graphite and the thicker lead shield. This thickness in the Pavia reactor is filled with graphite.

The calculations of the flux and dose profiles are being currently performed. In particular we continue to work on the comparison between the two different strategies to simulate the phantom irradiation and explain the preliminary results. Modifications have been planned in the MCNP modeling of the TRIGA Pavia reactor, to make it similar to the more detailed Casaccia simulation, for example from the point of view of the source description. On the other hand, simulations are being performed modifying some details of RC-1, to understand which are the structural characteristics that most affect the final results. For example, the Masonite layer can be replaced by graphite to compare the fluxes obtained in both situations. The aim of these strategies is to evaluate whether the column configuration that gave good results in Pavia simulations is also useful for this reactor. If this were the case, simulations will be performed to optimize the size of the irradiation compartment and the position and thickness of the neutron absorber.

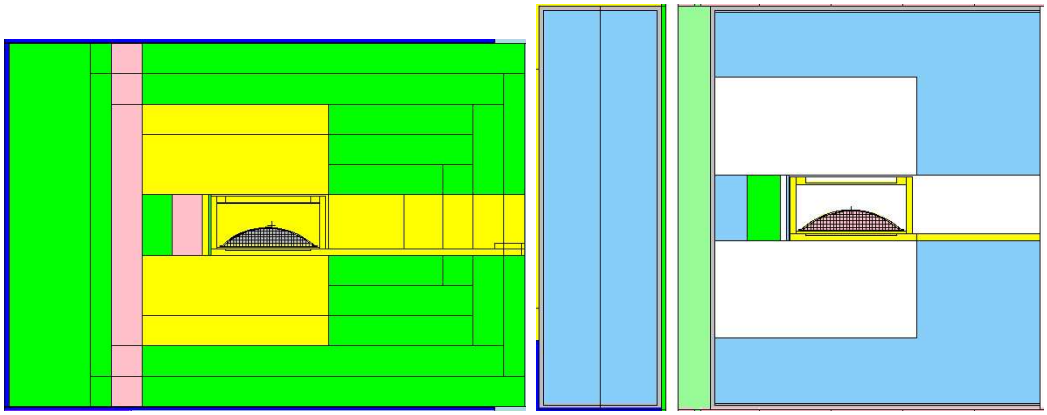

Figure 4.21: Comparison of the Thermal Column of the two reactors. On the left: TRIGA Pavia (yellow:air, green:graphite, pink:bismuth) on the right: RC-1 (white:air, green and light green: Lead, light blue:graphite).

4.5 The BNCT in Argentina[1]

4.5.1 Introduction

One of the collaborative projects we are currently participating in involves the National Atomic Energy Commission of Argentina (CNEA) (Comisión Nacional de Energía Atómica), Argentina[2]. Based on the availability of adequate neutron sources, human resources, clinical interest and a developed technology, BNCT is a solid project in Argentina, carried out by a number of research groups involved in the different scientific fields. Currently there are 11 groups working in BNCT research, coordinated by Dr. Sara Liberman and operating in the three atomic centers of CNEA, with the collaboration of the Roffo Institute of Oncology for the clinical part of the research.

4.5.2 The liver BNCT

Radiobiology

Based on the experience of the BNCT liver treatments performed in Pavia with the autotransplantation method, CNEA and the Roffo Institute of Oncology began a project that involves BNCT studies for the treatment of hepatic unresectable metastases from colon carcinoma. The proposed protocol is characterized by an important difference compared to the TAOrMINA method. It would avoid the high risk associated with the prolonged anhepatic phase in patients undergoing whole liver ex-situ BNCT followed by whole liver autograft. The novel BNCT technique proposed by Roffo Institute liver surgeons is based on partial liver autograft, following this procedure: administration of the boron compound, removal

[1]This brief summary of the BNCT liver project in Argentina and additional information described in the following section are based on private communications with S.J.Liberman.

[2]http://www.cnea.gov.ar/xxi/bnct/

of the left lateral liver section (segments II, III), irradiation according to the pre-established treatment plan, and re-implantation of this treated liver portion. After the effect of BNCT and adequate liver functions are verified in this part of the organ, a partial atrophy of the right, untreated liver would be induced by embolization of the portal vein. The hypothesis is that the atrophy of the untreated part of the organ would act as a stimulus for regeneration of the treated liver segments. When a sufficient amount of healthy liver mass is produced by regeneration, the atrophic right diseased part of the liver would be resected [67]. The advantages of this technique are that the patient would not undergo an anhepatic phase, and that the postoperative liver functionality would not depend on the outcome of BNCT because the patient would still have the right liver segments. To prove the feasibility of this technique it is necessary to verify that BNCT doses absorbed by healthy tissues during the treatment do not impair the regenerative process of healthy liver following a regenerative stimulus. A study was conducted on rats to evaluate the effects of BNCT mediated by BPA, GB-10 and BPA+GB-10 on short-term regenerative capacity of normal liver after partial hepatectomy. Biodistribution studies were performed to measure boron concentration in blood and tissues. The rats were infused with BPA, GB-10 or BPA+GB-10 and their abdomen was irradiated at RA-6 (CAB, Bariloche). Dose calculations were performed to guarantee that the dose delivered to normal tissue would not exceed the tolerance levels. After 21 days the rats underwent partial hepatectomy and 9 days later they were sacrificed to evaluate liver regeneration. Normal liver regeneration reached the control values of (liver weight)/(body weight) ratio for all the BNCT protocols tested. The rats were exposed to a physical dose similar to the dose delivered to the normal tissues during the two clinical applications in Pavia. These findings provide support for the future development of the proposed novel technique for the treatment of unresectable hepatic metastases.

Biodistribution

Work in other fields of the project is also in progress to finally apply BNCT to the treatment of liver metastases in a clinical trial. In 2005 ANMAT approved a protocol proposed by CNEA and Roffo Institute of Oncology for biodistribution studies in patients affected by liver metastases of colon carcinoma. The protocol foresees the inclusion of patients older than 18 years, with liver metastases only and having the primary tumour under control. Recently the first biodistribution study was performed with BPA in a patient scheduled for liver surgery. Blood and liver samples were taken for the measurement of the boron concentration. Measurements will be performed both in Buenos Aires (CAC) and in Pavia, where we will analyze samples by α spectrometry and obtain neutron autoradiography images. This biodistribution phase is of great importance not only for this novel method under study in Argentina, but also for the European groups that are developing liver BNCT applications. There is in fact a lack of statistically significant results of boron concentration measurements in human liver tissues, both normal and tumoural, that is often an obstacle for further development of the different projects. It would be undoubtedly useful to share the results and to create a solid

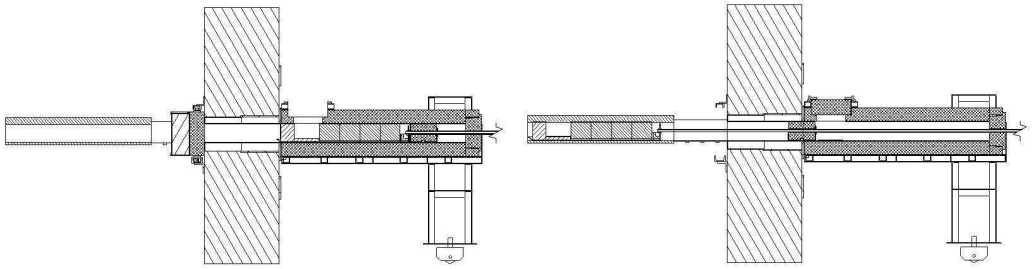

Figure 4.22: Technical drawings of the devices used to insert the samples in the column channel in Argentina.

background experience on which all BNCT liver research projects can be based.

The liver irradiation facility

The area of this project that we were most involved in was the physical characterization of the irradiation facility built in the Thermal Column of the RA-3 reactor, localized at Centro Atómico Ezeiza (CAE, Buenos Aires). RA-3 is an open pool reactor that can work up to 10 MW, and it is used for radioisotope production. It is equipped with a lateral Thermal Column filled with graphite blocks and shielded with a Boral layer between the graphite and the concrete external walls. It operates 5 days per week continually and thus it would not be possible to shut down the reactor to position the explanted liver at the designed irradiation location, and remove it at the end of irradiation. For this reason an external shielded device was built to allow sample insertion while the reactor is operating. A channel was prepared inside the Thermal Column, by extracting a number of graphite bars. An external tray was constructed so that it can be pushed by a tube along a guide rail up to the irradiation position. Once the shutter is closed, the samples are positioned in the sample holder on the tray, the upper shielding door is closed, the shutter is opened, the tray is pushed inside the column and an additional shield of graphite fills the space between the sample and the end of the channel, as shown in the technical drawings in Fig. 4.22. The irradiation position is shielded from the γ from the core with a bismuth block fixed at the end of the channel and another one positioned in the tray, before the sample holder. In addition, a layer 2 cm thick of bismuth is placed in the tray to serve as a base for the holder.

Some views of the devices for sample positioning are shown in Fig. 4.23 and 4.24, where details of the sample holder with the upper shielding door closed and open can be seen.

The compartment in which the sample holder is placed for irradiation has a length of 20 cm and a cross section of 15x15 cm^2.

The air channel was characterized by measuring the thermal neutron flux distribution and the γ dose rate distribution along the tunnel length, i.e. 1.5 m to 2.7 m from the beginning of the Thermal Column to the reactor core. The space inside the box for the samples was also characterized, demonstrating that the neutron

Figure 4.23: External views of the reactor external facility to position the tray in the irradiation facility.

Figure 4.24: Pictures of the tray that houses the samples for irradiation, with the upper shielding door closed (left) and with the upper door open for positioning of the samples (right).

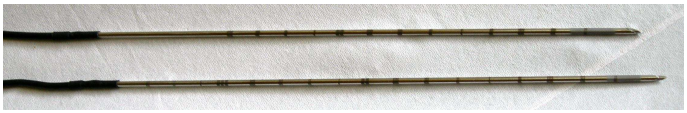

Figure 4.25: A picture of the SPND connected to the cables for the collection of the induced currents.

flux is highly thermalized in the irradiation position: the mean thermal neutron flux is nearly three orders of magnitude higher than the epithermal flux. The homogeneity along the longitudinal axis of the column is satisfactory inside the box: the difference between the maximum and the minimum neutron flux values is 20%; representing a homogeinity ratio of 1.25. Self Powered Neutron Detectors (SPND) were used for neutron flux measurements. A SPND is a coaxial cylindrical assembly consisting of a central cylinder of a conducting material with a high cross section for neutron capture surrounded by an insulator and by an external conductive sheath (collector) [68]. When the central emitter captures neutrons, it becomes β^- active and emits electrons that reach the external sheath through the insulator, polarizing the device. Using an amplifier connecting the emitter to the sheath, currents proportional to the thermal neutron flux can be collected. This kind of detectors can be constructed in very small sizes. This characteristic and the fact that they do not need a high voltage supply to operate makes an SPND a very manageable and useful tool for on line neutron measurements during patient irradiation. The material chosen as emitter is ^{103}Rh, that has a neutron capture cross section of 134 b, and allows currents above the picoampere range to be obtained. The emitter diameter was 1 mm. The insulator was made of Peek, a special plastic with good resistance to the radiation and a high resistivity ($10^{15} - 10^{16}$ Ω·cm). The external diameter of the insulator was 1.57 mm, and it was arranged to cover the 10 mm lenght of rhodium. The external sheath material was chosen to have the minimum interaction with the thermal neutron flux and the minimum residual radioactivity. Besides, it was necessary to build a compact device, whose sizes had to be comparable with the ones of the emitter and insulator assembly. Stainless steel was chosen as external sheat, in particular the needles used to perform biopsies were an adequate tool, having an internal diameter of 1.7 mm. The emitter and the insulator could be insercted inside the needle, and its lenght (200 mm) allowed to perform measurements at different depths in the tissue samples. This detector configuration has a number of advantages: the material is largely used in medicine and being a thin cylinder the measurement inside the sample does not damage the tissue. Fig. 4.25 shows a picture of the part of the detectors that enters the tissues. The currents produced were collected by a Keithley (mod. 6514) electrometer connected to a Desktop Computer.

Compared to the activation method used in Pavia, this kind of measurement is advantageous because it allows to obtain of flux values on-line, with a very simple analysis of the data collected during the irradiation.

To simulate liver irradiations, some gel phantoms were prepared for irradiation

Table 4.3: Elemental composition of the agarose solution used for the phantoms

element	H	O	C
mass percentage	11.03%	87.85%	1.12%

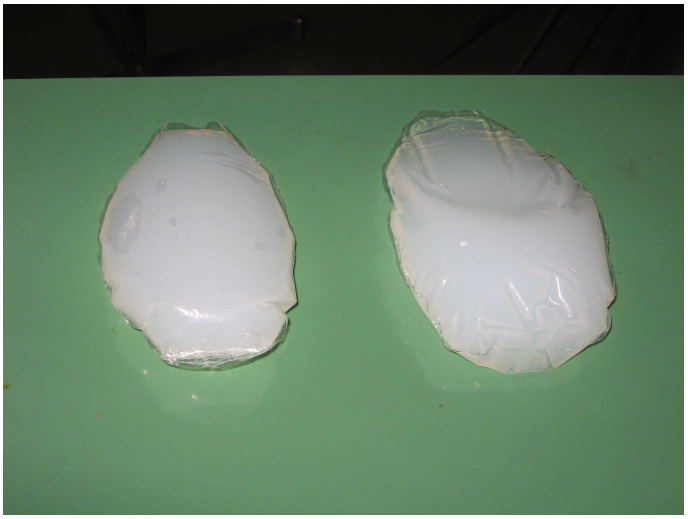

Figure 4.26: A picture of two agarose phantoms with different weights, prepared for thermal neutron irradiation in the Thermal Column of RA-3.

in the column facility[3]. The material chosen for the gels was a 2% solution of agarose ($C_{12}H_{14}O_2(OH)_4$) in water. This formulation yielded solid phantoms that keep their shape for several weeks without water loss at ambient temperature. The elemental composition of the agarose gel is reported in Tab. 4.3.

The solution was prepared and, still liquid, put in polyethylene bags shaped in the form of the liver portion that would be treated. Three phantoms were assessed for use in measurements, simulating different liver weights and dimensions. In Fig. 4.26 two phantoms with different weights are shown.

The aim of the measurements with the phantoms was to measure the thermal neutron flux profile inside the explanted organ. To this end, the phantoms were positioned in the acrylic box designed for the liver treatment. The irradiation position of the liver was conceived to maximize the uniformity of the thermal neutron flux distribution inside the organ. For this purpose, an inclined base was put inside the box to support the organ, with its thicker part leaning against the wall nearest the core. Besides, the phantoms were put in a polyethylene bag containing water, to simulate the preservation solution used to preserve the liver during irradiation, and in another polyethylene bag to reproduce the treatment conditions. The water volume that was needed to completely cover the liver was around 100 cm^3 (Fig. 4.27).

The box had two holes in the posterior side to allow the insertion of the detectors. Two detectors were used: the first was positioned along the longitudinal axis of the box, alongside the phantom, to monitor the thermal neutron flux profile

[3]The author participated in this measurement, during her stay at CNEA in May-June 2007.

Figure 4.27: A picture of the phantom positioned inside the polyethylene bag filled with water and placed in the acrylic box, on the inclined base.

in air. The other was implanted inside the phantom, along its principal axis, at half its height. The first measurement was taken with the detector positioned in the first centimeter from the box surface facing the core (Fig. 4.28).

When the detectors were inserted inside the box and positioned for irradiation, the reactor was operating at a power of 8 MW. For each measured point, certain of time is needed for the detector to reach a stationary current; this delay depends on the decay time of the rhodium. The current was measured over a period of 15 minutes for each point. After this time, the tray was removed from the column and the upper door was opened. We slid the detectors one centimeter backwards. This procedure was repeated to span the length of the phantom and build the thermal neutron flux profile. The results of one of these measurements, performed in a phantom that weighted about 300 g, are shown in Fig. 4.29.

For further characterization of the irradiation facility, the thermal neutron flux was measured inside a lateral liver lobe of a pig, whose weight and shape closely resemble those of sections II and III of a human liver [69] [70]. The lobe weight was about 310 g. Fig. 4.30 shows the liver positioned in the irradiation box.

As for the phantom irradiation, the liver lobe was also put inside two polyethylene bags, and submerged in water. Again, one of the two SPNDs was inserted inside the liver lobe along its principal axis, while the other was positioned inside the holder to measure the flux in air along an axis parallel to the liver. In this way the thermal neutron flux was measured where the flux attenuation is maximum compared to the situation in air. As in the case of the phantom, each measurement lasted 15 minutes for each point, with the reactor working at a power of 8 MW. The thermal neutron flux profiles inside the liver and in air are reported in Fig. 4.31. Comparing the thermal neutron flux profiles in air shown in the two graphs corresponding to the measurement in the liver and in the phantom, a difference of about 10% can be seen. This difference is due to a change in the reactor core con-

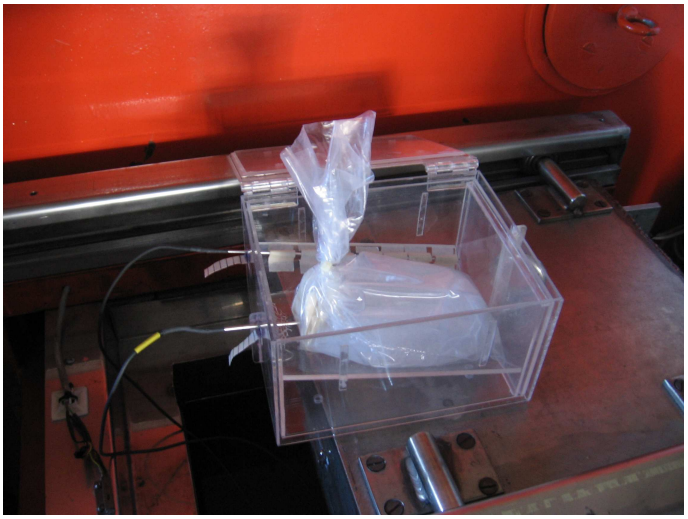

Figure 4.28: A picture of the acrylic box with the phantom and the detectors inserted inside the gel, before positioning in the tray for irradiation.

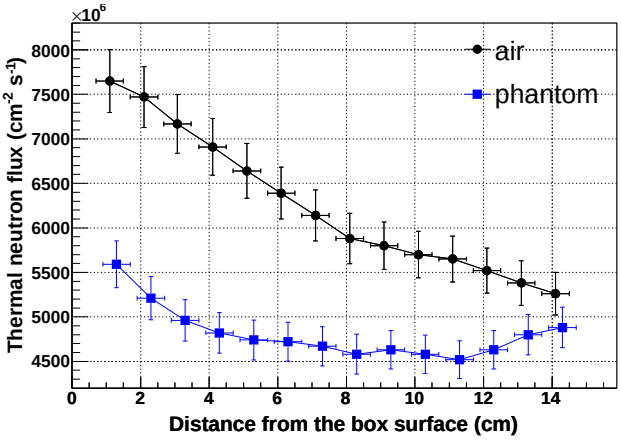

Figure 4.29: Measured data of the thermal neutron flux in air and inside the liver phantom. The measurement was performed using Self Powered Neutron Detectors (SPND).

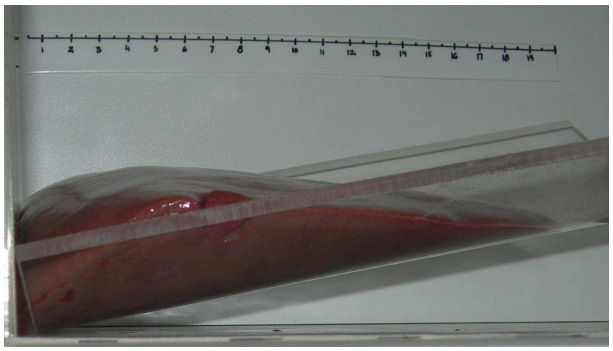

Figure 4.30: The position of the pig liver sample on the inclined base, that must be put inside the tray and pushed up to the irradiation position. The position of the liver inside the holder was chosen to expose the thickest part of the organ to the maximum neutron flux values, in order to keep a good level of uniformity of the thermal neutron flux distribution.

figuration between the two measurements. To take into account this change, the results of the measurements in the phantom were corrected for a factor calculated dividing the thermal flux in air measured in the two configurations. Fig. 4.32 is a comparison between the measured data inside the liver and inside the phantom, with the normalizing factor. The results are in good agreement, regarding the experimental errors, therefore the agarose phantoms are an adequate simulation for the liver tissues with respect to the thermal neutrons attenuation.

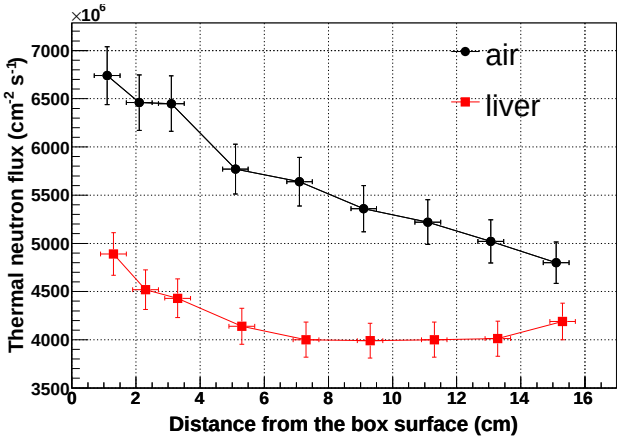

Figure 4.31: Measured data of the thermal neutron flux in air and inside the pig liver lobe. The measurement was performed using Self Powered Neutron Detectors (SPND).

Both the profile inside the liver lobe and in the phantom show a high grade of uniformity compared to the corresponding profile in air, due to the combination of different characteristics of the irradiation set-up. In fact, the thermal neutron flux in air decreases with the distance from the core, while the attenuation of the flux

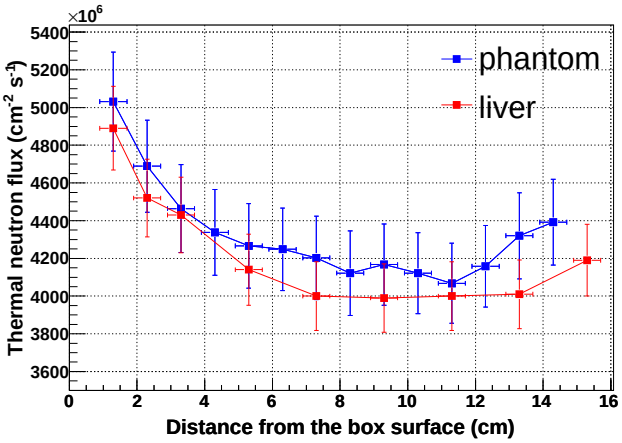

Figure 4.32: Comparison between the thermal neutron flux profile inside the pig liver lobe and inside the phantom.

in the liver is lower, because the liver thickness is smaller in the posterior parts. The inclined position takes advantage of the shape of the liver segments, such that the attenuation of the flux with the distance is compensated by the smaller amount of tissue that attenuates the flux in the posterior part of the organ. The resulting flux distribution is uniform enough to plan the liver irradiation in a fixed position. This would be a great advantage compared to the conditions at Pavia, where a 180^o rotation is needed in the present facility because the whole liver is irradiated. In the pig liver lobe, the ratio between maximum and minimum thermal neutron flux is less than 20%. Considering that 300 g is an upper limit for the mass of segments II and III of the human liver, this reveals a good level of uniformity of the irradiation field inside the organ. Given a minimum flux of $4\cdot 10^9$ cm^{-2} s^{-1}, a thermal neutron fluence of $4\cdot 10^{12}$ cm^{-2} could be reached with an irradiation time of less than 17 minutes. These measurements proved that a short irradiation in an adequate thermal neutron field would be possible at this facility without moving the organ during the treatment.

The simulation of the reactor[4]

The complete structure of the reactor was simulated using MCNP, version 5 [71]. The source was modeled with different strategies: some calculations were performed using the K-code and the SSW, SSR cards to build a plane recorded source coincident with the beginning of the Thermal Column. This source would be faster and easier to use after adequate validation, for all the calculations dealing with samples inside the Thermal Column. This calculation is currently being optimized and will not be described in this work. While this solution was under study, another source was built for calculations in the irradiation position. In particular, uniform sampling of the neutrons in the source volume was performed,

[4]This part of the work was performed in close collaboration with Mr Julián Pinto, CNEA, who is warmly acknowledged by the author.

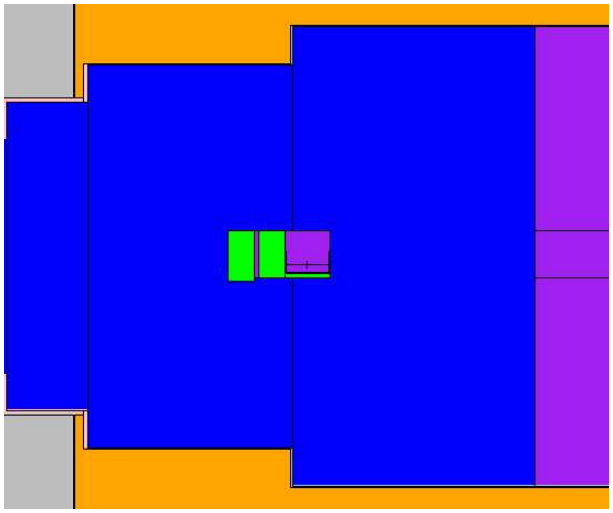

Figure 4.33: Simulation of the RA-3 Thermal Column with the acrylic box in the irradiation position and the channel between the box and the end of the column filled with graphite.

using the cell rejection criterion to exclude the zones of the core in which there is no fissile material. In fact some containers for radionuclides production are placed inside the core, between the fuel plates. The geometry of the source is modeled such that the core structure is made up of identical fuel plates for which the repeated structure capability of the simulation code can be applied.

The Thermal Column was simulated using the information from the original technical drawings and measurements on site; starting from the core up to the iron final door. The external device built to transport the samples to the irradiation position was not simulated because it does not affect the flux values and behaviour inside the column. Fig. 4.33 is a view of the column with an acrylic box placed in the irradiation position, with the channel filled with blocks of graphite. The bismuth blocks are visible, in green.

The acrylic box simulated in this calculation was equal to the one used to measure the thermal flux in air by means of thin cobalt foils. The calculation was intended to validate the code by comparing the experimental results and the MCNP results. When analyzing the results of MCNP, an important issue must be taken into account: the core model was built considering new fuel bars, with homogeneous composition. This simplification surely caused the MCNP results to be slightly different from the measured data. Measurements of the thermal neutron flux made by cobalt foils activation gave different results with different core configurations. The currents from SPNDs also changed with the modification of the core for a fixed reactor nominal power. Nevertheless, with the same nucleus configuration, the currents were reproducible in all the measurement sets performed. In Tab. 4.4, three different measurements of the thermal neutron flux performed with three core configurations in the center of the acrylic box surface facing the core are reported.

Table 4.4: Results of thermal neutron flux measurements performed with different reactor core configurations, and corresponding values of the currents collected by SPNDs

Thermal neutron flux ($cm^{-2}s^{-1}$)	SPND current (A)
$(6.8\pm 0.4)\cdot 10^{9}$	$1.38\cdot 10^{-11}$
$(8.2\pm 0.5)\cdot 10^{9}$	$1.67\cdot 10^{-11}$
$(9.0\pm 0.5)\cdot 10^{9}$	$1.84\cdot 10^{-11}$

The F4 tally was required in the position of the cobalt foil during the measurement. The result of the simulation for an F4 tally at that point was $(8.4 \pm 0.2)\cdot 10^{9}$ cm^{-2} s^{-1}, that is in good agreement with the measurement performed to date. The discrepancies between the calculations and the measured data depend on the simplified model of the source. This might involve inaccuracies in the neutron distribution which a KCODE calculation with an accurate reproduction of the fuel burnup would not. The plans for the future involve the use of a permanent monitor to determine the correction factor between the measured neutron flux in a certain core configuration and the calculated flux in the monitor position. The MCNP results would be adjusted by this factor to be used for treatment planning purposes.

4.6 Other BNCT applications developed in Argentina

The most advanced clinical area of the BNCT project in Argentina is the treatmnet of skin melanoma: a Phase II clinical trial, began in 2003 and is currently underway. The irradiation facility for Melanoma BNCT treatment was built at the Centro Atómico Bariloche (CAB), where a mixed thermal and epithermal neutron beam was extracted from the reactor RA-6, characterized and theoretically analyzed [72]. The first boron biodistribution studies began in 2001, in collaboration with the radiation therapy group of the Roffo Institute of Oncology [73]. In 2003 the National Agency of Drugs, Food and Technology (ANMAT) and the Nuclear regulatory Agency (ARN) approved a Phase I/II BNCT clinical trial, to evaluate the efficacy and toxicity of BNCT for cutaneous Melanoma in extremities. The protocol foresees the inclusion of 30 patients, with a post-treatment follow up of at least 12 months. Currently, a dose escalation study to establish the maximum tolerance dose for the skin is planned. BNCT is a treatment for patients not amenable to surgery due to the spread of the disease and with no prior treatment with standard chemotherapy and/or radiotherapy. In October 2003, the first patient was irradiated at RA-6 after the biodistribution study. Positioning was simulated at the Centro Atómico Constituyentes (CAC, Buenos Aires) and the treatment planning was based on the CT scan of the extremity and the measured ^{10}B concentration in blood [18]. This first treatment resulted in a good clinical outcome with low toxicity, and further patients could be treated. To date,

7 patients have been irradiated with encouraging results, i.e. no late toxicity and tumour growth delay in all cases [74].

In 2005 ANMAT approved a boron biodistribution study in patients with incurable thyroid cancer, after successful preclinical research in mouse and dog models using different boron carriers. The biodistribution studies are carried out in collaboration with different medical centers in Buenos Aires [75].

The other BNCT application that is currently being studied and developed is the treatment of liver metastases using a modification of the autotransplantation technique employed in Pavia as described in Section 4.5.2 in more details.

Significant efforts are devoted to radiobiological research, to extend the BNCT field of application to other tumours and to study the efficacy of new boron carriers. Two animal models were developed and employed in BNCT studies: an oral cancer model in the hamster cheek pouch [76] and an undifferentiated thyroid cancer model [77]. The studies in the hamster cheek pouch oral cancer model involve BNCT mediated by BPA and GB-10, a new boron carrier that was shown to cause selective effect in the tumour despite the fact that it is not selectively incorporated into tumour cells. As already mentioned in Chapter 1, this effect on the tumour depends on the higher radiosensitivity of the tumour blood vessels, due to the tumoural angiogenic process [35]. Within the context of this research field, a collaboration was born between the group coordinated by A. Schwint and ours. The aim is to collaborate on the technology, the procedures to measure boron concentrations and to visualize boron distributions by means of neutron autoradiography. Samples of oral hamster tumours, healthy liver and lung have already been sent to us. Some of them were used for quantitative measurements by α spectrometry and others to obtain radiographic images of the pouch sections. Fig. 4.34 is a comparison between a radiographic image of a section of precancerous pouch tissue from an animal injected with BPA and the histologic preparation of an adjacent section. These preliminary studies suggest differencies in boron uptake by the different tissue areas. This effect will be further investigated with a new series of autoradiographies.

The preliminary quantitative results are currently under evaluation. We report here the result of the first run of measurements, with a comparison between α spectrometry and ICP-AES performed at CAC (Centro Atómico Costituyentes), Buenos Aires (Tab. 4.5).

The values listed in Table 4.5 show that, apart from the hamster cheek pouch tumour and lung, the measurements are in good agreement, and further investigations are planned to better quantify BPA and the GB-10 uptake in the tissues and to verify the correspondence between BPA concentration values measured in lung and in liver using the two methods.

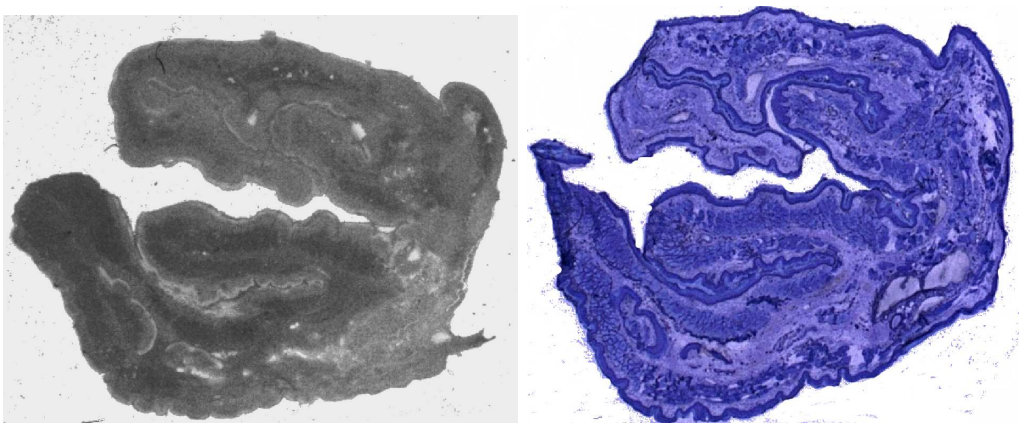

Figure 4.34: Comparison between the autoradiography of a hamster cheek pouch section (precancerous tissues) from an animal injected with BPA and the histologic preparation of an adjacent section. The different uptake by the different tissue areas can be seen in the grey scale image on the left.

Table 4.5: Comparison between α spectrometry and ICP-AES corresponding to samples of rat and the hamster cheek pouch oral cancer model following administration of BPA or GB-10

Tissue/protocol	GB-10 (50 mg ^{10}B/Kg)		BPA (31 mg ^{10}B/Kg)	
	Pavia	CAC	Pavia	CAC
Rat Liver	8.8± 0.4	8.5± 6.2	14.7± 0.9	17.9± 0.6
Rat Lung	23.2± 3.3	14.0± 6.3	16.0± 1.3	21.7± 6.2
Hamster Oral Tumour	68.9± 6.0	31.9± 21.4	29.6± 5.5	33.3± 17.4
Hamster Liver	38.1± 3.5	27.9± 11.0	13.9± 2.8	11.4± 4.5
Hamster Lung	68.4± 2.2	26.5± 23.1	15.7± 2.5	6.2± 2.6

Conclusions and Future Perspectives

Boron Neutron Capture Therapy is an experimental form of radiotherapy that has been studied and applied to a variety of tumours since the first clinical trials performed in the 1950s at the Brookhaven National Laboratories, USA. The selective boron uptake in the tumour makes this technique advantageous especially when the conventional treatments fail such as in the case of the metastatic disseminations. This characteristic demands to irradiate an entire organ or a large area of it with no need to know the precise spatial distribution of the tumoural nodules: the selectivity of the therapy is achieved by the drug targeting rather than by the irradiation field. Besides, the possibility to destroy also small sized nodules, that cannot be diagnosed before the treatment, gives a chance to lower the probability of tumour recurrence.

The application of BNCT to diffuse tumours is the research topic of our group since the first feasibility study dedicated to the autotrasplantation method, that lead to the treatment of two patients affected by hepatic metastases from colon adenocarcinoma [45]. Besides, a study on the BNCT application to lung tumours is being carried out, justified by the lack of effective treatments for many of the extremely aggressive diseases that can affect this organ. The strategies that were proposed for the metastases of the liver and the lung tumours are meant to take the best of the BNCT concept. Firstly, the liver can be extracted and irradiated in the Thermal Column in order to create a uniform thermal neutron field inside the organ, which is otherwise difficult to obtain inside the body because of the mass and position of the organ. Secondly, the lung can be irradiated using external collimated epithermal neutron beams, exploiting their penetration capability and the low density of the lung tissues. These strategies, concerning the liver research and the preliminary indications of the lung research, were presented in this thesis (Chapters 2, 3, 4). As a future plan for the study of the external irradiation of a human thorax, the employ of other anthropomorphic phantoms was planned. Apart from the voxel models, which are more precise in the organs definition and in the materials differentiation, a female model shall be used. EVE, the female counterpart of ADAM, cannot be irradiated using two opposite beams antero-posterior and postero-anterior, due to the presence of breast tissues. For

this reason an irradiation with a posterior-anterior and a lateral beams could be tested.

The encouraging results of the clinical phase of the liver research gave rise to other projects around the world to apply BNCT to hepatic metastases with the autotrasplant technique. Presently we are collaborating with three research groups, which are th University of Mainz, ENEA Casaccia (Rome) and CNEA (Comisión Nacional de Energia Atómica), Buenos Aires. The simulations and experimental measurements that we performed in the interest of these projects were also described showing how the methods invented and applied in Pavia could be further improved (Chapter 4). In particular we proposed a new configuration of the irradiation facility to ensure a better uniformity of the thermal neutron flux inside the liver with a set-up easy to realize. This purpose was taken into account for the modification of the thermal columns of the TRIGA reactors in Mainz and in Rome. The collaboration with CNEA, Argentina, is based on a sharing of experiences and measurement techniques, that would be helpful in the development of a new protocol for the liver treatment with partial autotrasplant. This project was inspired by the research made in Pavia, but tries to overcome the troubles associated with the anhepatic phase that the patient would undergo with the original Pavia technique. The future of our liver research is bound to the developments of these projects and to the possibility to re-start a clinical phase, with more patients, in order to obtain significant statistics in the results. As explained in Chapter 1, the effects of the treatment are to be fully understood especially from the clinical point of view, and further evaluation are essential to optimize the protocols.

The studies for the lung BNCT application gave encouraging preliminary results, both in the ^{10}B pharmacokinetic and in the dose distribution simulations point of view (Chapters 2 and 3). The next step will be a test of the whole procedure on rats with lung metastases, that will be infused with BPA and irradiated with an external neutron beam. The aim is to verify the BNCT effects on the tumour and on the surrounding healthy organs. To this end an horizontal channel of the TRIGA reactor will be dedicated to the realization of a neutron beam for little animals irradiations. The same channel will be used also for the realization of a Prompt Gamma Neutron Activation Analysis facility. The irradiation of a human thorax by using external neutron beams makes it necessary to have a good dosimetry in all the interested structures, toghether with information on the boron concentrations in all the tissues and blood. For the ^{10}B measurements in liquid samples or in tissues that cannot be cut into thin slices, a different method than α spectrometry is needed. The design of the beam is performed at present, and in the near future the realization and characterization of this beam is planned.

Another topic that we are exploring is the test of new borated compounds. *In vitro* analysis were scheduled for the uptake measurement of new generation drugs in DHD/K12/Trb cells. The substances in question are sugar-based carboranes, that have the property to carry ^{10}B atoms per molecule and have been previously demonstrated to have a good uptake in tumoural cells [78]. A group from the University of Firenze studied the possibility to fill liposomes with the icosahedral

carborane cage and two of its sugar derivatives [38]. The sugars could be an advantageous medium to carry the boron atoms inside the cell nucleus, being the building units mostly required by tumoural cells. Besides, liposomes are generally considered as efficient drug carriers. In particular cationic liposomes could be suitable BNCT carriers because they form stable complexes with BPA. The results of the study were that glucosyl and lactosyl carboranes were uptaken by the tested liposomes with high efficiency. In this way, the number of loaded liposomes to carry the right amount of boron into the cell nucleus would be low, and the BNCT would be far more effective. The first step of this research demonstrated that such kind of carriers can be easily produced, the next one will test their ability to carry the boron atoms inside the cells. This phase will be carried out at our laboratories, using the rat colon carcinoma cell line.

Appendix: the Monte Carlo method used to reproduce the experimental spectra

The method used for the study of the energy spectra obtained by thermal neutron irradiation of tissue samples with boron is described in this appendix.

A lung sample with boron and the detector geometry were simulated in a Monte Carlo code, in which the charged particles from the neutron interaction with the tissue elements were extracted, according to the cross sections of the reactions involved and the geometry of the apparatus. The tissue sample was simulated using the elemental composition of Tab. 2.3, which refers to the dry lung tissue. A boron concentration equal to the experimantal value as described in Chapter 2 was chosen: 4.0 ppm for a healthy sample and 13.3 for a tumoural one.

To compare the simulated and the measured spectra the mean number of reactions with boron and nitrogen were evaluated using their concentration and the cross sections of the processes involved. The total number of reaction is:

$$R = (n_B \sigma_B + n_N \sigma_N) V \phi t \tag{4.2}$$

where:

- σ_B is the microscopical cross section of the reaction on ^{10}B, 3837 b;
- σ_N is the microscopical cross section of the reaction on ^{14}N, 1.8 b;
- n_B and n_N are the number of ^{10}B and of ^{14}N atoms per unit of volume respectively;
- V is the total volume of the sample;
- ϕ is the neutron flux, $2.2 \cdot 10^9$ cm^{-2} s^{-1};
- t is the irradiation time.

Including V in the expression between brackets, the total number of ^{10}B and ^{14}N nuclei can be expressed as:

$$n_B V = (ppm \cdot 10^{-6} N_A / m_B) \cdot M \tag{4.3}$$

$$n_N V = (g\%(N) \cdot 10^{-2} N_A / m_N) \cdot M \tag{4.4}$$

where ppm is the boron concentration in parts per million, N_A is the Avogadro number, m_B and m_N are the atomic mass in grams of boron and nitrogen, M is the total mass of the sample and g%(N) is the percentage in grams of nitrogen in lung tissue. All these quantities were known, so the total number of reactions to be simulated in the Monte Carlo was calculated.

To simulate the process we assumed that the boron and nitrogen distributions were uniform in the sample. We analyzed a tumoural sample with 58 ppm of boron in the dry tissue which corresponds with $58 \cdot 0.23 = 13.3$ ppm in the fresh lung, and a healthy sample with 19.6 ppm of boron in the dry tissue which corresponds with $19.6 \cdot 0.23 = 4.5$ ppm in the fresh lung. The initial flight directions were isotropic in the 4π solid angle, but the geometric efficiency of the system lowered the angle to 2π. The first step was a Monte Carlo code that sampled the coordinates of the starting points of α, ^{7}Li and protons, the initial directions and the energies of the particles, taking into account the probabilities of the reactions branches. In order to verify if the Monte Carlo simulation was correct, we checked the uniformity of the sampling: in Fig. 4.35 the uniformity of the particles starting points in the tissue disk is reported, and in Fig. 4.36 the distribution of the sampling regarding the tissue depth, which is the third spatial coordinate that determines the starting point of a particle, is reported.

The uniformity of the distribution is a proof of the correct sampling in the Monte Carlo code. In this graph we can also check that the experimental ranges of the three radiation components were respected: 10.77 μm for the protons, 6.5 μm for the α and 4 μm for ^{7}Li respectively. In fact, the particles were uniformly sampled in a tissue thickness larger than the maximum proton range, and the histograms contains only information of the particles that had enough residual energy to be detected; in other words: the particles that were born in a depth less than their maximum range in lung tissue.

The results of this first Monte Carlo run were used as an input for SRIM, that uses the package TRIM (TRansport of Ions in Matter) which actually transported the different particles sampled in three separate calculations. The slab of material defined in SRIM was a compound with the composition of dry lung, as reported in the Tab.2.3. The results of the runs were three tables reporting the information on the position of the exit points and the residual energy of the particles. The energy data had to be corrected for the resolution of the silicon detector: they were broadened using a Gaussian function with the following standard deviations: 0.04 for α, 0.10 for protons and for ^{7}Li. In Fig.2.16 the three different components of the spectrum and the total histogram are shown for a healthy sample. The histograms of the residual energy were compared to the experimental results. The comparison between the measurement and the calculation for two samples of 50

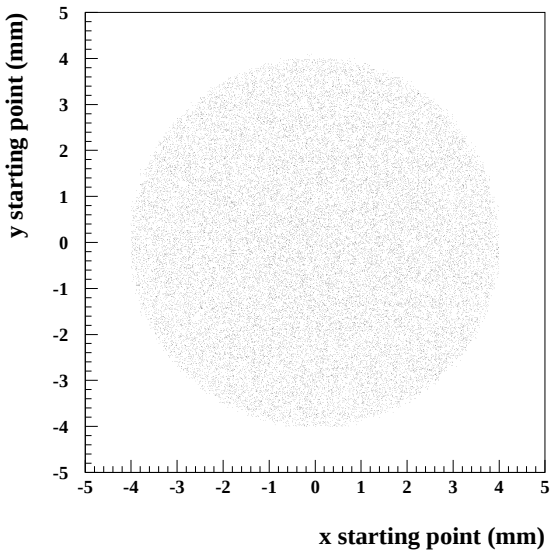

Figure 4.35: Scatter plot of the starting points of the α particles at a fixed depth. The uniformity of the distribution ensures that the starting point were correctly sampled.

μm (fresh sample thickness) were shown in Fig. 2.18 and 2.19, referring to an healthy and a tumoural thickness respectively.

The good agreement between simulation and experimental results proved that the experimental method gave a correct evaluation of the boron concentration in tissues, because the measured values were used to perform SRIM simulations and the resulting spectra were highly comparable.

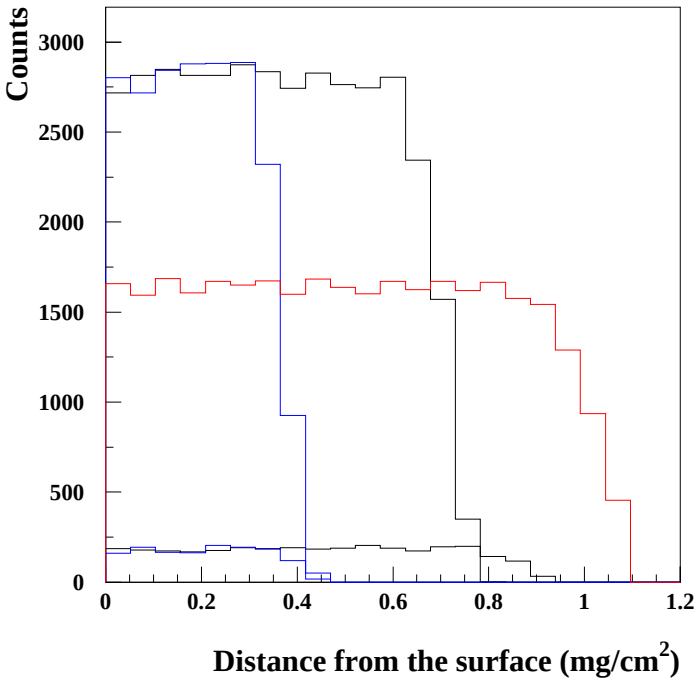

Figure 4.36: Distributions of the depths from which each particle started: red: protons, black: α and blue: ^{7}Li. The α and Li spectra have also a component at higher energy. The spatial coordinate along the depth of the tissue slice was sampled uniformly in the tissue thickness. The histograms refer to the particles that were detected, i.e. the ones with enough residual energy to exit from the tissue

Bibliography

[1] C.Soyland, S.P.Hassifjel, "Survival of Human Lung Epithelial Cells Following In Vitro Alpha-particle Irradiation with Absolute determination of the number of Alpha-particle Traversals of Individual Cells" Int. J. Rad. Biol. 76, 1315-1322 (2000)

[2] G.L.Locher, "Biological Effects and therapeutical possibilities of neutrons", Am. J. Roentgenol. Radium. Ther. 36, 1-13 (1936)

[3] L.E.Farr, W.H.Sweet, J.S.Robertson, G.S.Forster, H.B.Locksley, D.L.Sutherland, M.L.Mendelsohn, E.E.Stickey, "Neutron Capture Therapy with Boron in the treatment of Glioblastoma Multiforme", Am. J. Roentgenol. 71, 279-291 (1954)

[4] A.K.Asbury, R.G.Ojeman, S.L.Nielsen and W.H.Sweet, "Neuropathologic study of fourteen cases of malignant brain tumour treated by boron-10 slow neutron capture therapy", J. Neuropathol. Exp. Neurol. 31, 278-303 (1972)

[5] H.Hatanaka, "Clinical experience of boron-neutron capture therapy for gliomas-a comparison with conventional chemo-immuno-radiotherapy", In: H.Hatanaka ed Boron Neutron Capture Therapy for Tumours. Nishimura Co., Niigata 349-379 (1986)

[6] H.Hatanaka, Y.Nakagawa, "Clinical results of long-surviving brain tumour patients who underwent boron neutron capture therapy", Int. J. Radiat. Oncol. Biol. Phys. 28,1061-1066 (1994)

[7] Y.Nakagawa, H.Hatanaka, "Boron neutron capture therapy: clinical brain tumour studies", J. Neuro-Oncol. 33, 105-115 (1997)

[8] J.A.Coderre, E.E.Elowitz, M.Chadha, R.Bergland, J.Capala, D.D.Joel, H.B.Liu, D.N.Slatkin and D.A. Chanana, "Boron neutron capture therapy of glioblastoma multiforme using the p-borophenylalanine-fructose complex and epithermal neutrons: tryal design and early clinical results", J. Neuro-Oncol. 33, 141-152 (1997)

[9] A.Z.Diaz, A.D.Chanana, J.A.Coderre, R.Ma, "Retrospective review of the clinical BNCT trial at Brookhaven National laboratory", in Proceedings of the Ninth International Simposium on Neutron Capture Therapy for Cancer, Osaka 13-14 (2000)

[10] H.Madoc-Jones, R.Zamenhof, G.Solares, O.Harling, C-S.Yam, K.Riley, S.Kiger, D.Wazer, G.Rogers and M.Atkins, "A phase-I dose escalation trial of boron neutron capture therapy for subjects with subcutaneous melanoma of the extremities", in Y.Mishima ed, Cancer Neutron Capture Therapy, 707-716, Plenum Press, New York (1996)

[11] P.Busse, O.K.Harling, M.R.Palmer, W.S.Kiger, J.Kaplan, I.Kaplan, C.Chuang, J.Y.Goorley, K.Riley, T.H.Newton, G.A.Santa Cruz, X-Q.Lu and R.G Zamenhof, "A critical examination of the results from the Harward-MIT NCT program phase I clinical trial on neutron capture therapy for intracranial disease", J.Neuro-Oncol. 62, 111-121 (2003)

[12] R.L.Moss, "Progress towards boron capture therapy at the High Flux Reactor Petten", Basic Life Sci. 54, 169-183 (1990)

[13] D.Gabel and R.L.Moss editors, "Boron neutron capture therapy: toward clinical trials of glioma treatment" Plenum Press, New York (1992)

[14] W.Sauerwein et al. "Postoperative Treatment of glioblastoma with BNCT at the Petten irradiation facility", EORTC Protocol 11961 (1999)

[15] J.Capala, B.H.Stenstam, K.Skold, P.M Af Rosenschold, V.Giusti, C.Persson, E.Wallin, A.Brun, L.Franzen, J.Carlsson, J.Salford, C.Cerberg, B.Persson, L.Pellettieri, R.Henriksson, "Boron neutron capture therapy for glioblastoma multiforme: clinical studies in Sweden", J. Neuro-Oncol. 62(1-2) 135-144 (2003)

[16] H.Joensuu, L.Kankaanranta, T.Seppälä, I.Auterinen, M.Kallio, M.Kulvik, J.Laakso, J.Vähä talo, M.Kortesniemi, P.Kotiluoto, T.Seren, J.Karila, A.Brander, E.Järviluoma, P.Ryynänen, A.Paetau, I.Ruokonen, H.Minn, M.Tenhunen, J.Jääskeläinen, M.Färkkilä, and S.Savolainen, "Boron neutron capture therapy of brain tumours: clinical trials at the Finnish facility using borophenylalanine" J. Neuro-Oncol. 62(1-2) 123-134 (2003)

[17] T.Pinelli, A.Zonta, S.Altieri, S.Barni, A.Braghieri, P.Pedroni, P.Bruschi, P.Chiari, C.Ferrari, C.Zonta, "TAOrMINA: from the first idea to the application to the human liver", in: W.Sauerwein, R.Moss, A.Wittig, eds Research and Development in Neutron Capture Therapy. Bologna, Monduzzi Editore 1065-72 (2002)

[18] S.J.Gonzáles, M.R.Bonomi, G.A.Santa Cruz, H.R.Blaumann, O.A.Calzetta Larrieu, P. Menéndez, R.Jiménez Rebagliati, J.Longhino, D.B.Feld, M.A.Dagrosa, C.Angerich, S.G.Castiglia, D.A.Batistoni, S.J.Libermann, and

B.M.Roth, "First BNCT treatment of a skin melanoma in Argentina: dosimetric analysis and clinical outcome", Appl. Rad. Isotop. 61, 1101-1105 (2004)

[19] A.Wittig et al. "Early phase II study on BNCT in metastatic malignant melanoma using the boron carrier BPA", EORTC Protocol 11011 (2003)

[20] J.Burian, M.Marek, J.Ratai,et al. "Report on the first patient group of the phase I BNCT trial at the LVR-15 reactor", in: Sauerwein W, Moss R, Wittig A, editors. Research and Development in Neutron Capture Therapy, Bologna, Monduzzi Ed., 1107-1112 (2002)

[21] M.Suzuki, Y.Sakuray, S.Masunaga, Y.Kinashi, K.Nagata, A.Maruhashi, K.Ono, "Feasibility of boron neutron capture therapy (BNCT) for malignant pleural mesothelioma from a viewpoint of dose distribution analysis", Int. J. Radiat. Oncol. Biol. Phys. 66, 1584-89 (2006)

[22] S.Altieri, S.Bortolussi, P.Bruschi, F.Fossati, K.Vittor, R.Nano, A.Facoetti, P.Chiari, J.Bakeine, A.Clerici, C.Ferrari, O.Salvucci, "Boron Absorption Imaging in Rat Lung Colon Adenocarcinoma Metastases", J. of Phys. Conf. Series. 41, 123-126 (2006)

[23] "MCNP^{TM}-A General Monte Carlo N-Particle Transport Code", Version 4C, Judith F. Briesmeister, Editor, LA-13709-M (2000)

[24] S.Bortolussi, S.Altieri, P.Bruschi, P.Chiari, F.Fossati, A.Facoetti, R.Nano, A.Clerici, C.Ferrari, A.Zonta, C.Zonta, A.Marchetti, E.Solcia, J.J.Bakeine, O.Salvucci, "Boron Uptake Measurements in metastatic Tumours in Rat Lung", in Y.Nakagawa,T.Kobayashi, H.Fukuda, eds. Advances in Neutron Capture Therapy. pp 91-94, Takamatsu, Japan (2006)

[25] S.Altieri,S.Bortolussi, P.Bruschi, P.Chiari, F.Fossati, A.Facoetti, R.Nano, A.Clerici, C.Ferrari, A.Zonta, C.Zonta, A.Marchetti, E.Solcia, J.J.Bakeine, O.Salvucci, "Monte Carlo Dose Calculations for BNCT treatment of Diffuse Human Lung Tumours", in Y.Nakagawa,T.Kobayashi, H.Fukuda, eds. Advances in Neutron Capture Therapy. pp 91-94, Takamatsu, Japan (2006)

[26] J.L.Kiger, W.S Kiger, H.Patel, P.J.Binns, K.J.Riley, J.W.Hopewell, O.K.Harling and J.A.Coderre, "Effects of boron neutron capture therapy irradiation on the normal lung of rats", Appl. Radiat. Isot. 61, 969-973 (2004)

[27] V.A.Nievaart, R.L.Moss, J.L.Kloosterman, T.H.J.J.van der Hagen, H.van Dam, A.Wittig, M.Malago, and W.Sauerwein, "Design of a Rotating Facility for Extracorporal Treatment of an Explanted Liver with Disseminated Metastases by Boron Neutron Capture Therapy with an Epithermal Neutron Beam", Rad. Res. 166, 81-88 (2006)

[28] I.Kato, K.Ono, Y.Sakurai et al., "Effectiveness of BNCT for recurrent head and neck malignancies", Appl. Radiat. Isot. 61, 1069-1072 (2004)

[29] M.Suzuki, K.Nagata, S.Masunaga, et al, "Biodistribution of ^{10}B in a rat liver tumour model following intra-arterial administration of sodium borocaptate (BSH)/degradable starch microspheres (DSM) emulsion", Appl. Radiat. Isot. 61, 933-937, (2004)

[30] M.Suzuki, Y.Sakurai, S.Hargiwara, S.Masunaga, Y.Kinashi, K.Nagata, A.Murahashi, M.Kudo and K.Ono, "First Attempt of Boron Neutron Capture Therapy (BNCT) fro Hepatocellular Carcinoma", Jpn. J. Clin. Oncol. 37(5), 376-381, (2007)

[31] "Advances in Neutron Capture Therapy",ed. by Y.Nakagawa, T.Kobayashi, H.Fukuda, Takamatsu, Kagawa, Japan (2006)

[32] R.F.Barth, J.A.Coderre, M.Graca H.Vicente and T.E.Blue, "Boron Neutron Capture Therapy of Cancer: Current Status and Future Prospects", Clin. Cancer Res. 11(11), 3987-4002 (2005)

[33] S.Chandra, G.W.Kabalka, D.R.Lorey II, D.R.Smith, A.Coderre, "Imaging of Fluorine and Boron from Fluorinated Borophenylalanine in the same cell at organelle resolution by correlative ion microscopy and confocal laser scanning microscopy", Clin. Canc. Res. 8, 2675-2683 (2002)

[34] P.Carmeliet and R.K.Jain, "Angiogenesis in cancer and other deseases", Nature 407, 249-264 (2000)

[35] V.A.Trivillin, E.M.Heber, M.E.Itoiz, O.Calzetta, H.Blaumann, J.Longhino, and A.Schwint, "Therapeutic Success of Born Neutron Capture Therapy (BNCT) Mediated by a Chemically Non-selective Boron Agent in an Experimental Model of Oral Cancer: A New Paradigm in BNCT Radiobiology", Rad. Res. 166, 387-396 (2006)

[36] C-W.Lu, Y.Hung, "Bifunctional magnetic silica nanoparticles for highly efficient human stem cell labeling", Nano Letters, 7, 149-154 (2007)

[37] Q.Wei, E.B.Kullberg, L.Gedda, "Trastuzumab-conjugated boron-containing liposomes for tumor-cell targeting; development and cellular studies", Int. J. Onc. 23, 1159-1165 (2003)

[38] S.Ristori, J.Oberdisse, I.Grillo, A.Donati, O.Spalla, "Structural Characterization of Cationic Liposomes Loaded with Sugar-Based Carboranes", Bioph. J. 88, 535-547, (2005)

[39] T.U.Probst, "Methods for boron analysis for boron neutron capture therapy (BNCT).A review", Fresenius J. Anal. Chem. 364, 391-403 (1999)

[40] http://www.emedicine.com

[41] T.Pinelli, S.Altieri, F.Fossati, A.Zonta, C.Ferrari, U.Prati, L.Roveda, S.Ngnitejeu Tata, S.Barni, D.M Ferguson, "Operative modalities and Effects of BNCT on liver metastases from colon adenocarcinoma", in:

M.F.Hawthorne,K.Shelly, R.J.Wiersema, eds. Frontiers in Neutron Capture Therapy. New York:Kluwer Academic, Plenum Publishers, 1427-40 (2001)

[42] A.Cagnard, M.S.Martin, M.F.Michel, and F.Martin, "Interaction between two cellular subpopulations of a rat colonic carcinoma when inoculated to the syngeneic host", Int. J. Cancer, 36 273-279, (1985)

[43] D.Chiaraviglio, F.De Grazia, A.Zonta, S.Altieri, A.Braghieri, F.Fossati, P.Pedroni, T.Pinelli, A.Perotti Specchairello, G.Perlini, H.Rief, "Evaluation of selective Boron absorption in liver tumours", Strahlentherapie und Onkologie 165(2/3), 170-172 (1989)

[44] A.Braghieri, "Sviluppo di una metodologia per la misura di concentrazione di Boro mediante la reazione nucleare ^{10}B(n,α)^{7}Li indotta da neutroni termici", degree thesis 1986/1987

[45] A.Zonta, U.Prati, L.Roveda, C.Ferrari, S.Zonta, A.M.Clerici, C.Zonta, T.Pinelli, F.Fossati, S.Altieri, S.Bortolussi, P.Bruschi, R.Nano, S.Barni, P.Chiari and G.Mazzini, "Clinical lessons from the first applications of BNCT on unresectable liver metastases" J.of Phys.: Conf Series, 41, 484-495 (2006)

[46] C.Ferrari, A.Clerici, G.Mazzini, C.Zonta, S.Altieri, S.Bortolussi, F.Fossati, P.Bruschi, P.Chiari, P.Dionigi, A.Zonta, "The BNCT Resistant Fraction of Cancer Cells: an *In Vitro* Morphologic and Cytofluorimetric Study on Rat Colocarcinoma Cell Line" in Y.Nakagawa,T.Kobayashi, H.Fukuda, eds. Advances in Neutron Capture Therapy. pp 98-101 Takamatsu, Japan (2006)

[47] ICRU report 46. Photon,electron,proton and neutron interaction data for body tissues. International Commission on radiation Units and Measurements. Bethesda. MD(1992)

[48] R.Kramer, M.Zankl, G.Williams, G.Drexler, "The calculation of Dose from External Photon Exposures Using Reference Human Phantoms and monte Carlo Methods. Part I: The Male (ADAM) and female (EVE) Adult Mathematical Phantoms", GSF-Report S-88. Reprint July 1999. Institut fur Strhlenschutz GSF-Forschungszentrum fur Umwelt und Gesundheit, Neuherberg-Munchen, (1982)

[49] L.Casalini "Applicazione dei codici SABRINA ed MCNP al fantoccio antropomorfo ADAMO" CT WCD 00005 ENEA Internal report (1994)

[50] G.Gualdrini, L.Casalini, B.Morelli, "Monte Carlo Technique Applications in the field of Radiation Dosimetry at the ENEA RAdiation Protection Institute: a Review" RT/AMB/94/34 (Fourth Conference on Rad Prot Dosim, Orlando, Florida 1994)

[51] W.S.Sydner, M.R.Ford, G.G.Warner, "Estimated of absorbed fractions for monoenergetic photon sources uniformly distributed in various organs of a heterogeneous phantom", MIRD Phamplet No.5, revised, Society of Nuclear Medicine, New York (1978)

[52] ICRP-Report of the Task Group on Reference Man. ICRP Publication 23. Internal Commission on Radiological Protection, Pergamon Press, Oxford (1975)

[53] J.A.Coderre, J.C.Turcotte, K.J.Riley, P.J.Binns, O.K.Harling, W.S.Kiger, "Boron Neutron Capture Therapy: Cellular Targeting of High Linear Energy Transfer Radiation", Technology of Cancer Research & Treatment ISSN 1533-0346, vol 2, nr 5 (2003)

[54] J.A.Coderre, J.M.Morris, "The Radiation Biology of Boron Neutron Capture Therapy", Rad. Res. 151, 51-81 (1999)

[55] J.A.Coderre, M.S Makar, P.L.Micca et al. "Derivation of relative biological effectiveness for the high-let radiations produced during boron neutron capture irradiations of the 9L rat gliosarcoma in vitro and in vivo", Int. J. Radiat. Oncol. Biol. Phys. 27, 1121-9 (1993)

[56] F.M.Kong, J.A. Hayman, K.A. Griffith et al., "Final toxicity results of a radiation dose escalation study in patients with non-small cell lung cancer (NSCLC): predictors for radiation pneumonitis and fibrosis", Int. J. Radiat. Oncol. Biol. Phys. 65, 1075-86 (2006)

[57] K.J.Riley and O.K.Harling, "An improved prompt gamma neutron activation analysis facility using a focused diffracted neutron beam", NIM B 143, 414-421 (1998)

[58] K.W.Burn, L.Casalini, S.Martini, M.Mazzini, E.Nava, C.Petrovich, G.Rosi, M.Sarotto, R.Tinti, "An Epithermal Facility for Treating brain Gliomas at the TAPIRO Reactor", in: Applied Rad and Isotopes/ ICNCT-11 61-5 987-991, Elsevier Publisher, Boston (2004)

[59] S.Bortolussi and S.Altieri, "Thermal Neutron irradiation Field Design for Boron Neutron Capture Therapy of Human Explanted Liver", Med. Phys. in press

[60] Technical Foundation of Triga, General Atomics, San Diego (1958)

[61] B.E.Watt, "Energy spectrum of neutrons from thermal fission of ^{235}U", Phys. Rev. 87 (1952)

[62] K.H.Beckurts, K.Wirtz, "Neutron Physics", Springer Verlag, Berline (1964)

[63] C.H.Wetscott, "Effective Cross Sections Values of Well Moderated Therma Reactor Spectra", Report AECL no 1101 (1960)

[64] C.H.Wetscott, W.H.Walker, T.K.Alexander, "Effective Cross Section and Cadmium Ratios for the Neutron Spectra of Nuclear Reactors", in Proceedings of the International Conference on the Peaceful Uses of Atomic Energy, Geneva, 1958, P/202 70, (USA, New York 1959)

[65] J.H.Lamarsh, "Introduction to Nuclear Engineering", Addison-Wesley Publishing Company, New York (1975)

[66] ATTILA - 3D multi-group Sn particle transport code, version 6, Transpire, Inc. (2005).

[67] J.Cardoso, V.Trivillin, E.Heber, D.Nigg, O.Cazetta, H.Blaumann, J.Longhino, M.Itoiz, E.Bumaschny, E.Pozzi, A.Shwint, "Effect of Boron Neutron Capture Therapy (BNCT) on Normal Liver Regeneration: Towards a Novel Therapy for Liver Metastases", Int. J. Radiat. Biol. 83(10), 699-706 (2007)

[68] M.E.Miller, L.E.Mariani, M.L.Sztejnberg Gonçalves-Carralves, M.Skumanic, S.I.Thorp, "Implantable self-powered detector for on-line determnation of neutron flux in patients during NCT treatment" Appl. Radiat. Isot. 61, 1033-1037 (2004)

[69] M.Miller, *Personal Communication*

[70] V.Crawley and M.A. Gadan, "Caracterización preliminar de la facilidad de irradiación de muestras biológicas del reactor RA-3 para implementación del tratamiento de metástasis en hígado con BNCT", 2007, degree tesis

[71] X-5 Monte Carlo Team, "MCNP - A General Monte Carlo N-Particle Transport Code, Version 5", April 24, 2003 (Revised 10/3/05) LA-UR-03-1987

[72] H.R.Blaumann, S.J.González, J.Longhino, G.A.Santa Cruz, O.A.Calzetta Larrieu, M.R.Bonomi, B.M.C.Roth, "Boron neutron capture therapy of Skin Melanomas at the RA-6 reactor: a procedural approach to beam set up and performance evaluation for upcoming clinical trials", Med. Phys. 31(1), 70-80 (2004)

[73] S.Liberman, A.Dagrosa, R.Jimenéz Rebagliati, M.Bonomi, B.Roth, L.Turjanski, S.Castiglia, S.González, P.Menéndez, R.Cabrini, M.Roberti, D.Batistoni, "Biodistribution studies of borophenylalanine- furctose in melanoma and brain tumour patients in Argentina", Appl. Radiat. Isot. 61, 1095-1100 (2004)

[74] B.M.Roth, M.R.Bonomi, S.J.González, R.J.Rebagliati, P.Menénedez, G.A.Santa Cruz, M.R.Casal, H.R.Blaumann, O.A.Calzetta Larrieu, D.Feld, D.Batistoni, J.Longhino, S.Castiglia, S.J.Liberman, "BNCT Clinical Trials of Skin Melanoma patients in Argentina", in: Y.Nakagawa, T.Kobayashi, H.Fukuda ed., Advances in Neutron Capture Therapy, Proceedings of ICNCT-12, Takamatsu, Kagawa, Japan (2006)

[75] A.Dagrosa, M.Viaggi, R.J.Rebagliati, V.Castillo, D.Batistoni, R.Cabrini, S.Castiglia, G.Juvenal, M.Pisarev, "Biodistribution of p-borophenylalanine (BPA) in dogs with spontaneous undifferentiated tyroid carcinoma (UTC)" Appl. Radiat. Isot. 61, 911-915, (2004)

[76] E.Kreimann, M.Itoiz, A.Dagrosa, R.Garavaglia, S.Farias, D.Batistoni, A.Schwint, "The Hamster Cheek Pouch as a Model of oral cancer for boron Neutron Capture Therapy Studies: Selective Delivery of Boron by Borophenylalanine" Canc. Res. 61, 8775-8781 (2001)

[77] A.Dagrosa, M.Viaggi, R.Cabrini, J.Dadino, G.Juvenal, M.Pisarev, "Selective Uptake of p-borophenylalanine (BPA) by Undiferentiated Carcinoma for Boron neutron Capture Therapy", Tyroid, 12(1) 7-12 (2002)

[78] L.F.Tietze, U.Bethe, U.Griesbach, M.Nakaichi, T.Hasegawa, H.Nakamura and Y.Yamamoto, "Ortho-Carboranyl Glycosides for the treatment of cancer by boron neutron capture therapy", Bioorg. Med. Chem. 9, 1747-1752 (2001)

List of publications

- S.Bortolussi and S.Altieri, "Thermal Neutron Irradiation Field Design for Boron Neutron Capture Therapy of human Explanted Liver", Med. Phys. in press

- S.Bortolussi, S.Altieri, P.Bruschi, P.Chiari, F.Fossati, A.Facoetti, R.Nano, A.Clerici, C.Ferrari, A.Zonta, C.Zonta, A.Marchetti, E.Solcia, J.Bakeine, O.Salvucci, "Boron Uptake Measurement in Metastatic Tumours in Rat Lung" in Y.Nakagawa, T.Kobayashi, H.Fukuda, eds. Advances in Neutron Capture Therapy. pp 91-94, Takamatsu, Japan (2006)

- S.Altieri, S.Bortolussi, P.Bruschi, P.Chiari, F.Fossati, A.Facoetti, R.Nano, A.Clerici, C.Ferrari, A.Zonta, C.Zonta, A.Marchetti, E.Solcia, J.Bakeine, O.Salvucci, "Monte Carlo Dose Calculations for BNCT Treatment of Diffuse Human Lung Tumours" in Y.Nakagawa, T.Kobayashi, H.Fukuda, eds. Advances in Neutron Capture Therapy. pp 500-503 Takamatsu, Japan (2006)

- C.Ferrari, A.Clerici, G.Mazzini, C.Zonta, S.Altieri, S.Bortolussi, F.Fossati, P.Bruschi, P.Chiari, P.Dionigi, A.Zonta, "The BNCT Resistant Fraction of Cancer Cells: an *In Vitro* Morphologic and Cytofluorimetric Study on Rat Colocarcinoma Cell Line" in Y.Nakagawa, T.Kobayashi, H.Fukuda, eds. Advances in Neutron Capture Therapy. pp 98-101 Takamatsu, Japan (2006)

- G.Gambarini, S.Agosteo, S.Altieri, S.Bortolussi, M.Carrara, S.Gay, M.Mariani, C.Petrovich, G.Rosi, E.Vanossi, "Dose Imaging with Gel Dosimeters in Phantoms Exposed in Reactor Thermal Columns Designed for BNCT" in Y.Nakagawa, T.Kobayashi, H.Fukuda, eds. Advances in Neutron Capture Therapy. pp 417-420 Takamatsu, Japan (2006)

- S.Altieri, S.Bortolussi, P.Bruschi, F.Fossati, K.Vittor, R.Nano, A.Facoetti, P.Chiari, J.Bakeine, A.Clerici, C.Ferrari, O.Salvucci, "Boron Absorption Imaging in Rat Lung Colon Adenocarcinoma Metastases", J.of Phys. Conf Series, 41, 123-126 (2006)

- A.Zonta, U.Prati, L.Roveda, C.Ferrari, S.Zonta, A.M.Clerici, C.Zonta, T.Pinelli, F.Fossati, S.Altieri, S.Bortolussi, P.Bruschi, R.Nano, S.Barni, P.Chiari and

G.Mazzini, "Clinical lessons from the first applications of BNCT on unresectable liver metastases" J.of Phys, Conf Series, 41, 484-495 (2006)

- S.Altieri, S.Bortolussi, "Application of Neutron Capture Therapy to Widespread Tumours", in Ricerca Scientifica ed Educazione Permanente: 11th International Conference on Nuclear reaction Mechanisms, vol. 126 pp 601-608, Milano (2006)

- S.Altieri, A.Braghieri, S.Bortolussi, P.Bruschi, F.Fossati, P.Pedroni, T.Pinelli, A.Zonta, C.Ferrari, U.Prati, L.Roveda, S.Barni, P.Chiari, R.Nano, "Boron Concentration imaging for BNCT", 5th International Conference on Isotopes, Brussel, Belgium (2005)

- S.Altieri, A.Braghieri, S.Bortolussi, P.Bruschi, F.Fossati, P.Pedroni, T.Pinelli, A.Zonta, C.Ferrari, U.Prati, L.Roveda, S.Barni, P.Chiari, R.Nano, "Neutron radiography of Human Liver Metastases after BPA Infusion" 11th World Congress on Neutron Capture therapy, Boston (2004)

Acknowledgements

I am deeply grateful to dr Saverio Altieri, who shared with me the birth of this ambitious BNCT project in Pavia. Thanks for the help, the discussions, the work hours spent together in these years, and for being the best tutor a phD student could look for.

A deep acknowledgement goes to dr Sander Nievaart who helped me through all my phD career and especially in preparing this thesis. I would like to thank him for the time that he dedicated to me and for the friendship that binds us. I really appreciate his personality and his way to face this work.

I would like to thank dr Raymond Moss who accepted to be the referee of this thesis and contributed to make it more complete and written in a better english.

I thank dr Kenneth W.Burn, for teaching me thousands of things regarding MCNP, for sharing conversations and scientific discussions.

Vorrei esprimere tutto l'apprezzamento per il lavoro del sig. Piero Bruschi, di cui ammiro l'esperienza, le capacità e il saggio punto di vista sulle cose. Un grazie e un "in bocca al lupo" a Sabrina, per l'avventura che sta iniziando. Grazie anche a tutti coloro che danno il proprio contributo al nostro esperimento: biologi, chimici e medici.

I am really grateful to dr Marcelo Miller who gave me hospitality in his research group, where I learned a lot and where I immediately felt at home. Thanks to dr Silvia Thorp, for showing me her precise and expert work in the laboratory.

For her incredible skill, experience and personality I would like to thank dr Amanda Schwint, because in her group I found competence, passion, and results. And because she is a friend. I really would like to be like her a day...

Special thanks to dr Sara Libermann, chief of the BNCT project in Buenos Aires, who I really admire.

For the advice, the support and the kind friendship I would like to thank prof. Wolfgang Sauerwein and dr Andrea Wittig.

I would like to thank prof. Jeffrey A. Coderre from MIT for sharing his experience and helping us in the lung project. We are proud to go on with our research supported by the results that he and his staff reached in Boston.

Hoping that our collaboration will be long and full of encouraging results, I thank dr Gabriele Hampel, dr Birgit Wortman and dr Arturo Lizon Aguilar for the discussions about the Mainz reactor and its simulations. In Mainz a special

greeting to Chris, with my best wishes for his career and life.

Ringrazio i miei genitori perchè con il tempo mi accorgo che il loro lavoro è sempre stato più difficile e importante del mio. Grazie alla loro presenza e alla loro convinzione sono potuta arrivare fin qui e posso sempre inventare nuovi obiettivi. Grazie a Claudia, più giovane, ma più grande e più saggia di me in tantissimi aspetti. Grazie al resto della famiglia per esserci sempre.

Special greetings to all the BNCT friends, especially to the ones that were at the young researchers meeting in Birmingham. To dr Silvio Nadalin, a cousin that I didn't know to have, I say "mandi, si viodin a Morsan!". I hope to see all of you in Florence, at the next ICNCT.

Quiero agradecer a todos los que en Argentina compartieron algo conmigo. Todos fueron importantes para mi, y el recuerdo de los días pasados allá me llena de nostalgia y de ganas de volver. Primero mil gracias van a Julián Pinto y a Mario Gadan, compañeros de: trabajo, jazz, rock, mate, conversaciones sobre películas, literatura, epistemología, sociedad, historia, viajes... paseos en la capital, pizzas, fiestas, cafés, Havanna, golosinas...los extraño un montón! Gracias a Emiliano, por llevarme a recorrer Buenos Aires con su maravillosa familia. Gracias a los chicos de los almuerzos en la cocina de Instrumentación y Control: Marcelo, por presentarme a la compañia y por invitarme a su casa, donde encontré una muy buena onda y estuve re-bien! Gracias al flaco Oscar por compartir una de mis pasiones más grandes, a Daniel, compañero y nuevo hermano, a Pablo mi paisano, a Pepe por hablarme de tango, a todos por preparar aquel asado que nunca me voy a olvidar! Gracias a las "damas de la BNCT", con ellas hice una reunión muy divertida de BNCT en el Departamento de Odontología de la UBA, y muchas otras cenas y conversaciones sobre ciencia y mucho más. Un saludo a los muchachos que trabajan en el reactor, sobre todo a Adrián. Gracias a la gente que conocí afuera del centro atómico, sobre todo a Daniela e Inés por abrirme la puerta y hospedarme como si nos conociéramos desde siempre...faltaba sólo Estela! En esa casa, gracias también a Ricardo y a su familia, encontré humanidad, historias, confianza, sabiduría, y pude comprender un poco más de las personas que quiero. Gracias a Nacho, Diego, y a sus padres, por el cariño que me mostraron. Gracias a Lelian y a Willy por hacerme sentir en mi casa.

Un "arrivederci in giro" ai miei compagni di dottorato, in particolare al Maira che mi mancherá moltissimo, e ad Irina e Lia con cui ho condiviso un'estate surreale al Dipartimento.

Ai vecchi amici tutta la mia riconoscenza per tutto quello che la loro presenza significa nella mia vita: senza di loro il senso di troppe cose sfuggirebbe altrove. Andrea: perchè nell'inaspettato corso degli eventi la tua prospettiva è quella che dà pienezza alla mia visione. Fede e Stefi: vicine o lontane siete voi a cui mi ispiro nelle infinite scelte che mi trovo a fare ogni giorno. Laura: sei un incredibile modello di donna, vivere con te mi ha insegnato tantissimo! Forna e Valeria: per dimostrarci che gli atti coraggiosi si possono compiere, e per farci vedere quanto rendano felici, Schiab: "...sogno un viaggio morbido, dentro al mio spirito...", Sabrina: perchè il suo affetto non mi lascia mai, Lo: per le lunghe chiacchierate sui nostri prediletti della letteratura e del cinema...e a tutti gli altri, che hanno

vissuto con me momenti che restano. Grazie a Lella e Pilo per una bellissima vacanza strappata alle fatiche della tesi, ci rivediamo presto!

Grazie a Estela perché la sua storia mi ha fatto capire quanta forza sia necessaria e si possa trovare dentro di sè per realizzare i propri progetti e poterne, alla fine, apprezzare la grandezza.

Grazie a Fer, per essere un universo che non smette mai di affascinarmi. (...¿Vamos a brillar mi amor?)